

Composite Bulges: The Coexistence of Classical Bulges and Disky Pseudobulges in S0 and Spiral Galaxies

Peter Erwin^{1,2,7}, Roberto P. Saglia^{1,2}, Maximilian Fabricius^{1,2}, Jens Thomas^{1,2},
Nina Nowak³, Stephanie Rusli^{1,2}, Ralf Bender^{1,2}, Juan Carlos Vega Beltrán⁴,
and John E. Beckman^{4,5,6}

¹Max-Planck-Institut für extraterrestrische Physik, Giessenbachstrasse, 85748 Garching, Germany

²Universitäts-Sternwarte München, Scheinerstrasse 1, D-81679 München, Germany

³Stockholm University, Department of Astronomy, Oskar Klein Centre, SE-10691 Stockholm, Sweden

⁴Instituto de Astrofísica de Canarias, C/ Via Láctea s/n, 38200 La Laguna, Tenerife, Spain

⁵Departamento de Astrofísica, Universidad de La Laguna, Avda. Astrofísico Fco. Sánchez s/n, 38200, La Laguna, Tenerife, Spain

⁶Consejo Superior de Investigaciones Científicas, Spain

⁷Guest investigator of the UK Astronomy Data Centre

9 November 2018

ABSTRACT

We study nine S0–Sb galaxies with (photometric) bulges consisting of two distinct components. The outer component is a flattened, kinematically cool, disklike structure: a “disky pseudobulge”. Embedded inside is a rounder, kinematically hot spheroid: a “classical bulge”. This indicates that pseudobulges and classical bulges are not mutually exclusive: some galaxies have both.

The diskly pseudobulges almost always have an exponential disk (scale lengths = 125–870 pc, mean ~ 440 pc) with disk-related subcomponents: nuclear rings, bars, and/or spiral arms. They constitute 11–59% of the galaxy stellar mass (mean $PB/T = 0.33$), with stellar masses $\sim 7 \times 10^9$ – $9 \times 10^{10} M_{\odot}$. Classical-bulge components have Sérsic indices of 0.9–2.2, effective radii of 25–430 pc and stellar masses of 5×10^8 – $3 \times 10^{10} M_{\odot}$ (usually $< 10\%$ of the galaxy’s stellar mass; mean $B/T = 0.06$). The classical bulges show rotation, but are kinematically hotter than the diskly pseudobulges. Dynamical modeling of three systems indicates that velocity dispersions are isotropic in the classical bulges and equatorially biased in the diskly pseudobulges.

In the mass–radius and mass–stellar mass density planes, classical-bulge components follow sequences defined by ellipticals and (larger) classical bulges. Diskly pseudobulges *also* fall on this sequence; they are more compact than similar-mass large-scale disks. Although some classical bulges are quite compact, they are distinct from nuclear star clusters in both size and mass, and coexist with nuclear clusters in at least two galaxies.

Since almost all the galaxies in this study are barred, they probably *also* host boxy/peanut-shaped bulges (vertically thickened inner parts of bars). NGC 3368 shows evidence for such a zone outside its diskly pseudobulge, making it a galaxy with all three types of “bulge”.

Key words: galaxies: bulges – galaxies: structure – galaxies: elliptical and lenticular, cD – galaxies: spiral – galaxies: kinematics and dynamics – galaxies: evolution.

1 INTRODUCTION

In the standard picture of galaxy structure, disk galaxies have two main stellar components. The defining component is the disk: a highly flattened structure dominated by rotation, often (but not always) with a radial density profile which is exponential; disks often have significant substructure,

particularly bars and spiral arms. The secondary component, present in early and intermediate Hubble types, is the bulge. Traditionally, the bulge has been seen as something very like a small elliptical galaxy embedded within the disk: more spheroidal than the disk, with stellar motions dominated by velocity dispersion rather than rotation,

and having a strongly concentrated structure – e.g., having a surface brightness profile similar or identical to the stereotypical $R^{1/4}$ profile of an elliptical). In addition, the stellar populations of bulges were said to resemble those of ellipticals in being older (and possibly more metal-rich and alpha-enhanced) than the majority of stars in the disk. (See, e.g., Wyse et al. 1997 and Renzini 1999 for reviews.) Taken all together, this seemed to argue for a bulge formation mechanism similar to that proposed for ellipticals, either via monolithic collapse or by rapid, violent mergers of initial subcomponents at high redshift.

The past decade or two has seen the growing realization that this picture is probably *not* true for many bulges, at least when bulges are defined as the excess stellar light in the central regions of the galaxy when compared to the dominant exponential profile of the disk.¹ Instead, bulges are now seen as falling into two rather different classes: classical bulges (the traditional model) and *pseudobulges* (e.g., Kormendy 1993; Kormendy & Kennicutt 2004), which are conceived of as something much more like disks than spheroids; i.e., they are flattened and dominated by rotation, with profiles which are close to exponential. Added to this complexity is the existence of so-called “boxy” and “peanut-shaped” bulges, which are now well understood as the vertically thickened inner parts of bars (see Athanassoula 2005, for a discussion of the distinctions); confusingly, these structures are also sometimes called pseudobulges.

Although some authors are careful to point out the possibility that classical bulges could coexist with pseudobulges (see, e.g., Athanassoula 2005; Fisher & Drory 2010), it is common to suggest that galaxies have one or the other, but not both. For example, in observational surveys such as those of Fisher & Drory (2008) or Gadotti (2009), photometrically identified bulges are classified as either classical or pseudobulge. Similarly, in studies of how central supermassive black holes (SMBHs) relate to their host galaxies, disk galaxies are divided into those with classical bulges and those with pseudobulges (e.g., Hu 2008; Greene et al. 2010; Kormendy et al. 2011).

In this paper, we present evidence for the *coexistence* in nine galaxies of both a classical bulge – that is, a round, kinematically hot stellar structure which is significantly larger than a nuclear star cluster – and a disk pseudobulge – that is, a flattened stellar system, distinct from the main disk, whose kinematics are at least partly dominated by rotation and which (usually) hosts nuclear bars, nuclear rings, or other disk morphology.

Two of the galaxies discussed here – NGC 3368 and NGC 3489 – were previously discussed, in an abbreviated fashion, in Nowak et al. (2010), using the term “composite pseudobulges”. Some analysis of the morphological substructure in NGC 3945 and NGC 4371 has been previously presented in Erwin & Sparke (1999) and Erwin et al. (2003).

The outline of this paper is as follows. After some initial discussion of data sources and reduction (Section 2), we lay out our terminology in Section 3. We introduce our methodology for identifying classical bulges by considering

in Section 4 two examples of *simple* classical-bulge-plus-disk systems (galaxies with *only* a classical bulge in addition to their disk). With this as a reference, we then consider two galaxies (NGC 3945 and NGC 4371) in some detail in Section 5, demonstrating first that much of their photometrically defined bulges are *not* classical bulges as previously defined, but something else: (disky) pseudobulges. We then go on to show that inside each pseudobulge is an additional structure which *does* resemble a classical bulge. The evidence for composite bulges in seven other galaxies follows a similar pattern, but is postponed to the Appendix (Section A) so as not to interrupt the flow of the paper. Section 7 uses the results of Schwarzschild modeling for three composite-bulge galaxies to investigate the 3D stellar dynamics of the classical-bulge and disk-pseudobulge components. Section 8 considers these composite-bulge galaxies and their subcomponents, including an analysis of their place in the mass-radius and surface-density–mass diagrams and a demonstration that the classical-bulge components, while generally rather small, are not in the same class as nuclear star clusters. Finally, Section 9 summarizes our findings.

2 DATA SOURCES

2.1 Imaging Data and Surface-Brightness Profiles

Imaging data for this study comes from a variety of sources; for each galaxy, we specify the individual images used and their origins. Some of the large-scale, ground-based optical images come from the WIYN Survey (Erwin & Sparke 2003), the INT-WFC observations of Erwin et al. (2008), or from the Sloan Digital Sky Survey (SDSS; York et al. 2000); for the latter, we use Data Release 7 (DR7; Abazajian et al. 2009). Other ground-based image sources include WHT-INGRID *K*-band images from Knapen et al. (2003), available via NED, and images from the European Southern Observatory (ESO) archive and the Isaac Newton Group (ING) archive.

For high-resolution imaging of the central regions of galaxies, we rely on archival images from the *Hubble Space Telescope*, obtained with the Wide Field Planetary Camera 2 (WFPC2), the Wide Field Channel of the Advanced Camera for Surveys (ACS-WFC), or the NICMOS2 and NICMOS3 near-IR imagers. In some cases – i.e., when *HST* imaging data is lacking or when the centre of a galaxy is particularly dusty – we use adaptive-optics *K*-band images derived from our VLT-SINFONI IFU observations by collapsing the datacubes along the wavelength direction. The latter observations are described in more detail in Nowak et al. (2010), Rusli et al. (2011) and Erwin et al. (2014).

The surface-brightness profiles we construct and analyze combine data from multiple images for each galaxy: high-resolution data from *HST* or AO imaging for the smallest radii, where good spatial resolution is critical, and non-AO ground-based imaging for larger radii, since the galaxies extend beyond the high-resolution imaging fields of view. To combine these data, we must match the overall intensity scaling, and we must also account for the fact that the high-resolution images are too small for accurate background subtraction. (The VLT-SINFONI AO observations were taken

¹ Very compact central concentrations – e.g., nuclear star clusters – are considered separate objects and are excluded from this definition.

with offsets to blank sky, but these were spaced too far apart in time for accurate removal of the overall background levels.) The problem is then to find the correct multiplicative scaling k to match the background-corrected “inner” profile (from the high-resolution image) with the “outer” profile (from the low-resolution image, which is large enough for its own background to be properly estimated), while also determining the unknown background level B_i in the high-resolution image, so that we can transform the observed inner profile I_i to a corrected profile I'_i :

$$I'_i = k(I_i - B_i). \quad (1)$$

Fortunately, these two issues can be dealt with in combination, by taking advantage of the fact that the same galaxy was observed in both images. The trick is to identify a radial overlap zone between the two profiles (outside the region where seeing distorts the low-resolution data) and iteratively fit for the values of k and B_i which minimize the difference $I'_i(r) - I_o(r)$ for values of r in the overlap zone (with I_o being the outer profile). The two profiles are then merged at the best-matching radius in the overlap region. Although the profiles we analyze are usually major-axis cuts, in practice we determine k and B_i using profiles from ellipse fits with fixed position angle and ellipticity, to increase the signal-to-noise ratio. This approach is ideal when the high- and low-resolution images were taken with the same filter; in some cases, we are forced to match and combine profiles from images with dissimilar filters (e.g., F814W and R , or K and z).

When decomposing our surface-brightness profiles – which are typically cuts along the major axis of the galaxy – we do not attempt to correct for PSF convolution, though we do exclude the inner 2–3 pixels of the profile from the fit. For several galaxies with *HST* images, we estimated the possible effects of neglecting PSF convolution by also extracting profiles from images which had been deconvolved using the Lucy-Richardson algorithm (via the IRAF task `lucy`) and TinyTim-generated PSFs. (This was not possible for all galaxies, since for some galaxies we rely on SINFONI data for which PSFs cannot be determined with nearly the same precision.) Comparison of fits to both uncorrected and “deconvolved” profiles of the same galaxy showed that parameters for the central (classical) bulges differ by $\lesssim 15\%$ in the Sérsic index n and $\lesssim 3\%$ for other parameters.

2.2 Spectroscopic Data

Some of the spectroscopic data used for NGC 2859 and NGC 4371 is based on previously unpublished data obtained with the ISIS double spectrograph on the 4.2m William Herschel Telescope. Details of the observations are provided in the Appendix (Section B).

For NGC 3368, NGC 3945 and NGC 4371 we use long-slit data obtained with the Marcario Low Resolution Spectrograph at the Hobby-Eberly Telescope, previously presented in Fabricius et al. (2012). For NGC 3368 and NGC 4699, we also use IFU data from our SINFONI K -band SMBH measurement program (Nowak et al. 2010); Erwin et al. (2014).

2.2.1 Other Sources

We also make use of various published long-slit and IFU kinematic data; the specific sources are listed in the discussions of each galaxy. We note here some datasets provided directly to us. For NGC 1068, this includes both long-slit data from Shapiro et al. (2003), provided by Joris Gerssen, and SINFONI data for NGC 1068 (Davies et al. 2007), provided by Ric Davies. Large-scale SINFONI kinematic data for NGC 3368 (Hicks et al. 2013) were provided by Erin Hicks. Finally, for NGC 4262 we make use of OASIS IFU data (McDermid et al. 2006), provided by Richard McDermid.

3 TERMINOLOGY AND DEFINITIONS: WHAT DO WE MEAN BY “CLASSICAL BULGE” AND “PSEUDOBUULGE”?

The terms “pseudobulge” and “classical bulge” are unfortunately rather ambiguous at present. Sometimes they are defined in terms of their presumed formation methods: e.g., pseudobulges are central concentrations of stars formed from bar- or spiral-driven inflows of gas in the disk plane, or even by any process that does not explicitly involve major mergers, while classical bulges are those structures formed by violent relaxation in major mergers (usually at high redshifts). The fundamental problem with such approaches is that there are few if any clear observational predictions for how to distinguish such formation methods in nearby galaxies.

For example, the formation of central “bulges” by the merger of massive star-forming clumps in gas-rich, high- z disks can produce thick, dispersion-dominated central structures with $\sim R^{1/4}$ light profiles and α -enhanced metallicities (e.g., Immeli et al. 2004; Elmegreen et al. 2008), fulfilling most of the traditional criteria for classical bulges. If one insists on major mergers as the formation mechanism, then these are not classical bulges – but we would have little or no way to distinguish these structures at $z \sim 0$ from “proper” classical bulges. Other theoretical studies of this formation mechanism argue that the resulting bulges should be smaller and more exponential-like, with Sérsic indices of ~ 2 or even ~ 1 , and significant rotation (e.g., Hopkins et al. 2012; Inoue & Saitoh 2012). What this means is that a classification of structures in present-day galaxies based on their supposed formation mechanisms, though desirable, is probably still premature.

If we turn to the more feasible approach of observationally-based classification, we still find considerable discord, if not an outright cacophony. Some surveys classify the central region of a galaxy as classical or pseudobulge depending on the presence or absence of certain morphological features: e.g., a smooth light distribution means a classical bulge, while the presence of dust lanes, spiral arms, rings, nuclear-scale bars, or so-called boxy/peanut-shaped isophotes means a pseudobulge (Kormendy & Kennicutt 2004; Fisher & Drory 2008, e.g.). Other studies make distinctions based on photometric profiles of the “bulge” component that results from a bulge-disk decomposition – e.g., pseudobulges are by definition any central structure with a Sérsic index < 2 , or even any such structure with $n < 4$

(Laurikainen et al. 2009) – or some combination of mean surface brightness and size for the bulge component (e.g., Gadotti 2009).

Because of this confusion, we feel it is important to be clear about our terminology and our methods for identifying and classifying different types of “bulges”. As part of our analysis, we first identify what we call **photometric bulges**. This term refers to the region of a galaxy where the observed stellar surface brightness is brighter than an inward extrapolation of the outer disk component, or is brighter than the inward extrapolation of a previously identified disk pseudobulge. We require that the photometric bulge should be more extended than a simple nuclear star cluster (i.e., the half-light radius should be $\gtrsim 10$ pc). This is, as the name suggests, a purely photometric classification, and is used only as a preliminary tool (and for comparison with the results of purely photometric methodologies).

We then analyse the photometric bulges and classify them into two categories:

- **Classical bulge:** This is a photometric bulge which is some type of kinematically hot spheroid. That is, it must be clearly *rounder* in a three-dimensional sense than the main galaxy disk (i.e., $(c/a)_{\text{bulge}} > (c/a)_{\text{disk}}$, where c is the vertical scale length and a is the radial) *and* must have stellar kinematics which are dominated by velocity dispersion rather than rotation.

- **Disk pseudobulge:** This is a photometric bulge which is “disklike” in *two* main ways: it has a flattening similar or identical to that of the main galaxy disk, and the stellar kinematics are dominated by rotation rather than velocity dispersion at least some point within the photometric bulge region. We also consider the presence of clear morphological features such as bars, rings and spiral arms to be additional signatures of a disk pseudobulge, but do not rely on them alone.

It is important to note that our definition of classical bulge does *not* assume a particular surface-brightness profile shape: we are not assuming that kinematically hot spheroids must have de Vaucouleurs $R^{1/4}$ profiles, nor that they must have Sérsic indices greater than some minimum value.

We also note that we are not considering several characteristics which are sometimes, as alluded to previously, discussed as indicative of “pseudobulges” (Kormendy & Kennicutt 2004). For example, we are mostly not concerned with the presence or absence of dust in the centres of these galaxies, since this can sometimes be due to off-plane or counter-rotating gas (likely the result of accretion), and in other cases may merely indicate that the disk and bulge are co-extensive. Since many of the galaxies we consider are lenticular, we do not require the presence of current or recent star formation as a pseudobulge indicator either. Thus, we are explicitly including what Fisher et al. (2009) called “inactive pseudobulges” (objects in their sample which had what they considered the morphological and photometric signatures of pseudobulges but which showed little or no evidence for recent star formation; see also Fisher & Drory 2010).

Finally, we are, for the most part, explicitly excluding boxy/peanut-shaped bulges from consideration in this study. As Athanassoula (2005) pointed out, these are the vertically thickened inner parts of bars, the result of a common dynamical instability which appears to accompany the formation

of most bars. As such, they are *not* the sort of highly flattened, axisymmetric structures we are most interested in. None the less, we *do* consider the question of their possible co-existence with disk pseudobulges and classical bulges later on in the paper (Section 8.4).

In Section 4, we present two cases of S0 galaxies with purely classical bulges, as a way of providing both examples of how we identify classical bulges and some context for the composite bulges we discuss later. In Section 5 we then go on to analyze two composite-bulge S0 galaxies in detail; we start by identifying disk pseudobulges in each galaxy. While we would ideally like to present an example or two of “pure disk pseudobulge” systems before moving on to the composite bulges, we have encountered difficulty in trying to identify any clear examples in the very nearby (e.g., $D \lesssim 20$ Mpc), early-type disk galaxy population for which the necessary data (particularly stellar kinematics with the right combination of high spatial resolution and radial extent) exist. The problem is not so much identifying candidate disk pseudobulges in other nearby galaxies (as numerous others have done), but rather being able to clearly demonstrate that these are *not also* composite bulge galaxies: i.e., that there are no classical bulges, however small, inside these galaxies. The fact that we do not present any examples of S0–Sb disk galaxies with pure disk pseudobulges should not, however, be taken as a claim that such systems are absent in the local universe.

4 METHODS AND APPLICATIONS: SIMPLE CLASSICAL BULGES

4.1 Basic Methodology

How does one identify the “bulge” of a galaxy, and how does one determine whether such a structure is more like a classical bulge or a disk pseudobulge? Our basic approach has three steps. First, we identify the photometric bulge via a standard Sérsic + exponential decomposition of the entire galaxy. The outer boundary of the (photometric) “bulge-dominated” region is then identified by finding the radius R_{bd} where the Sérsic and exponential components are equal in brightness:

$$\mu_{\text{Ser}}(R_{bd}) = \mu_{\text{exp}}(R_{bd}) \quad (2)$$

Note that this radius may vary somewhat depending on the wavelengths of the data being used for the fit.

Second, we analyse the morphology of the photometric bulge region, focusing especially on the shape of the isophotes. Our working assumption is that the photometric bulge and the outer disk share a common equatorial plane (i.e., they have the same line of nodes and, most importantly, the same inclination to the line of sight). This means that if the bulge is intrinsically rounder (more spheroidal) than the disk, its projected isophotes should appear rounder than those of the outer disk; in the extreme case of a spherical bulge, we would expect to see the elliptical isophotes of the (projected) outer disk give way to circular isophotes at small radii, where the bulge dominates the light.

Finally, we analyse the stellar kinematics in the photometric bulge region, trying to determine whether they are more dominated by rotation or velocity dispersion. Traditionally, one way of using stellar kinematics to discriminate

between classical bulges and pseudobulges (going back to Kormendy 1982) has been to note the position of the bulge in question on the V/σ - ϵ diagram (Illingworth 1977), where V and σ are the “characteristic” stellar velocity and velocity dispersion and ϵ is the ellipticity.² One can define a curve in this diagram which corresponds to an “isotropic oblate rotator” (IOR), a simple model for a classical bulge or elliptical with isotropic velocity dispersion and possible flattening due to modest amounts of stellar rotation (e.g., Binney 1978, 2005). If the object clearly lies above the IOR curve, then the argument is that the object is too dominated by rotation to be considered a classical bulge. (Kinematically hot systems with little or no rotation but significant anisotropy will tend to lie below the IOR line.) This is one of the methods by which some of the original “pseudobulges” (avant la lettre) were identified (Kormendy 1982, 1993). Recent discussion of this diagram, primarily in the context of elliptical and S0 galaxies and taking advantage of 2D kinematics, include, e.g., Cappellari et al. (2007), Spolaor et al. (2010), and Emselfem et al. (2011).

There are, however, some problems with the V/σ - ϵ approach. The underlying theoretical arguments for the reference IOR models presuppose simple, coherent stellar systems with unique, unambiguous values for the ellipticity, velocity and velocity dispersion. The original application envisaged was elliptical galaxies, where at least the domain (the entire galaxy) is unambiguous. But in the case of complex systems such as a bulge embedded within a disk containing secondary structures (nuclear rings, bars, etc.), it is not at all clear how one is supposed to define “the” ellipticity; nor is it clear how to define “the” velocity dispersion when the latter can vary significantly with radius. Even the common technique of choosing the *maximum* stellar velocity as “the” velocity runs into trouble if the rotation curve continues to rise throughout the bulge region and on into the disk-dominated part of the galaxy (or if the rotation curve has multiple peaks).

Faced with these difficulties, we opt for a different approach: we define a simple *local* measurement of the relative importance of rotation versus dispersion, by deprojecting the observed rotation to its in-plane value $V_{\text{dp}} = V_{\text{obs}}/\sin i$ and then dividing this by the observed velocity dispersion σ at the same radius. The resulting quantity – V_{dp}/σ – is a continually varying function of the radius, not a “universal” value for an entire galaxy (or entire galactic component). We adopt an admittedly crude and ad-hoc limit of $V_{\text{dp}}/\sigma = 1$ as the dividing line between kinematically “cool” and kinematically “hot” systems, so that classical bulges should have $V_{\text{dp}}/\sigma < 1$ within the region where they dominate the galaxy’s light. In the following subsections we provide some partial justification for this criterion by showing that galaxies with simple disk + spheroidal bulge morphologies do seem to have $V_{\text{dp}}/\sigma < 1$ within their bulge-dominated regions.

Since we identify the photometric bulge region via decomposition of the major-axis profile, it makes sense to use major-axis value of V_{dp}/σ . This lets us use major-axis long-

slit spectroscopy, which is in many cases the only available stellar kinematic data – or the only data covering the full radial range of interest – for the galaxies we examine.

To show how this approach works in the simple case of disk galaxies *without* pseudobulges, the following subsections apply our methodology to two S0s with classical bulges.

4.2 Simple Classical Bulge Example: NGC 7457

NGC 7457 is a nearby ($D = 12.9$ Mpc)³ low-luminosity S0 galaxy, seen at moderate inclination ($i \approx 58^\circ$; Gutiérrez et al. 2011); it has a central velocity dispersion of only ~ 60 – 70 km s⁻¹ (e.g., Trager et al. 1998; Wegner & et al. 2003; Ho et al. 2009). Although it has been suggested as a possible pseudobulge host in the past, largely on the basis of supposed deviations from the Faber-Jackson relation (e.g., Kormendy 1993; Pinkney et al. 2003), more recent analyses clearly identify it as having a classical bulge (e.g., Fisher & Drory 2008, 2010; Kormendy et al. 2011).

The upper left panel of Figure 1 shows the V -band isophotes for NGC 7457, based on an archival image from the Jacobus Kapteyn Telescope (JKT) of the ING (see Gutiérrez et al. 2011, for details). The upper right panel shows our B/D decomposition of a major-axis cut which combines data from the V -band image with data from an HST WFPC2 F555W image (for $r < 6$ arcsec). The fit excluded both the outer part of the disk (which has an antitruncated profile; Gutiérrez et al. 2011) and the inner nuclear excess at $r < 0.35$ arcsec, which has been attributed to either AGN emission (Gebhardt et al. 2003) or a nuclear star cluster (Graham & Spitler 2009). The bulge/disk crossover radius is at $R_{bd} = 6.2$ arcsec; the disk is clearly the dominant component at $r \gtrsim 15$ – 20 arcsec.

Turning to the isophotes shapes, the lower left panel of Figure 1 shows the results of fitting ellipses to both images. The ellipticity stays roughly constant in to $a \sim 12$ arcsec, and then becomes progressively rounder inside. This is consistent with the influence of a round bulge embedded within a highly elliptical (inclined) disk, so we have evidence that the photometric bulge identified in the B/D decomposition is a rounder (and thus more spheroidal) object than the disk.

Finally, the lower right panel of Figure 1 shows V_{dp}/σ as a function of radius along the major axis, using the long-slit kinematic data of Simien & Prugniel (1997). Within the photometric bulge region, V_{dp}/σ is consistently < 1 (in fact, it never gets above ~ 0.6); it increases to larger radii, finally becoming > 1 at $r \gtrsim 15$ arcsec. Note that V_{dp}/σ continues to increase as we move into the (photometric and morphological) disk region, reaching values $\gtrsim 2$ in the region which is unambiguously disk-dominated.

As a crude approximation, then, we can identify “kinematically disklike” regions as having $V_{\text{dp}}/\sigma > 1$.

4.3 Simple Classical Bulge Example: NGC 1332

With a K -band luminosity of $1.56 \times 10^{11} L_\odot$ and a central velocity dispersion of 328 km s⁻¹ (Rusli et al. 2011),

² V is usually taken to be the maximum stellar rotation velocity V_{max} and σ is some “central” value; the ellipticity is sometimes the maximum observed value and sometimes a mean value.

³ Based on the SBF distance of Tonry et al. (2001) and the Mei et al. (2005) correction.

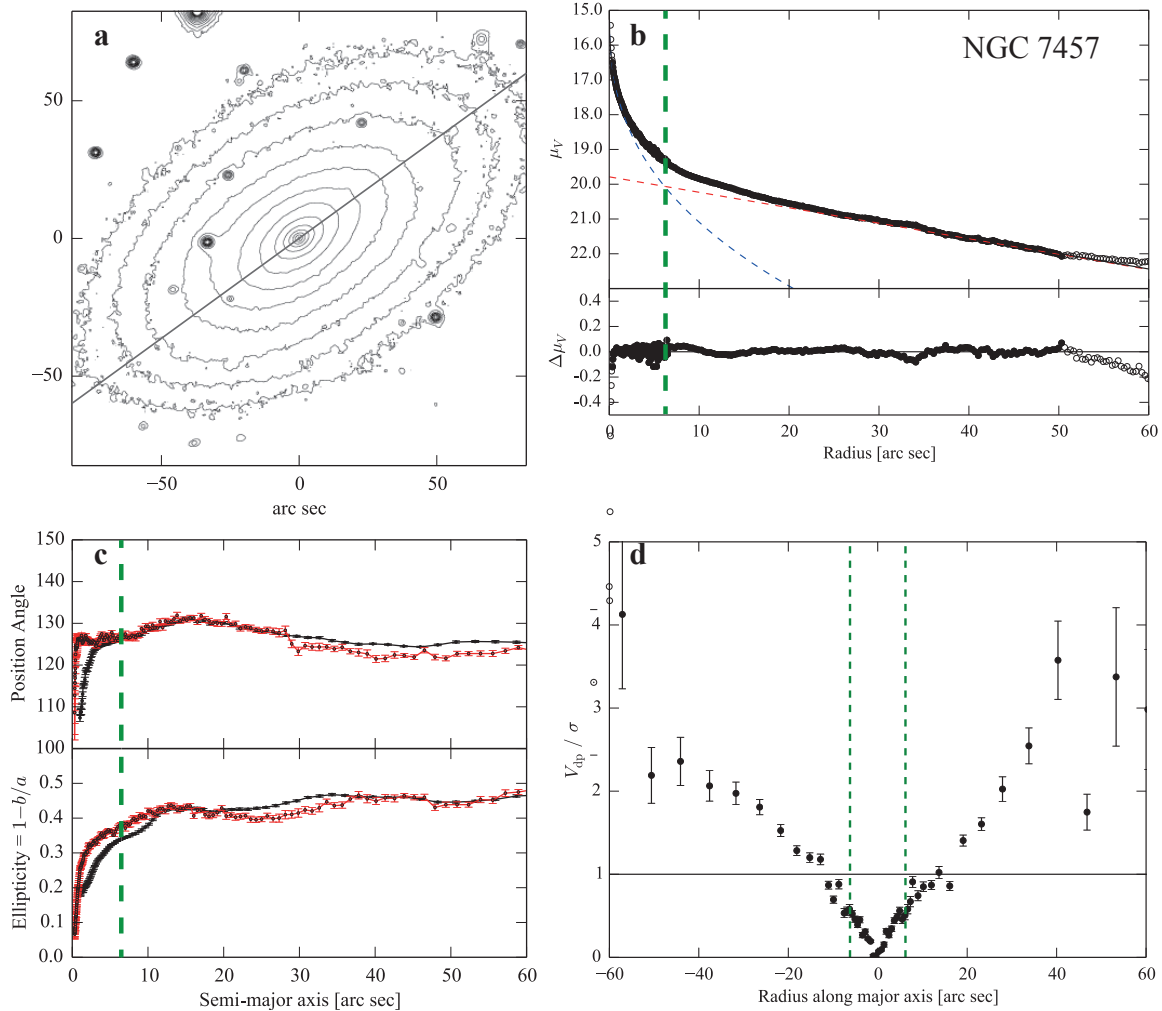


Figure 1. Evidence for a classical bulge in the low-mass S0 galaxy NGC 7457. **a:** log-scaled V -band isophotes (JKT image); gray line marks major axis (PA = 126°). **b:** Bulge-disk decomposition of major-axis profile. Data (black circles) combine major-axis cuts through *HST* WFPC2 F555W image ($r < 6.6$ arcsec) and ground-based V -band image. Dashed lines are Sérsic + exponential fit to the data for $r = 0.4$ –50 arcsec (filled circles), with residuals in lower sub-panel; data at $r > 50$ arcsec are part of a shallower outer zone in the antitruncated disk profile. Vertical dashed green line marks “bulge=disk” radius R_{bd} , where Sérsic and exponential components are equally bright; this sets the boundary of the “photometric bulge region”. **c:** Ellipticity and position angle of ellipse fits to V -band image (black) and *HST* image (red). **d:** Plot of deprojected stellar rotation velocity divided by local velocity dispersion V_{dp}/σ along the major axis, using long-slit data from Simien & Prugniel (1997). Vertical dashed lines mark the photometric bulge region $|R| < R_{bd}$; $V_{dp}/\sigma < 1$ inside, indicating a kinematically hot region (i.e., a classical bulge).

NGC 1332 is one of the most massive S0 galaxies in the nearby universe ($D = 22.3$ Mpc, from Tonry et al. 2001 and Mei et al. 2005); it also hosts a central supermassive black hole with a mass of $1.45 \times 10^9 M_{\odot}$ (Rusli et al. 2011).

Figure 2 shows the overall morphology of the galaxy in panel a: a highly elliptical outer disk with a distinctly rounder inner zone. Decomposition of the major-axis profile (panel b, combining data from a ground-based R -band image with *HST* WFPC2 F814W data at smaller radii and data from our SINFONI K -band datacube at the very smallest radii to reduce the effects of circumnuclear dust extinction; see Rusli et al. 2011 for details) shows a photometric bulge dominating the light at $r < R_{bd} = 12$ arcsec. As was the case for NGC 7457, the isophotes in the bulge-dominated

region are clearly rounder (panel c) than those of the outer disk.

Previous B/D decompositions for this galaxy (both 1D and 2D) are discussed in Rusli et al. (2011). Of particular note is the fact that their 2D decomposition had a best fit using a Sérsic bulge component with ellipticity = 0.27, in contrast to the best-fitting exponential disk ellipticity of 0.73. This is clear support for the idea that the photometric bulge corresponds to a region which is significantly rounder than the disk. The slight twisting and rounding of isophotes between $a \sim 20$ and 40 arcsec may indicate a very weak bar or lens, but otherwise this galaxy is very close to an ideal exponential disk + Sérsic bulge system.

Finally, panel d of Figure 2 shows the radial trend of V_{dp}/σ , using data from Kuijken et al. (1996) as re-reduced

by Rusli et al. (2011). V_{dp}/σ clearly reaches a plateau value ($\sim 0.5\text{--}0.6$) within the photometric bulge; as was the case for NGC 7457, the ratio only becomes > 1 outside the photometric bulge region.

As in the case of NGC 7457, we conclude that the photometric bulge in NGC 1332 is a structure which is clearly rounder than the disk and has stellar kinematics dominated by velocity dispersion: in other words, a classical bulge.

5 COMPOSITE BULGES: DETAILED EXAMPLES

In this section, we turn to a set of galaxies whose photometric bulges show significantly more complex structure than was true for the two S0 galaxies considered in the previous section. Basic parameters for these galaxies are presented in Table 1.

We begin by examining two S0 galaxies – NGC 3945 and NGC 4371 – in detail, as paradigms for the analysis we apply to the whole set. Individual details and analysis for the other galaxies are discussed in the Appendix (Section A).

5.1 Composite Bulge Example: NGC 3945

NGC 3945 is a double-barred S0 galaxy (Erwin & Sparke 1999; Erwin 2004) which was originally singled out as an unusual object by Kormendy (1982); it had the largest value of $(V_{\text{max}}/\sigma_0)^{*4}$ of any of the galaxies in his sample (see also Figure 17 of Kormendy & Kennicutt 2004), indicating an unusually high degree of rotational support for a “bulge”.

Erwin & Sparke (1999) re-examined this galaxy using *HST* imaging. They pointed out that much of the inner region (i.e., the photometric bulge) appeared to be similar to a small exponential disk, complete with a nuclear bar surrounded by a stellar ring, embedded inside the main body of the galaxy, and that this region had a flattening roughly consistent with that of the outer disk. Erwin et al. (2003) revisited this analysis by performing B/D decompositions and a further analysis of the original kinematics of Kormendy (1982); they noted the existence of a separate photometric component within the inner 2 arcsec, with isophotes which were rounder than the main part of the photometric bulge (and the outer disk). Because NGC 3945 is such a paradigmatic case for the phenomenon of composite bulges, we repeat most of their analysis here, with the addition of *HST* STIS stellar kinematics from Gültekin et al. (2009) which enables us to explore the kinematic status of the classical bulge; we also make use of new, large-scale kinematics obtained with the HET.

5.1.1 Photometric Bulge as Disky Pseudobulge

As we did for the pure-classical-bulge S0s in the previous section, we performed a simple B/D decomposition of the major-axis profile (panel b of Figure 3). This is not entirely successful, since the outer disk is *not* a simple exponential;

⁴ This is the ratio of the observed V_{max}/σ_0 to the value expected for an isotropic oblate rotator having the same ellipticity; the value for NGC 3945 was 1.82.

instead, it is distorted by the presence of a very luminous outer ring, which we exclude from the fit. (On the other hand, this profile largely avoids any contribution from the primary bar, which is oriented close to the galaxy minor axis.) None the less, there *is* a clear inner excess which dominates the light at $r \lesssim 20$ arcsec; from our fit, we find $R_{bd} = 17$ arcsec.

The fit in Figure 3 is somewhat different from the global B/D decomposition presented in Erwin et al. (2003), which used an ellipse-fit profile rather than a major-axis cut, and tried to fit the outer ring beyond 80 arcsec with the same exponential component. That fit increased the role of the Sérsic component (in part because it included light from the bar, which our cut largely avoids because the bar is oriented almost perpendicular to the major axis), moving R_{bd} out to ~ 30 arcsec; a similar R_{bd} value can be seen in the ellipse-fit-based B/D decomposition of this galaxy in Fisher & Drory (2010). If we use either of those fits instead, the photometric bulge region becomes larger, but the conclusions of our analysis remain unchanged.

Thus far, our analysis of this galaxy has not shown any clear deviation from the simple classical-bulge systems discussed in Section 4. Something rather different does emerge, however, when we look at the isophote shapes in the photometric bulge region (panels c and e of Figure 3). The ellipticity of this region is quite large: it reaches a maximum value of 0.36 at $a \approx 10$ arcsec, which is close to that of the outer disk. Given that these isophotes may still be distorted by light from the (primary) bar outside, it is possible that the underlying shape is actually the *same* as the outer disk; in any case, it suggests that much of the photometric bulge region is nearly as flat as the outer disk.

Unsharp masking (panel d of Figure 3) shows the signature of a stellar nuclear ring in this region (with $a \sim 6.5$ arcsec); additional unsharp masking also reveals the presence of a nuclear bar inside the ring (see Figure 2 of Erwin & Sparke 1999). This inner bar actually produces a *minimum* in the ellipticity at $a \approx 2.6$ arcsec because it is oriented close to the minor axis of the galaxy. The presence of these structures reinforces the idea that the photometric bulge of NGC 3945 is predominantly a disklike structure.

Finally, panel f of Figure 3 shows V_{dp}/σ , using our HET kinematics. In contrast to the simple classical-bulge galaxies studied above, V_{dp}/σ reaches a peak value > 2 within the photometric bulge region. This is clear, dramatic evidence that the photometric bulge region is *not* a simple, kinematically hot structure; instead, the local stellar motions are sufficiently dominated by rotation as to resemble the *disk* regions of NGC 1332 and NGC 7457. Combined with the previous morphological evidence, this makes NGC 3945 one of the clearest cases of an S0 galaxy with a diskly pseudobulge.

5.1.2 Inner Photometric Bulge as Classical Bulge

All of the foregoing is strong evidence that the photometric bulge of NGC 3945 is mostly, if not entirely, a diskly pseudobulge. However, there is also good evidence that the innermost regions of the galaxy are dominated by a separate component, distinct from the pseudobulge.

The inner part ($r < 20$ arcsec) of the major-axis surface-brightness profile (panel b of Figure 4) has two interesting

Table 1. Galaxies with Composite Bulges

Galaxy	RC3 Type	D Mpc	Source	M_B	PA deg	i deg	R_{bd} arcsec
(1)	(2)	(3)	(4)	(5)	(6)	(7)	(8)
NGC 1068	(R)SA(rs)b	14.2	1	-21.23	86	31/40	24
NGC 1543	(R)SB(l)0 ⁰	20.0	2	-20.12	—	20?	26
NGC 1553	SA(r)0 ⁰	18.0	2	-21.08	152	48	16
NGC 2859	R)SB(r)0 ⁺	24.2	1	-20.21	85	32	52
NGC 3368	SAB(rs)ab	10.5	3	-20.37	172	50	52
NGC 3945	(R)SB(rs)0 ⁺	19.8	1	-19.94	158	55	17
NGC 4262	SB(s)0 ^{-?}	15.4	4	-18.72	155	30	7.2
NGC 4371	SB(r)0 ⁺	16.9	4	-19.49	90	58	32
NGC 4699	SAB(rs)b	18.9	1	-21.33	35	37	44

Basic characteristics of galaxies with composite bulges. Column 1: Galaxy name. Column 2: Hubble type (RC3). Column 3: Distance. Column 4: Source for distance: 1 = Virgocentric-infall-corrected redshift from HyperLeda; 2 = Tonry et al. (2001), with correction from Mei et al. (2005); 3 = Freedman et al. (2001); 4 = Blakeslee et al. (2009). Column 5: absolute B luminosity (HyperLeda B_{tc} + adopted distance). Column 6: adopted position angle of disk. Column 7: adopted inclination. Column 8: Radius where luminosity of Sérsic component = luminosity of exponential component from initial photometric decomposition (see text).

Table 2. Imaging and Spectroscopic Data Summary

Galaxy	Telescope/Instrument Imaging	Filter	Source	Telescope/Instrument Spectroscopy	Source
(1)	(2)	(3)	(4)	(5)	(6)
NGC 1068	VLT-SINFONI (AO)	H	1	VLT-SINFONI (AO)	1
	<i>HST</i> -NICMOS3	F200N		Gemini-GMOS	2
	2MASS	K		KNPO-4m-RCFS	3
	SDSS	i		...	
NGC 1543	<i>HST</i> -WFPC2	F814W		...	
	<i>Spitzer</i> -IRAC	IRAC2		...	
NGC 1553	<i>HST</i> -WFPC2	F814W		CTIO-4m-RCS	4
	<i>HST</i> -NICMOS2	F160W		ESO-1.52m-B&C	5
	<i>Spitzer</i> -IRAC	IRAC1		...	
NGC 2859	<i>HST</i> -ACS/WFC	F814W		WHT-ISIS	6
	WIYN-3.5m	R	7	WHT-SAURON	8
	SDSS	i		...	
NGC 3368	VLT-SINFONI (AO)	K	9	VLT-SINFONI (AO)	9
	<i>HST</i> -NICMOS2	F160W		HET-MLRS	10
	WHT-INGRID	K	11	...	
	SDSS	r		...	
NGC 3945	<i>HST</i> -WFPC2	F814W		<i>HST</i> -STIS	12
	WIYN-3.5m	R	7	HET-MLRS	10
NGC 4262	<i>HST</i> -ACS/WFC	F850LP		WHT-OASIS	13
	SDSS	i		WHT-SAURON	14
NGC 4371	<i>HST</i> -ACS/WFC	F850LP		VLT-SINFONI (AO)	15
	INT-WFC	r	16	WHT-ISIS	6
NGC 4699	VLT-SINFONI (AO)	K	15	VLT-SINFONI (AO)	15
	SDSS	i,z		Las Campanas-2.5m-MS	17

Imaging and spectroscopic data used for the composite-bulge galaxies. For each galaxy, we list the data in order of decreasing spatial resolution (e.g., *HST* or AO data, followed by ground-based data). Column 1: Galaxy name. Column 2: Telescope + instrument or survey for imaging data (“AO” = adaptive optics used). Column 3: Filter used for imaging data. Column 4: Source of imaging data, if not from public telescope archives. Column 5: Telescope + instrument for spectroscopic/kinematic data. Column 6: Source of spectroscopic/kinematic data. References: 1 = Davies et al. (2007); 2 = Gerssen et al. (2006); 3 = Shapiro et al. (2003); 4 = Kormendy (1984); 5 = Longo et al. (1994); 6 = this paper (Appendix B); 7 = Erwin & Sparke (2003); 8 = de Lorenzo-Cáceres et al. (2008); 9 = Nowak et al. (2010); 10 = Fabricius et al. (2012); 11 = Knapen et al. (2003); 12 = Gültekin et al. (2009); 13 = McDermid et al. (2006); 14 = Emsellem et al. (2004); 15 = Erwin et al., in prep.; 16 = Erwin et al. (2008); 17 = Bower et al. (1993).

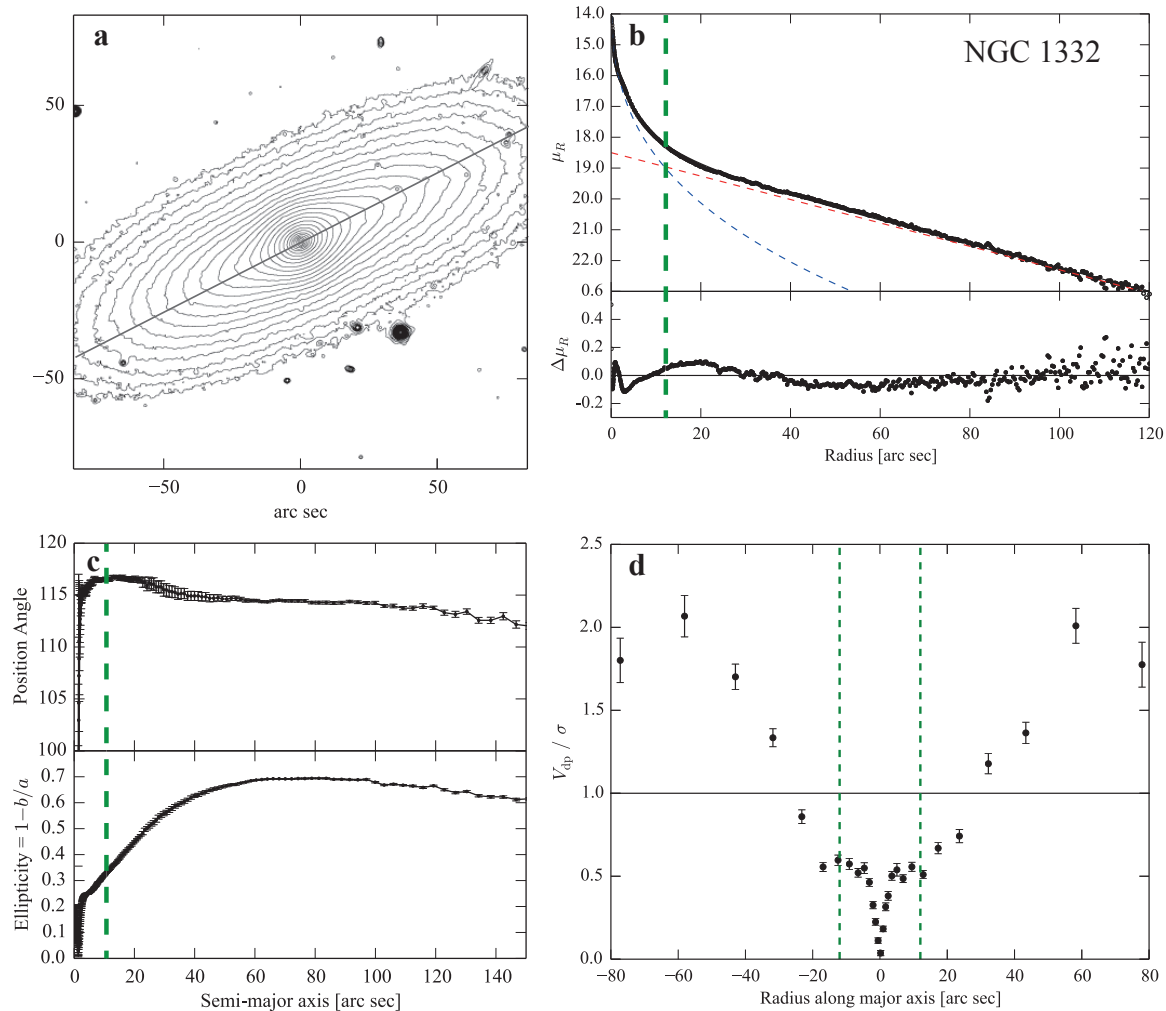


Figure 2. As for Figure 1, but now showing evidence for a classical bulge in the high-mass S0 galaxy NGC 1332. **a:** log-scaled R -band isophotes (NTT-EMMI image); gray line marks major axis (PA = 117°). **b:** Bulge-disk decomposition of major-axis profile. Data (black circles) combine ellipse fits to SINFONI 100mas and HST-WFPC2 F814W images ($r < 2.6$ arcsec) and ground-based R -band image. Dashed lines are Sérsic + exponential fit to the data, with residuals in lower sub-panel. Vertical dashed green line marks “bulge=disk” radius R_{bd} , where Sérsic and exponential components are equally bright; this sets the boundary of photometric bulge region. **c:** Ellipticity and position angle of ellipse fits to R -band image. **d:** Plot of V_{dp}/σ along major axis, using long-slit data from Kuijken et al. (1996) as re-reduced by Rusli et al. (2011). Vertical dashed lines mark the photometric bulge region $|R| < R_{bd}$; V_{dp}/σ is < 1 inside, indicating a kinematically hot region (i.e., a classical bulge).

characteristics: first, most of the profile is very nearly a perfect exponential; second, the inner $r \lesssim 2$ arcsec show a steep central excess. Erwin et al. (2003) pointed out that this profile appeared eerily similar to that of an exponential plus an inner Sérsic component, and proceeded to treat it in just that fashion. Panel b of Figure 4 produces a revised version of that fit, this time including the contribution from the lens/outer-disk (dashed green line in the bottom left corner of the upper panel). Although the details of the fit are slightly different from Erwin et al. (2003), the result is still an excellent match to the profile; the small deviations at $r < 5$ arcsec are due to the presence of the inner bar and its surrounding nuclear ring. Given this *inner* decomposition, we can identify a new, much smaller photometric bulge region, with $R_{bd,i} = 1.1$ arcsec (we use $R_{bd,i}$ to indicate an *inner* bulge = disk radius, in contrast to the R_{bd} value from the global decomposition of the previous subsection).

The inner ellipse fits – particularly those of the HST image – show that the region inside $R_{bd,i} = 1.1$ arcsec is distinctly *rounder* than the main part of the diskly pseudobulge (and rounder than the outer disk), with an ellipticity ≈ 0.21 (panel c of Figure 4). Photometrically and morphologically, then, we have evidence for a distinct central component, rounder than the outer disk *and* the diskly pseudobulge.

What about the stellar kinematics? Here, we make use of the HST-STIS kinematics published by Gültekin et al. (2009). Panel d of Figure 4 shows that V_{dp}/σ reaches a plateau value of ~ 0.5 in the region $\lesssim 1.1$ arcsec. Since the stellar kinematics of this central structure appear dominated by random motions, much like the larger classical bulges of NGC 1332 and NGC 7457 (above), we conclude that this inner structure is a (small) classical bulge.

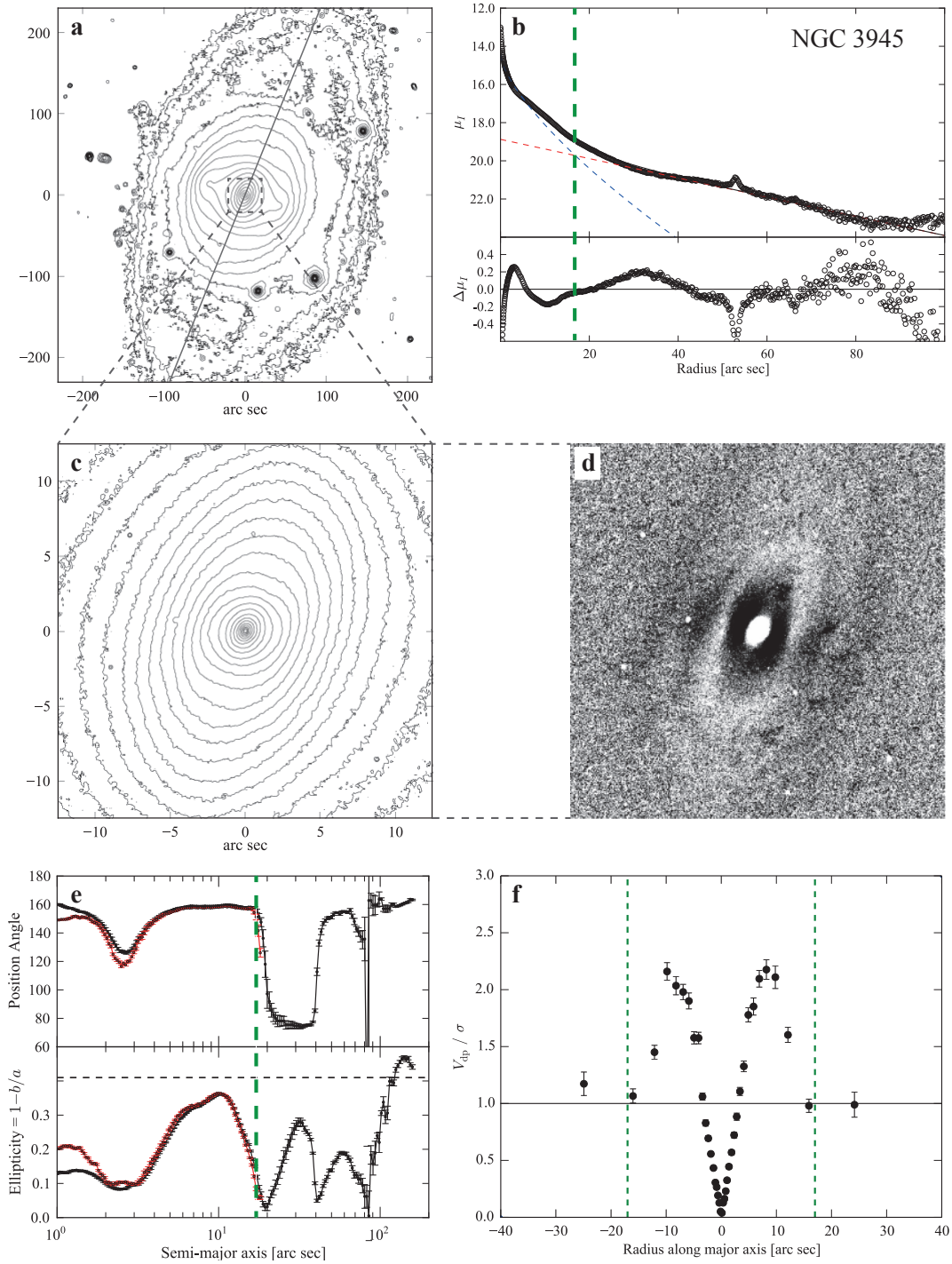


Figure 3. Evidence for a disk pseudobulge in the S0 galaxy NGC 3945. **a:** log-scaled R -band isophotes (WIYN image, smoothed with 15-pixel-wide median filter); gray diagonal line marks major axis (PA = 158°). **b:** Bulge-disk decomposition of WIYN major-axis profile. Dashed lines show Sérsic + exponential fit to the data, with residuals in lower sub-panel. Vertical dashed green line marks “bulge=disk” radius R_{bd} , where Sérsic and exponential components are equally bright; this sets the boundary of the photometric bulge. **c:** Close-up of photometric bulge region, (log-scaled isophotes from *HST* F814W WFPC2 image). **d:** Unsharp mask (using $\sigma = 15$ pixel Gaussian kernel) of inner region on the same scale as panel c, showing stellar nuclear ring. **e:** Ellipse fits to WIYN and *HST* images; note that the ellipticity reaches ~ 0.36 , similar to outer disk value (horizontal dashed line), in the photometric bulge; this suggests that at least part of the photometric bulge has flattening similar to the outer disk. **f:** Deprojected stellar rotation velocity divided by local velocity dispersion V_{dp}/σ along the major axis, using HET long-slit data. Vertical dashed lines mark the photometric bulge region $|R| < R_{bd}$; V_{dp}/σ rises to > 2 in this region, indicating a kinematically cool region more like a disk.

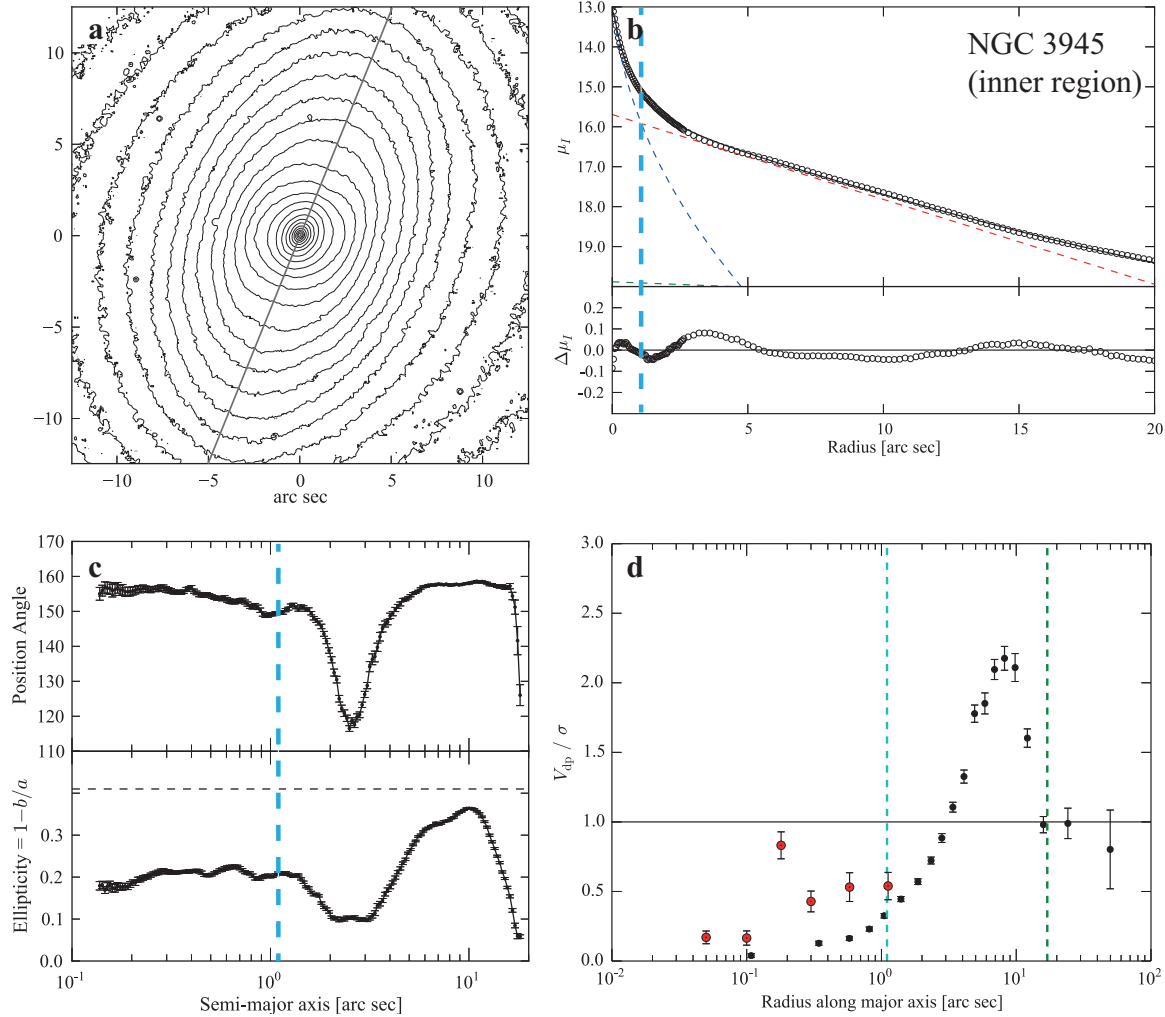


Figure 4. Evidence for a small classical bulge inside the disk pseudobulge of NGC 3945. **a:** Close-up of main photometric bulge region from *HST* WFPC2 F814W image, gray line marks major-axis PA. **b:** major-axis profile from *HST* F814W WFPC2 image, with Sérsic + two-exponential fit (dashed lines) and residuals from fit in lower sub-panel. Vertical dashed blue line marks inner “bulge=disk” radius $R_{bd,i}$, where the Sérsic and exponential components of this fit are equally bright; this sets the boundary of the *inner* photometric bulge. **c:** Ellipse fits to *HST* image; ellipticity in the inner photometric bulge region ($a \lesssim 1.1$ arcsec) is ~ 0.21 , much less than that of the disk pseudobulge outside. **d:** Deprojected, folded stellar rotation velocity divided by local velocity dispersion V_{dp}/σ along the major axis, using *HST* STIS data from Gültekin et al. (2009) [red] and HET long-slit data [black]. Vertical dashed blue and green lines mark the inner and main photometric bulge regions $|R| < R_{bd,i}$, respectively. In the inner region ($r \lesssim 1$ arcsec), V_{dp}/σ remains well below 1, suggesting a kinematically hot region.

5.2 Composite Bulge Example: NGC 4371

Like NGC 3945, NGC 4371 was noted by Kormendy (1982) for its rather large value of $(V_{max}/\sigma_0)^*$ – second only to NGC 3945 in his sample. The variation in ellipticity of the inner isophotes in this barred S0 galaxies led Wozniak et al. (1995) to suggest that the galaxy might have a total of *three* bars: the obvious large outer bar and two more in the photometric bulge region. Using *HST* images, Erwin & Sparke (1999) were able to show that the apparent signature of the inner two “bars” was actually the result of a bright, stellar nuclear ring distorting the isophotes (see also Erwin et al. 2001).

5.2.1 Photometric Bulge as Disky Pseudobulge

Our B/D decomposition of the major-axis profile is shown in panel b of Figure 5. The fit shows significant residuals, due in part to the presence of the nuclear ring at $a \sim 10$ arcsec; however, it does allow us to define the photometric bulge boundary as $R_{bd} = 25$ arcsec. (This is smaller than the bulge region defined by the decomposition of Fisher & Drory 2010, presumably because their ellipse-fit-derived profile includes light from the bar, which our major-axis cut largely excludes.)

As was the case for NGC 3945, a close-up of the photometric bulge region shows very elliptical isophotes interior to those defining the bar (panels c and e of Figure 5); the peak ellipticity of ~ 0.40 is close to that of the outer disk. (Note that the plotted ellipticity in panel e peaks at 0.54 at $a \sim 140$ arcsec due to the presence of an outer ring; the true

outer-disk ellipticity of 0.45 is determined from isophotes further out; see, e.g., Fig 3b of Erwin et al. 2005.) Unsharp masking (panel d) shows the nuclear ring, which is a purely stellar phenomenon with no signs of gas, dust, or ongoing star formation, though Comerón et al. (2010) did find that the ring has a slightly bluer colour than the surrounding light in their *HST* colour map. Unlike the case of NGC 3945, there is no evidence for a nuclear bar in this galaxy.

The peculiarly box-shaped isophotes interior to the nuclear ring, which are visible at $a \sim 5\text{--}7\text{arcsec}$ and which produce the local ellipticity minimum in the ellipse fits, can be explained as the side effect of adding the isophotes of an elliptical ring to those of a rounder structure inside (see Erwin et al. 2001).

Finally, analysis of our major-axis WHT-ISIS spectroscopy shows that the V_{dp}/σ profile (panel f) has a peak of ~ 1.5 within the photometric bulge region – in fact, the peak is more or less at the radius of the nuclear ring. Once again, we have good evidence that the photometric bulge region is kinematically more like a disk than a classical spheroid, in addition to the clear morphological evidence for a disky pseudobulge.

5.2.2 Inner Photometric Bulge as Classical Bulge

Although the inner profile is not as clean and simple as that of NGC 3945, we can still identify a clear central excess at $r \lesssim 5$ arcsec. Panel b of Figure 6 shows a plausible decomposition, where we treat the inner disk + nuclear ring as a single component with a broken-exponential profile (Erwin et al. 2008). (See Erwin et al. 2014 for a more complex, 2D decomposition which yields similar results in terms of the classical bulge.) As we did for NGC 3945, we can define an inner value of $R_{\text{bd},i} = 5$ arcsec, where the Sérsic component is brighter than the sum of the outer exponential plus the nuclear-ring/inner-disk component.

The ellipticity of the *HST* isophotes interior to this radius (panel c of Figure 6) is consistently ≈ 0.30 (the variation at $a \approx 0.3\text{--}0.6$ arcsec is due to a circumnuclear dust ring, noted by Comerón et al. 2010). Moreover, the stellar kinematics for this region (panel d of the same figure) shows that V_{dp}/σ reaches a plateau of ~ 0.65 within $R_{\text{bd},i} = 5$ arcsec, so the kinematics of this region are dominated by velocity dispersion instead of rotation. In other words, the inner $r < 5$ arcsec of this galaxy appears to be dominated by a classical bulge.

6 OTHER COMPOSITE BULGES

Detailed discussion and analysis of the other seven composite-bulge galaxies can be found in Appendix A. We note here that not all these galaxies are as clear-cut as the two just discussed (NGC 3945 and NGC 4371). For example, we lack kinematic data with high enough spatial resolution to properly resolve the interior of the classical-bulge region for some of those galaxies. In most such cases, however, V_{dp}/σ is significantly < 1 in the (resolved) region just *outside* the classical bulge, so it is unlikely that V_{dp}/σ is actually > 1 inside the classical bulge.

For some galaxies, we use profiles from position angles other than the galaxy major axis, especially when strong

Table 5. B/T Values

Name (1)	$B/T_{\star,\text{cl}}$ (2)	$B/T_{\star,\text{phot}}$ (3)	B/T_L (lit.) (4)	Source (5)
NGC 1068	0.021	0.40	0.11	L10
NGC 1543	0.10	0.00	0.34	L10
NGC 1553	0.031	0.41	0.23	L10
NGC 2859	0.070	0.38	0.29, 0.47	L10, F12
NGC 3368	0.024	0.54	0.26, 0.41	F11, F12
NGC 3945	0.045	0.37	0.39, 0.36	L10, F12
NGC 4262	0.045	0.65	0.55	L10
NGC 4371	0.093	0.27	0.22, 0.38	L10, F12
NGC 4699	0.089	0.71	0.34	L04

Bulge-to-total values for composite-bulge galaxies. Column 1: Galaxy name. Column 2: Ratio of classical bulge stellar mass to total galaxy stellar mass. Column 3: Ratio of photometric bulge stellar mass to total galaxy stellar mass, from simple 1-D decomposition. Column 4: Near-IR B/T luminosity values from the literature. Column 5: Sources for values in Column 4 – L04 = 2D K -band decompositions of Laurikainen et al. (2004); L10 = 2D K -band decompositions of Laurikainen et al. (2010); F11 = “near-IR” 1D decompositions of Fisher & Drory (2011); F12 = H -band 1D decompositions of Fabricius et al. (2012).

nuclear bars are present. This includes profiles perpendicular to nuclear bars (when present), to minimize its contribution, as well as alternate cases where we use a profile along the nuclear-bar major axis, including an extra component to account for the bar contribution.

The results of these analyses, combined with the previous ones for NGC 3945 and NGC 4371, are presented in Tables 3–5.

7 STELLAR DYNAMICS OF CLASSICAL BULGES AND DISKY PSEUDOBULGES

Three of the composite-bulge galaxies, along with one of the example pure-classical-bulge galaxies (NGC 1332), have been observed with the SINFONI IFU during a project measuring supermassive black hole masses in galaxy centres (Nowak et al. 2007, 2008, 2010; Rusli et al. 2011, 2013; Erwin et al. 2014). As part of the analysis, we perform Schwarzschild orbit-superposition modeling in order to reproduce both the stellar light distribution and the observed stellar kinematics; see Thomas et al. (2004), Nowak et al. (2010) and Rusli et al. (2011) for details. Briefly stated, this involves constructing a galaxy potential from the combination of a central SMBH and one or more deprojected, 3D luminosity-density distributions (e.g., a components for the classical bulge and one for the disky-pseudobulge+outer-disk), converted to 3D stellar mass density distributions via a stellar mass-to-light (M/L) ratio. Trial values of the SMBH mass and the stellar M/L ratios are assigned, and then several tens of thousands of sample orbits are integrated in the potential. The resulting orbit library is weighted to produce the best match to the observed light distribution and the observed stellar kinematics, and the process is then iterated with new values of M/L and SMBH mass to map out the χ^2 landscape.

The end result, in addition to best-fit values for the stellar M/L ratios and the SMBH mass, is a library of stel-

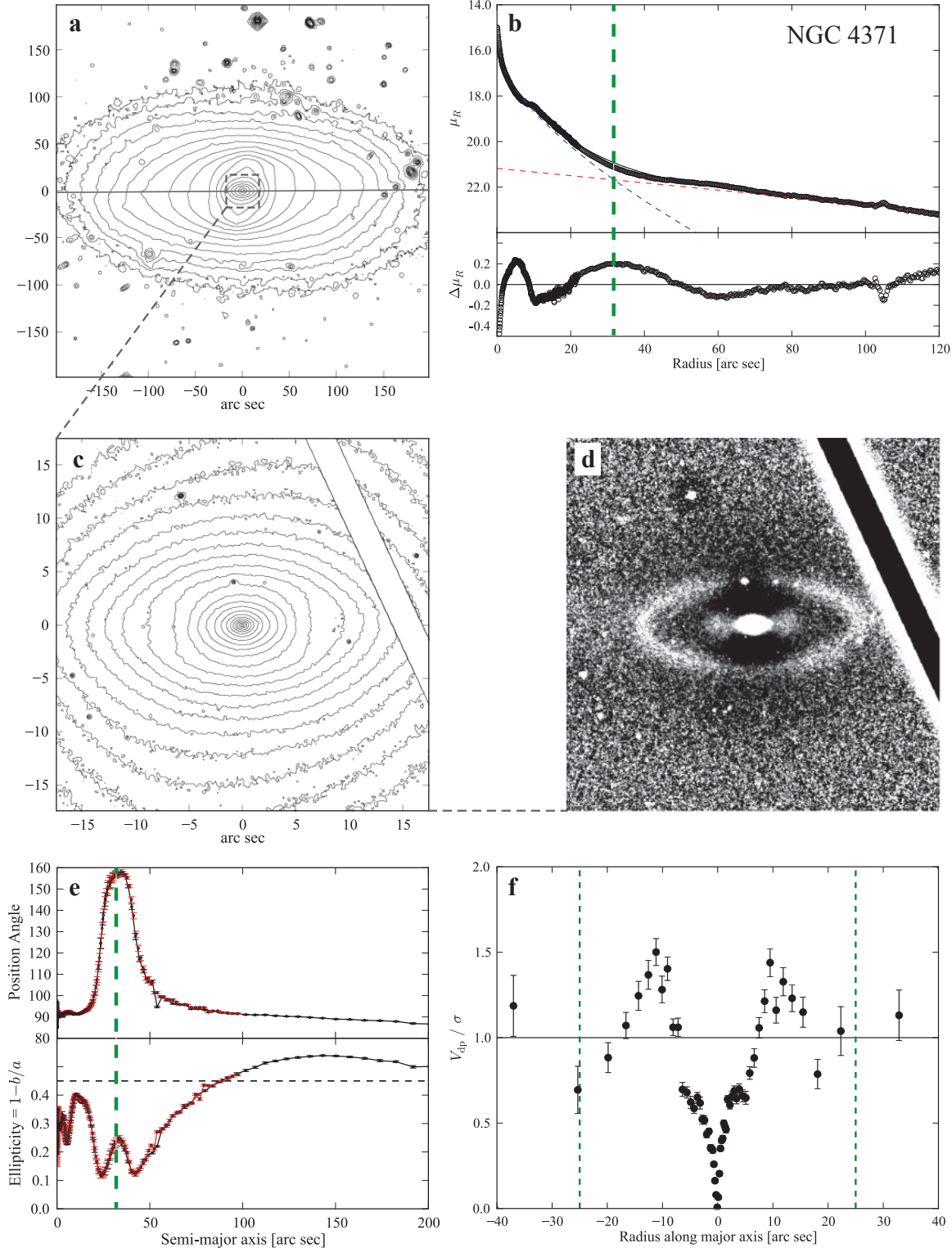


Figure 5. Evidence for a disk pseudobulge in the S0 galaxy NGC 4371. **a:** log-scaled R -band isophotes (INT-WFC image, smoothed with 15-pixel-wide median filter); gray line marks major axis (PA = 90.4°). **b:** Bulge-disk decomposition of INT-WFC major-axis profile. Dashed lines represent Sérsic + exponential fit to the data, with residuals plotted in lower sub-panel. Vertical dashed green line marks “bulge=disk” radius R_{bd} , where the Sérsic and exponential components are equally bright; this sets the boundary of the “photometric bulge”. **c:** Close-up of photometric bulge region (log-scaled contours from *HST* ACS-WFC F850LP image). **d:** Unsharp mask ($\sigma = 20$ pixels) of same region, showing stellar nuclear ring. **e:** Ellipse fits to INT-WFC and *HST* (red) images; note that ellipticity reaches ~ 0.40 , almost as high as the outer disk value (horizontal dashed line), in photometric bulge; this suggests that at least part of the photometric bulge has flattening similar to the outer disk. **f:** Deprojected stellar rotation velocity divided by local velocity dispersion V_{dp}/σ along major axis, using WHT-ISIS long-slit data. Vertical dashed lines mark the photometric bulge region $|R| < R_{bd}$; V_{dp}/σ rises to ~ 1.5 in this region, indicating a kinematically cool region more like a disk.

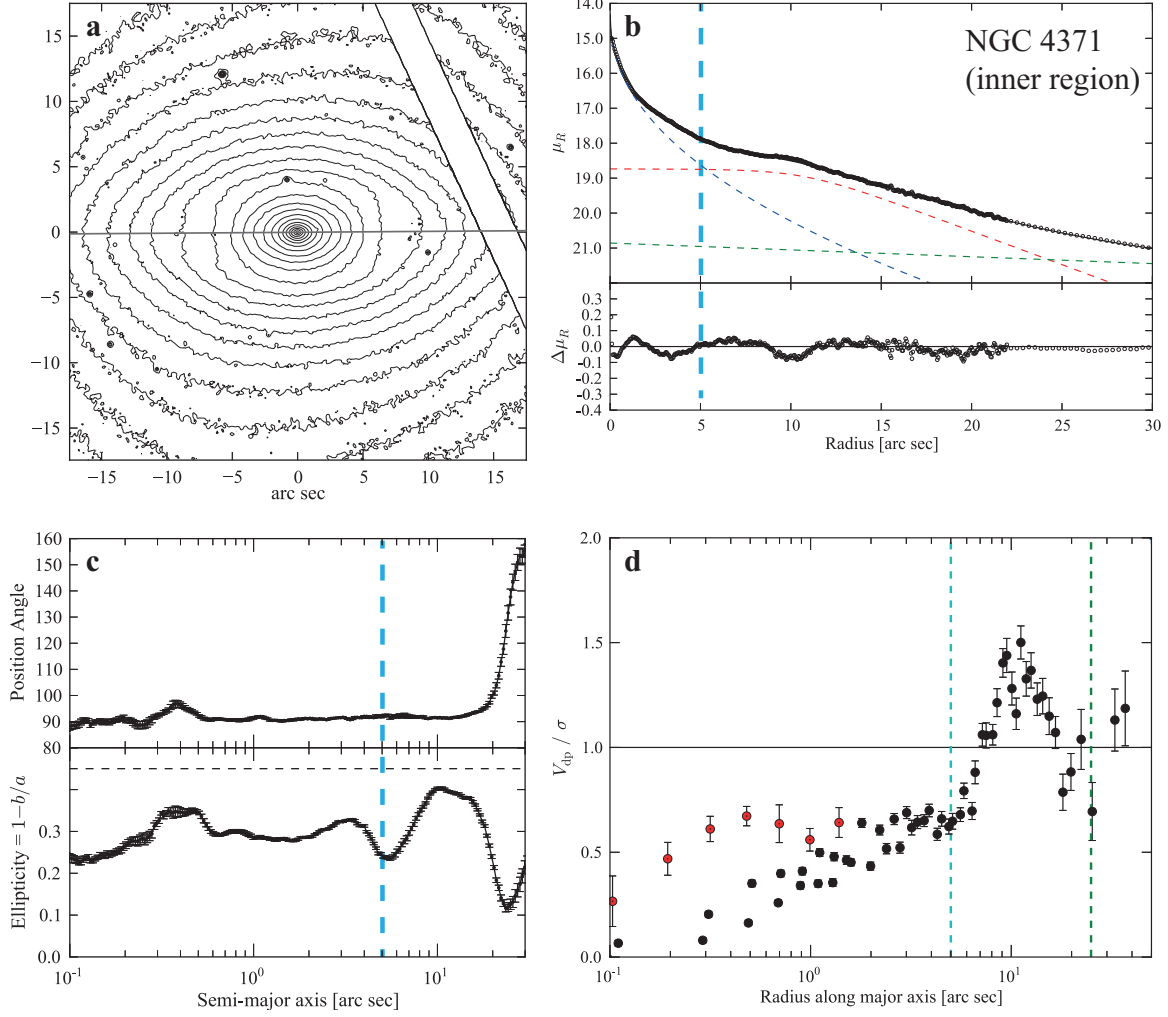


Figure 6. Evidence for a classical bulge inside the disk pseudobulge of NGC 4371. **a:** Close-up of main photometric bulge region from *HST* ACS-WFC F850LP image; gray line marks major-axis PA. **b:** major-axis profile from *HST* ($r < 22$ arcsec) and INT-WFC images, with fit (Sérsic + broken-exponential + outer exponential; dashed lines) and residuals from fit in lower sub-panel. Vertical dashed blue line marks inner “bulge=disk” radius $R_{bd,i}$, where the Sérsic component has surface brightness equal to the sum of the disk components; this sets the boundary of the *inner* “photometric bulge”. **c:** Ellipse fits to the *HST* image; note that ellipticity in the inner photometric bulge region ($a \lesssim 5$ arcsec) is ~ 0.28 , significantly less than that of the disk pseudobulge outside. **d:** Deprojected, folded stellar rotation velocity divided by local velocity dispersion V_{dp}/σ along the major axis, with WHT-ISIS long-slit data [black] and SINFONI AO data [red]. Vertical dashed blue and green lines mark the inner and main photometric bulge regions $|R| < R_{bd,i}$, respectively. In the inner region ($r \gtrsim 5$ arcsec), V_{dp}/σ reaches a plateau value of ≈ 0.65 , suggesting a kinematically hot region (i.e., a classical bulge).

lar orbits and corresponding weights which can be used to investigate the phase-space distribution of the stars and to look for things such as radial trends in 3D stellar dynamical quantities. We have previously made use of best-fit orbit libraries to study radial anisotropy trends in core and non-core elliptical galaxies (Thomas et al. 2014); here, we use the best-fit models for the S0 NGC 1332 (which has only a classical bulge) and the composite-bulge galaxies NGC 3368, NGC 4371 and NGC 4699 to explore how the models might shed light on the internal 3D kinematics of composite bulges.

Data and modeling for NGC 1332 and NGC 3368 have already been presented in Rusli et al. (2011) and Nowak et al. (2010), respectively; full data and modeling results, including SMBH measurements, for the other galaxies will be presented elsewhere (Erwin et al. 2014). Once the best-fitting model is determined, stellar-dynamical quantities can

be extracted using the weighted means of orbits in different radial and angular bins.

Working in cylindrical coordinates (R, φ, z) , we compute the velocity anisotropy by comparing the vertical dispersion σ_z^2 with the mean velocity dispersion in the equatorial plane σ_e^2 ; the latter is defined as

$$\sigma_e^2 = (\sigma_R^2 + \sigma_\varphi^2)/2. \quad (3)$$

All of these values are averages of the orbits over angular bins running from $\theta = -23^\circ$ to $\theta = +23^\circ$ with respect to the equatorial plane at each radius, using the orbit weights from the best-fitting solution. We then define the anisotropy β_{eq} as

$$\beta_{\text{eq}} = 1 - \sigma_e^2/\sigma_z^2; \quad (4)$$

this is ~ 0 for the isotropic case and < 0 for planar-biased

Table 3. Disky Pseudobulge Characteristics

Galaxy	Exp. Profile?	Max(V_{dp}/σ)	Disky Features	μ_0 (mag arcsec $^{-2}$)	h (arcsec)	(pc)	$\log M_\star$ (M_\odot)
(1)	(2)	(3)	(4)	(5)	(6)	(7)	(8)
NGC 1068	Y	2.80	bar, spirals	13.12 (<i>K</i>)	6.80	468	10.89
NGC 1543	Y	— ¹	bar, NR	17.15 (<i>I</i>)	7.03	665	9.84
NGC 1553	Y?	1.38	bar, NR/spirals	15.31 (<i>I</i>)	5.33	466	10.57
NGC 2859	Y	1.56	bar, NR/spirals	16.88 (<i>i</i>)	4.45	522	10.49
NGC 3368	Y	1.36	bar, spirals	12.71 (<i>K</i>)	3.05	149	9.85
NGC 3945	Y	2.18	bar, NR	15.69 (<i>I</i>)	5.11	491	10.43
NGC 4262	Y	1.58	NR	14.45 (<i>i</i>)	1.66	124	10.09
NGC 4371	Y[*]	1.50	NR	— ²	— ²	— ²	9.88
NGC 4699	Y	1.36 ³	bar, spirals	15.83 (<i>z</i>)	7.61	697	10.97

Column 1: Galaxy name. Column 2: Indicates whether surface-brightness profile is exponential. Column 3: Maximum value of V_{dp}/σ in the diskly pseudobulge. Column 4: “Disky” features found in the pseudobulge region (NR = nuclear ring); note that for NGC 1068 and NGC 3368, the bars are only seen clearly in the near-IR. Column 5: Central surface brightness of exponential component of diskly pseudobulge; band is listed in parentheses. Columns 6–7: Exponential scale length of same, listed in both angular and linear sizes. Column 8: Logarithm of estimated stellar mass of diskly pseudobulge (including nuclear bar components; see text). Notes: 1 = galaxy too close to face-on to reliably deproject velocities; 2 = In NGC 4371, the diskly pseudobulge profile is distorted by the strong nuclear ring, and is not modeled as a simple exponential (see Section 5.2.2); 3 = kinematics do not extend to edge of pseudobulge, so this may be only a *lower* limit on Max(V_{dp}/σ).

Table 4. Classical Bulge Parameters

Name	n	R_e (arcsec)	R_e (pc)	μ_e (mag arcsec $^{-2}$)	ϵ	$\log M_\star$ (M_\odot)
(1)	(2)	(3)	(4)	(5)	(6)	(7)
NGC 1068	0.98	0.50	34	11.05 (<i>K</i>)	0.14	9.47
NGC 1543	1.50	2.73	258	17.02 (<i>I</i>)	0.05	9.49
NGC 1553	1.66	1.48	129	15.73 (<i>I</i>)	0.1	9.32
NGC 2859	1.68	1.06	124	17.00 (<i>i</i>)	0.15	9.47
NGC 3368	1.34	0.63	31	13.38 (<i>K</i>)	0.00	8.73
NGC 3945	2.02	1.24	119	16.20 (<i>I</i>)	0.20	9.63
NGC 4262	0.89	0.30	23	15.02 (<i>i</i>)	0.05	8.70
NGC 4371	2.18	5.20	427	18.70 (<i>z</i>)	0.30	9.64
NGC 4699	1.43	2.15	247	15.42 (<i>z</i>)	0.11	10.46

Characteristics the of the classical bulges in our composite-bulge galaxies. Column 1: Galaxy name. Columns 2–5: Parameters of Sérsic fit; effective radius is given in both angular and linear sizes, and the band of the μ_e value is in parenthesis (these are usually based on the reddest available images, which vary from galaxy to galaxy). Column 6: Adopted mean isophotal ellipticity of classical bulge. Column 7: Logarithm of estimated stellar mass (see text).

anisotropy. For comparison, $\beta_{\text{eq}} \approx -1.0$ for the Galactic disk in the Solar neighborhood (using $z = 0$ values from Table 1 of Bond et al. 2010), or -1.2 for the Galactic thick disk (using dispersions from Table 5 of Carollo et al. 2010).

Figure 7 shows the radial trend of the anisotropy for the simple classical-bulge S0 NGC 1332 and for three composite-bulge galaxies. We also plot the radial trends of $V_\varphi/\langle\sigma\rangle$, where V_φ is the intrinsic mean rotation velocity measured in the two bins closest to the equatorial plane and $\langle\sigma\rangle$ is the total velocity dispersion:

$$\langle\sigma\rangle = \sqrt{(\sigma_R^2 + \sigma_\varphi^2 + \sigma_z^2)/3}. \quad (5)$$

For all galaxies, the anisotropy parameter β_{eq} is ~ 0 in the classical-bulge region, and decreases outside, indicating a shift from isotropic velocity dispersion to a dispersion which

is dominated by planar motions. The latter is what we expect for flattened, disklike structures, and supports the idea that the diskly pseudobulges are indeed dynamically distinct from the classical bulges.

In most cases, the $V_\varphi/\langle\sigma\rangle$ profiles show a trend similar to what we have seen in the major-axis V_{dp}/σ profiles: dispersion-dominated kinematics within the classical-bulge region and rotation-dominated kinematics in the diskly pseudobulge (or main disk in the case of NGC 1332) outside. The exception is NGC 4371, where there is also an *inner* peak in $V_\varphi/\langle\sigma\rangle$ at $r \sim 0.4$ arcsec, deep within the classical-bulge region. Curiously, the radius where $V_\varphi/\langle\sigma\rangle$ reaches its local maximum is also where the isophotal ellipticity has a local maximum (panel c of Figure 6), though *HST* colour maps indicate that this is also a region marked by strong

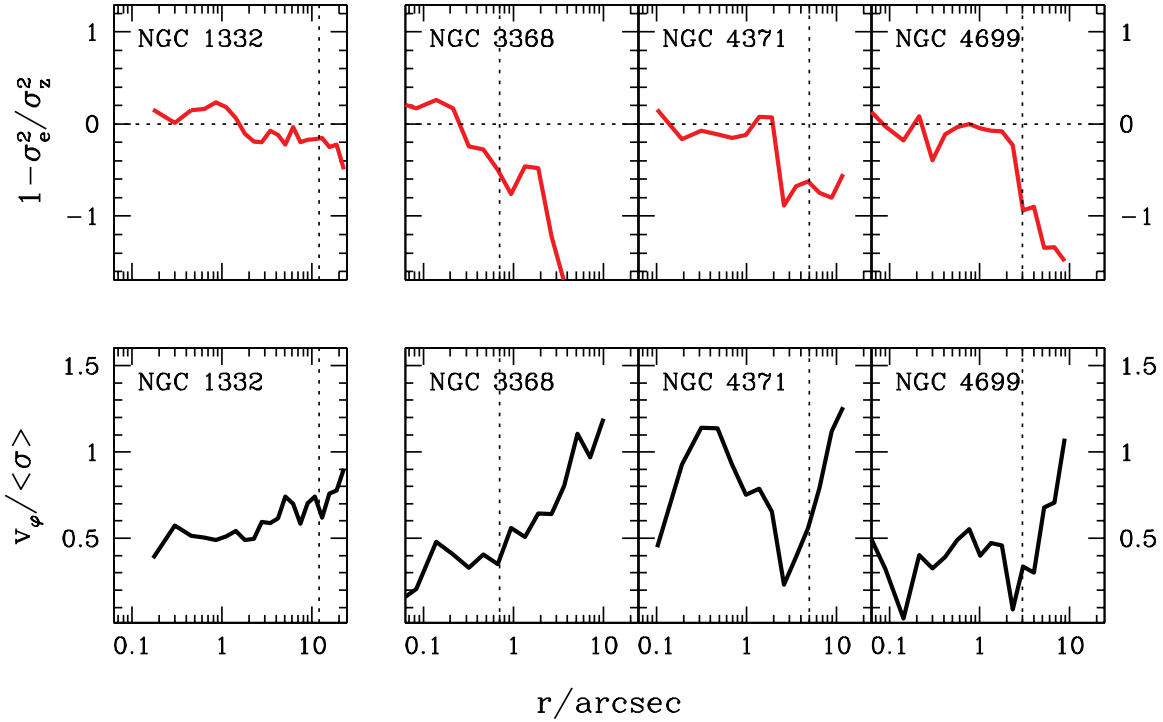


Figure 7. 3D stellar kinematics from dynamical modeling of galaxies observed with SINFONI, for the classical-bulge galaxy NGC 1332 (left panels) and three of the composite-bulge galaxies (right set of panels). Vertical dashed lines mark R_{bd} for NGC 1332 and $R_{bd,i}$ for the classical bulges in the composite-bulge galaxies; regions to the left of these lines are dominated by the classical bulge components. Top panels: $\beta_{\text{eq}} = 1 - \sigma_e^2/\sigma_z^2$, which measures the relative anisotropy of planar ($\sigma_e^2 = (\sigma_R^2 + \sigma_\phi^2)/2$) versus vertical (σ_z^2) velocity dispersion in the best-fitting models; values near zero indicate isotropic velocity dispersions, while more negative values mean planar dispersions dominate over vertical dispersions. Lower panels: local ratio of mean rotation velocity V_ϕ to total mean velocity dispersion in the models.

circumnuclear dust (see Comerón et al. 2010). This might represent the existence of an additional disk component with $r \sim 30$ pc deep inside the classical bulge.

8 DISCUSSION

In the preceding sections of this paper (and in the Appendix) we have provided a kind of existence proof demonstrating that at least some lenticular and early-type spiral galaxies can host *both* disk pseudobulges *and* compact classical bulges, with the latter nestled inside the former. This shows that classical bulges and pseudobulges are not always exclusive phenomena.

The disk pseudobulges can almost always be described with exponential profiles,⁵ with the addition of various disk-like features: nuclear bars, stellar rings, or spiral arms. Our major-axis decompositions yield exponential scale lengths of 125–870 pc, with a mean of 440 pc. These are relatively massive structures, with stellar masses ranging from 7.1×10^9 to $9.4 \times 10^{10} M_\odot$ (mean = $3.3 \times 10^{10} M_\odot$), or anywhere from 11 to 59 per cent of the total galaxy stellar mass (mean fraction = 33 per cent). Thus in many cases a significant fraction of the galaxy’s stars are part of the disk pseudobulge. (See Section 8.3 for details on the computation of the disk-pseudobulge stellar masses.)

⁵ The main exception is NGC 4371, where the disk pseudobulge is better fit with a broken-exponential profile; see Section 5.2.2.

The classical bulges, in contrast, are relatively compact, low-mass structures. Our fits yield Sérsic indices of 0.89–2.18 (mean index = 1.52), half-light radii between 23 and 426 pc (mean $R_e = 143$ pc), and stellar masses ranging from 5.0×10^8 to $2.9 \times 10^{10} M_\odot$. (See Section 8.2 for details of the stellar-mass estimation.) In only two galaxies is the stellar mass of the classical bulge more than 10 per cent of the galaxy’s total stellar mass (NGC 1543 and NGC 4699, where it is 13.1 and 11.3 per cent, respectively), and the mean value is only 5.9 per cent.

8.1 Hints Concerning the Frequency of Composite Bulges

How common are composite-bulge systems? The disadvantage of an existence-proof study such as this one is that it can do little, by itself, to answer this question. The galaxies discussed in this paper are unfortunately not drawn from any well-defined sample which has been consistently analysed with the same degree of spatial resolution in both imaging and spectroscopy, primarily because the necessary combined data (particularly high-resolution spectroscopy for stellar kinematics) are not available for most nearby galaxies. We *can* note that most of our galaxies are part of a sample of early-type barred galaxies originally studied by Erwin & Sparke (2003) and expanded by Erwin et al. (2005), which does allow us to put some very crude lower limits. Of the 25 barred S0 galaxies in the aforementioned sample with $i > 30^\circ$, we can identify three which are composite bulge

hosts (NGC 2859, NGC 3945 and NGC 4371). Of the 34 barred S0/a–Sb barred galaxies with the same inclination cutoff, there are three more galaxies from our composite-bulge set (NGC 1068, NGC 3368 and NGC 4699). This suggests that *at least* ~ 10 per cent of S0–Sb barred galaxies are probably composite-bulge systems. The true frequency could be much higher – though it clearly cannot be 100 per cent, as there are clearly some galaxies with classical bulges but no disk pseudobulges (e.g., NGC 1332 and NGC 7457, Sections 4.2 and 4.3).

If we take the presence of nuclear bars as indicators of disk pseudobulges, as is often done (e.g., Kormendy & Kennicutt 2004; Fisher & Drory 2008), then the recent review of Erwin (2011) suggests that disk pseudobulges (with or without classical bulges) can be found in at least 20 per cent of early-type (S0–Sab) disk galaxies. The presence of nuclear bars as indicators of disk pseudobulges also means that weaker, less luminous disk pseudobulges may be lurking within more dominant classical bulges. For example, at least four of the galaxies classified as having classical bulges in the recent studies of Fisher & Drory (2008) and Fisher & Drory (2010) have nuclear bars: NGC 3031, NGC 3992, NGC 4548 and NGC 6684 (Elmegreen et al. 1995; Erwin 2004; Gutiérrez et al. 2011; Erwin 2014b).

Fisher & Drory (2010) argued that galaxies with composite bulges would not be clearly distinguishable from galaxies with only a disk pseudobulge when using 1-D surface-brightness profiles, unless the classical bulge were very luminous; they suggested that some of the galaxies with what they called “inactive pseudobulges”⁶ might harbor classical bulges as well, if the latter had relatively small Sérsic indices (e.g., $\lesssim 3$). This is exactly what we find: all of our classical-bulge components have Sérsic indices $\lesssim 2.2$. Of the four galaxies in common with their sample (NGC 1543, NGC 3368, NGC 3945 and NGC 4371), all are classified by Fisher & Drory as “inactive pseudobulges” based on the mid-IR colours. It is worth noting that their 1-D decompositions produced Sérsic indices for the *photometric bulges* of $n < 2$ for all but one of these galaxies (NGC 4371), so one cannot conclude from the Sérsic index of the photometric bulge alone that a galaxy is *lacking* a classical-bulge component.

8.2 Embedded Classical Bulges Compared with Other “Spheroid” Systems

Table 4 presents the structural characteristics of the classical bulges in our composite-bulge systems. The listed colours come from aperture photometry on SDSS images (or *HST* images in the case of NGC 3945; Erwin et al. 2003); we use the colour-to- M/L calibrations of Bell et al. (2003) to calculate the resulting stellar masses. The exception to this is NGC 1068, where the bright AGN point source makes accurate stellar colour measurements in the inner few arcseconds very difficult. Instead, we adopted a K -band M/L ratio of 0.7, using the lower end of the age estimate (5–12 Gyr) from the near-IR spectroscopy of Storchi-Bergmann

et al. (2012) and the average M/L ratios of Longhetti & Saracco (2009).⁷

In this paper, we refer to these compact, inner components as “classical bulges” because they fulfill at least some of the standard criteria for classical bulges. The fact that they have rounder isophotes than the outer disk, yet share similar or identical position angles, suggests they are approximately oblate spheroids (with little triaxiality) which are rounder (in an edge-on, vertical sense) than the disk. In addition, we have clear evidence that the classical bulges are kinematically hot, with V_{dp}/σ always < 1 , in the cases of NGC 1068, NGC 3368, NGC 3945, NGC 4371 and NGC 4699, where the available kinematic data comes from observations with high enough spatial resolution to resolve the classical bulge region. In other galaxies, such as NGC 2859.

The one exception to the usual classical-bulge paradigm is in the luminosity profiles. Traditionally, classical bulges have been claimed to have $R^{1/4}$ profiles – i.e., a Sérsic index of $n = 4$. More recent formulations have suggested an approximate dividing line of $n = 2$, with classical bulges having higher values and pseudobulges (of whatever kind) having lower (e.g., Fisher & Drory 2010). Almost all of the objects we find have $n < 2$; only for NGC 3945 and NGC 4371 is $n \gtrsim 2$. So one *could* argue, purely on the basis of the Sérsic indices, that most of our central structures are a peculiar species of round, kinematically hot “pseudobulge.” However, we prefer to consider the possibility that classical bulges can have a range of surface-brightness profiles, and that their primary characteristics remain their overall shape, their lack of disk substructure, and pressure-dominated stellar kinematics.

There are other kinematically hot, round stellar systems which are not considered classical bulges, of course. As we have seen, the classical bulge parts of composite bulges span a range of sizes, with half-light radii from ~ 400 down to ~ 25 pc. The lower end of this range is sufficiently small that one might wonder whether some of these objects would really be better understood as “nuclear star clusters” (NSCs), which are extremely common in late-type spirals and at least moderately common in earlier-type disks (see, e.g., the review by Böker 2008).

In Figures 8 and 9, we plot the classical bulge components of our composite bulges in the context of other “spheroids” – that is, stellar systems dominated by velocity dispersion – ranging from NSCs, dwarf spheroidals and ultracompact dwarfs to giant ellipticals. For the latter three classes of objects, we use the aggregated data compiled by Misgeld & Hilker (2011).

To those data we have added the (photometric) bulges of S0–Sa galaxies from Table 1 of Laurikainen et al. (2010) (red stars). These are more modern measurements based on 2D decompositions of near-IR images, which helps ensure that light belonging to the bar is not counted as part of the bulge. (We note that these decompositions do not account for the possibility of composite bulges, and we exclude the seven galaxies in their sample which are studied in this paper.) We converted their K -band measurements to stellar masses using the M/L ratios of Bell et al. (2003) and colours

⁶ Low Sérsic indices and/or disk morphologies combined with mid-IR colours indicative of low star-formation rates.

⁷ <http://www.brera.inaf.it/utenti/marcella/mtol.html>

from HyperLEDA. In particular, we used $(B - V)_e$ colours, which are a better approximation to the bulge colours than the total galaxy colour.⁸ We also include the bulges of unbarred S0–Sbc galaxies from Balcells et al. (2007), converting their K -band magnitudes to stellar masses in the same fashion (green stars). Finally, we plot NSCs using a compilation of masses from Erwin & Gadotti (2012) and half-light radii primarily from Böker et al. (2004) and Walcher et al. (2005), with some additional values from Ho & Filippenko (1996), Graham & Spitler (2009), Barth et al. (2009), Kormendy et al. (2010) and Seth et al. (2010).

What Figure 8 shows is that the structures we identify as classical bulges in the composite-bulge systems fall into the “bulge” section of the plot, not the “nuclear cluster” section. Elliptical galaxies⁹ and classical bulges form a clear, relatively tight sequence in the $R_e - M_*$ plane, and our classical bulges either fall directly into this sequence or form a natural extension of it. Similarly, in Figure 9, our classical bulges fall into the same (loose) sequence formed by giant ellipticals and larger classical bulges.

Although the smallest classical bulges are undeniably small, and begin to approach the most massive NSCs in size (half-light radius), they are significantly more massive. Moreover, in at least two of the composite-bulge galaxies (NGC 1543 and NGC 1553) there is evidence for distinct nuclear star clusters with half-light radii ~ 4 pc located *inside* the classical bulge components. While we cannot rule out the possibility of an as-yet undetected population of central spheroids with masses $\sim 10^8 M_\odot$ and $R_e \sim 10$ – 20 pc, which would provide continuity between the classical bulges and NSCs, for the time being we consider them to be distinct phenomena.

8.3 Disky Pseudobulges in the Mass-Size-Density Planes

As we have seen, the classical-bulge components of our composite-bulge systems appear to follow the same trends as (larger) classical bulge and ellipticals, at least in the $R_e - M_*$ and $(\Sigma_*)_e - M_*$ planes. What about the diskly pseudobulges: do they resemble large-scale disks, classical bulges, or something else? Figure 10 and 11 show where the diskly pseudobulges (filled blue diamonds) fall in the same diagrams used for Figures 8 and 9; we have desaturated the previously plotted points to allow the pseudobulge data points to stand out more clearly. We also plot the (large-scale) disk components from the S0/spiral decompositions of Balcells et al. (2007) and Laurikainen et al. (2010) as filled grey diamonds.

The stellar masses of our diskly pseudobulges – and the main disks from the Laurikainen et al. (2010) and Balcells et al. (2007) samples – plotted in Figures 10 and 11 come from the same general colour-to- M/L estimates (based on

⁸ For two galaxies without $(B - V)_e$ colours (NGC 5636 and NGC 5953), we used $g - r$ colours measured within an aperture of 5 arcsec radius on SDSS images; we were unable to find or measure colours for NGC 3892, which is excluded from the plots.

⁹ Here we are excluding dE galaxies – roughly, those “ellipticals” with $M_* \lesssim 5 \times 10^9 M_\odot$ – which tend to form a separate sequence merging into the dwarf spheroidals; see, e.g., arguments in Kormendy & Bender (2012), where dE and dSph are together termed “spheroidals”.

Bell et al. 2003) as used for the classical-bulge components in the preceding section. For most of the diskly pseudobulges, we use the exponential component from the inner decomposition (e.g., panel b of Figure 4) and assume that the diskly pseudobulge is an exponential disk with an ellipticity equal to that of the outer disk. (For NGC 4371, we use the plotted broken-exponential fit from panel b of Figure 6.) In the cases of NGC 1068, NGC 1543 and NGC 2859, where the inner fits specifically exclude the contribution of bright inner bars, we include an additional flux term to account for the inner bar itself (e.g., Erwin 2011). The half-light radii are computed using the best-fitting exponential scale lengths from the inner decompositions (e.g., panel b of Figure 4) – i.e., excluding any contribution from the classical bulge component. (The half-light radii for the large-scale disks are also estimated this way.) For diskly pseudobulges with significant inner bars, this may mis-estimate the true half-light radius, but probably by less than a factor of 2, which means a very small shift on the plots.

What we can see from Figures 10 and 11 is that in terms of size, stellar mass, and mean density, diskly pseudobulges actually fall into the bulge/elliptical sequence, just like the classical bulges (albeit with masses and sizes that are on average larger than the classical bulges). Although some of the diskly pseudobulges are as massive as large-scale stellar disks, they are roughly a factor of ~ 5 times more compact. This suggests that their formation mechanisms are probably not the same as those involved in large-scale disks. It also is an indication that otherwise unclassified objects which fall on the classical-bulge/elliptical sequence in the mass-size and mass-density planes may not always be kinematically hot spheroidal systems.

(We note in passing that the precise location and distribution of large-scale disks on plots such as these may depend partly on Hubble type. For example, disks in very late type spirals may lie further to the left in the $R_e - M_*$ plane; see, e.g., Fig. 9 of Laurikainen et al. 2010 or Figs. 18 and 20 of Kormendy & Bender 2012.)

8.4 What About Boxy/Peanut-Shaped Pseudobulges?

Athanassoula (2005) argued that instead of lumping the central regions of disk galaxies into just two types – classical bulges versus pseudobulges – one could, from a theoretical point of view, distinguish at least three possible structures: classical bulges, “disc-like bulges” (i.e., what we have been calling diskly pseudobulges), and boxy/peanut-shaped bulges, which are actually the vertically thickened inner parts of bars. She even suggested that some galaxies might contain all three at the same time.

In this paper, we have identified a number of disk galaxies containing *both* classical bulges and diskly pseudobulges; what about boxy/peanut-bulges? We have avoided dealing with the latter in order to concentrate on the contrasting diskly and spheroidal nature of the pseudobulges and classical bulges we are interested in; moreover, the traditional approach to identifying boxy/peanut-shaped bulges relies on galaxies which are edge-on, not moderately inclined. None the less, all but one of the galaxies discussed in this paper are barred. The extensive survey of edge-on galaxies by Lütticke et al. (2000) found that the frequency of boxy

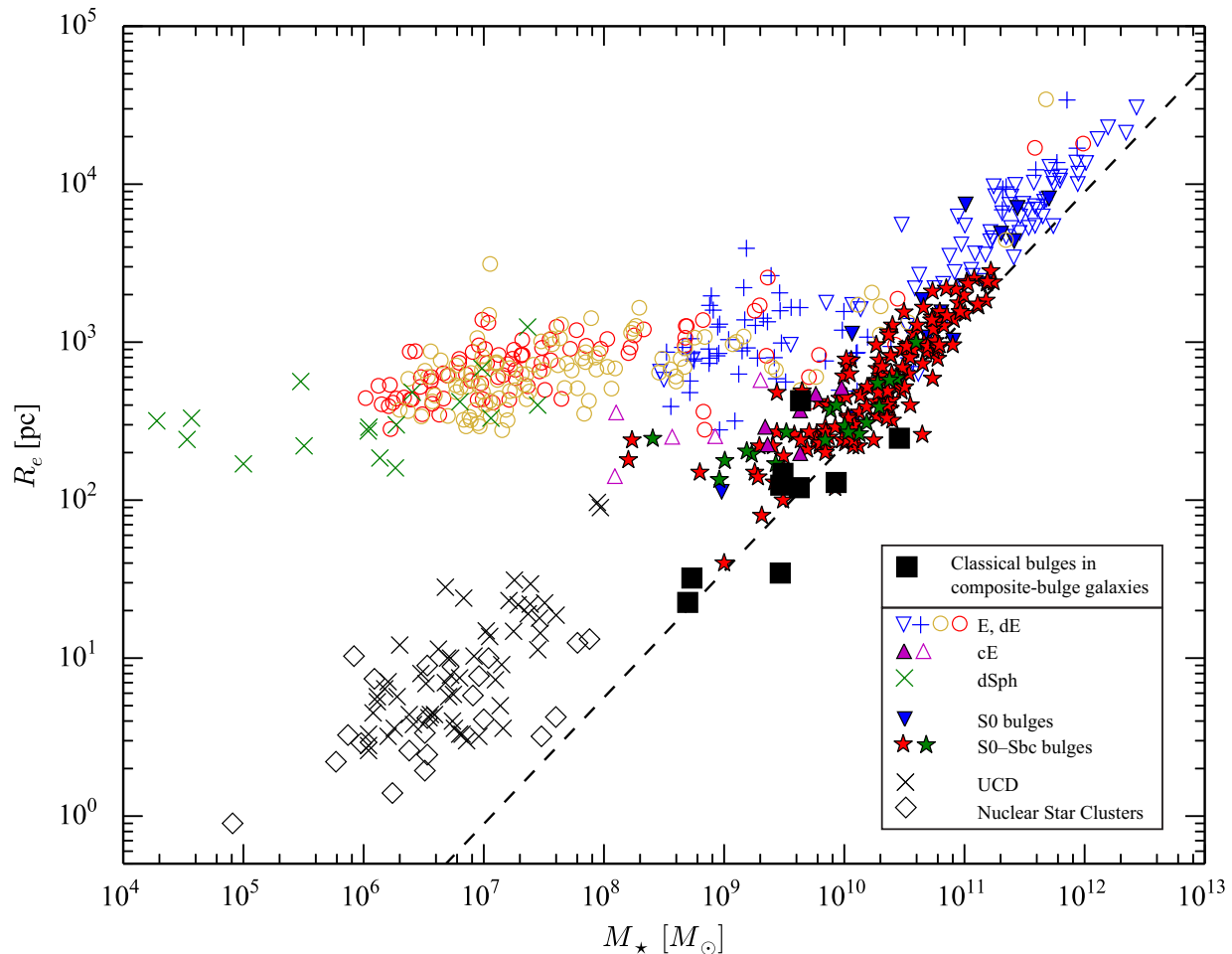


Figure 8. Half-light radius versus total stellar mass for a variety of “spheroids” or “hot stellar systems”, based partly on Figure 4 of Misgeld & Hilker (2011). All except the squares, diamonds and stars are taken from their compilation: open and filled blue (inverted) triangles are ellipticals and bulges of S0 galaxies, respectively, from Bender et al. (1993); blue plus signs and red and orange open circles are E and dE galaxies from the ACS Virgo Cluster Survey (Ferrarese et al. 2006), the Hydra I Cluster (Misgeld et al. 2008) and the Centaurus Cluster (Misgeld et al. 2009), respectively; magenta triangles are compact ellipticals (open triangles are Coma galaxies from Price et al. 2009); and green and black \times symbols are dSph galaxies and UCDs, respectively. Red stars are bulges of S0–Sa galaxies from the 2D decompositions of Laurikainen et al. (2010); green stars are bulges of unbarred S0–Sbc galaxies from Balcells et al. (2007); and open black diamonds are nuclear star clusters (see text for sources). Finally, the filled black squares are the *classical* bulge components of our composite-bulge galaxies; they appear to fall into the narrow sequence defined by ellipticals and (early-type disk) bulges. The dashed line is the “zone of avoidance” from Eqn. 8 of Misgeld & Hilker (2011).

and peanut-shaped bulges was consistent with most if not all barred galaxies having a vertically thickened inner region (a box/peanut structure, or B/P structure). Bureau et al. (2006) identified a number of edge-on galaxies which appeared to have both B/P structures *and* disk pseudobulges, so the coexistence of those two structures is certainly plausible. (Due to low spatial resolution and the presence of strong dust extinction in the central regions, small embedded classical bulges would have been difficult to find in their galaxies, if any such were present.)

More recently, Erwin & Debattista (2013) identified several morphological signatures of the B/P structure in barred galaxies which can be seen when the galaxy is only moderately inclined (i.e., $i \sim 40\text{--}70^\circ$), if the bar is favorably aligned with respect to the disk major axis. Since NGC 1068, NGC 1543, NGC 2859 and NGC 4262 are close to face-on (mostly $i \lesssim 30^\circ$), we would not expect to see signatures

of the B/P structure. Additionally, the bars in NGC 3945 and NGC 4371 are oriented very close to the minor axes of their respective host galaxies. The latter orientation is one which minimizes the signature of the B/P structure; Erwin & Debattista did not find this signature in those three galaxies. However, they *did* identify NGC 3368 as an example of a galaxy with a visible projected B/P structure; as we noted in Section A3, this is probably responsible for the slightly boxy isophotes *outside* the disk pseudobulge – see Figure 12. Thus, NGC 3368 is a clear case of a galaxy matching the suggestion of Athanassoula (2005) that disk galaxies can simultaneously host classical bulges, disk pseudobulges, *and* box/peanut bulges.

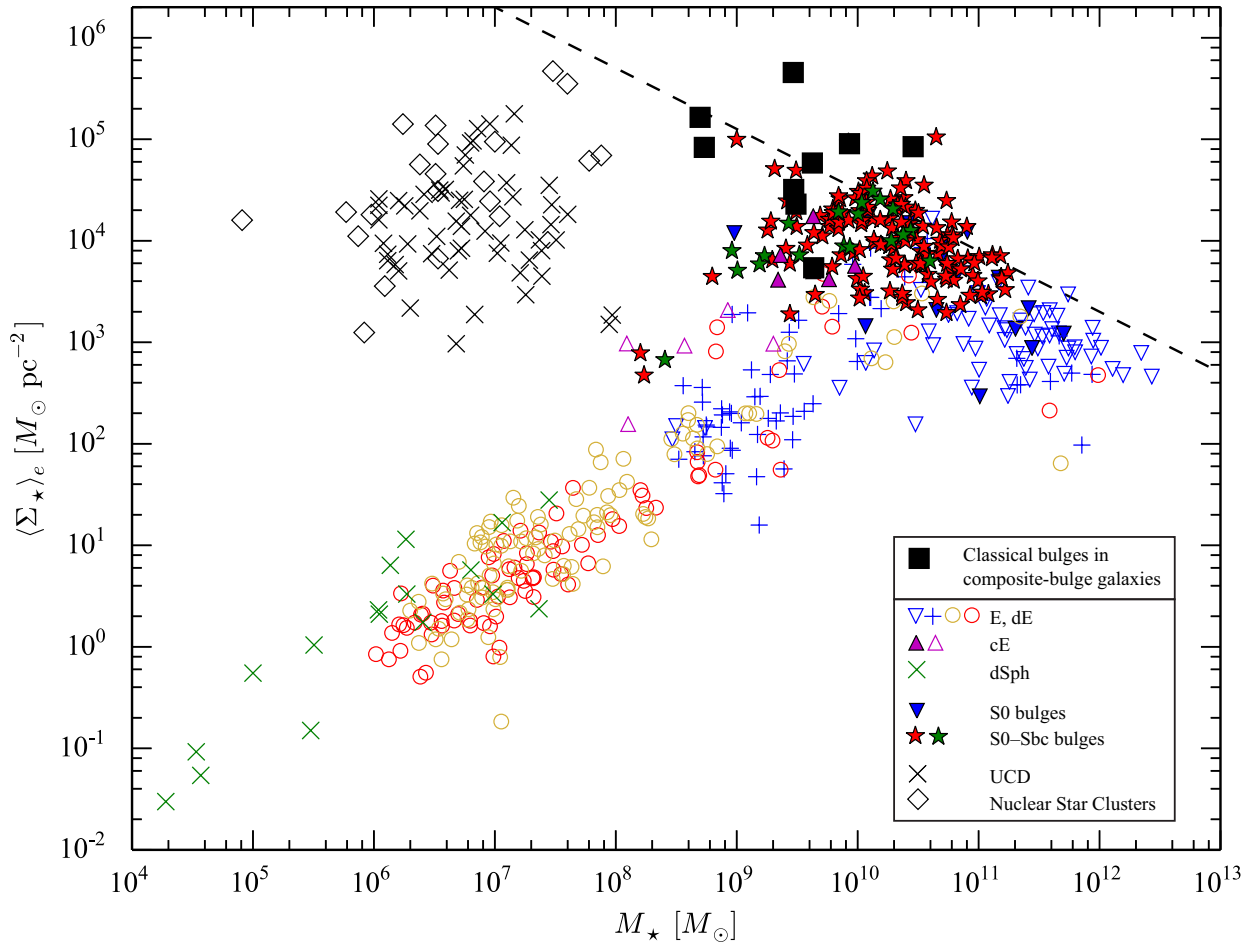


Figure 9. As for Figure 8, but now showing mean stellar mass density within the half-light radius versus total stellar mass for the same systems.

8.5 Speculations on Formation

8.5.1 Morphology: Disky Pseudobulges Are (Mostly) Found Inside Bars

Most discussions of pseudobulges (see, e.g., Kormendy & Kennicutt 2004) portray them as secondary structures formed late in a galaxy’s history, usually via some form of bar-driven gas inflow and subsequent star formation in the central regions of the galaxy. The fact that almost all the galaxies discussed in this paper are barred is at least broadly consistent with the hypothesis of bar-driven formation. What is perhaps not yet clear is whether bar-driven inflow and star formation can readily create diskly pseudobulges as large and as massive as some of those we identify. A possible additional issue is the fact that star-formation inside the bars of early-type disks in the local universe is usually observed taking place in nuclear *rings*. Several of our diskly pseudobulges do feature nuclear rings (Table 3), which argues for a connection; the question is whether the rest of the diskly pseudobulge, both inside and outside the ring, was formed the same way.

Wozniak & Michel-Dansac (2009) studied a high-resolution disk galaxy simulation and noted the formation of an extended “nuclear disk” inside the bar, due to gas-driven bar inflow and star formation. This disk apparently

gave rise to an independently rotating nuclear bar, with a gaseous nuclear ring of radius ~ 400 pc. The reported size of the disk – ~ 500 pc after 2 Gyr – is consistent with some of our diskly pseudobulges, and the mass ($7 \times 10^9 M_{\odot}$, 34 per cent of the galaxy’s total stellar mass) is as well. More recently, Cole et al. (2014) have reported on a detailed disk-galaxy simulation in which a similar large nuclear disk formed inside a bar, and compared it to the diskly pseudobulges in NGC 3368, NGC 3945, and NGC 4371. The nuclear disk in the simulation was more extended (relative to the size of the bar) than is the case for the three diskly pseudobulges, but did have a similar mass fraction (29% of the simulated galaxy’s total stellar mass). So it appears that at least some detailed, high-resolution simulations *can* produce barred galaxies with diskly pseudobulges similar to those seen in real galaxies.

We note that three of the composite-bulge galaxies do pose some more general problems for the bar-driven formation scenario, because their bars are weak, missing, or simply too small. NGC 1068, though formally unbarred, does at least appear to have a large-scale bar surrounding its diskly pseudobulge (Erwin 2004, and references therein); however, this bar is quite weak, and is sometimes considered an “oval disk” rather than a true bar (Kormendy & Norman 1979; Kormendy & Kennicutt 2004). It is not clear whether such a

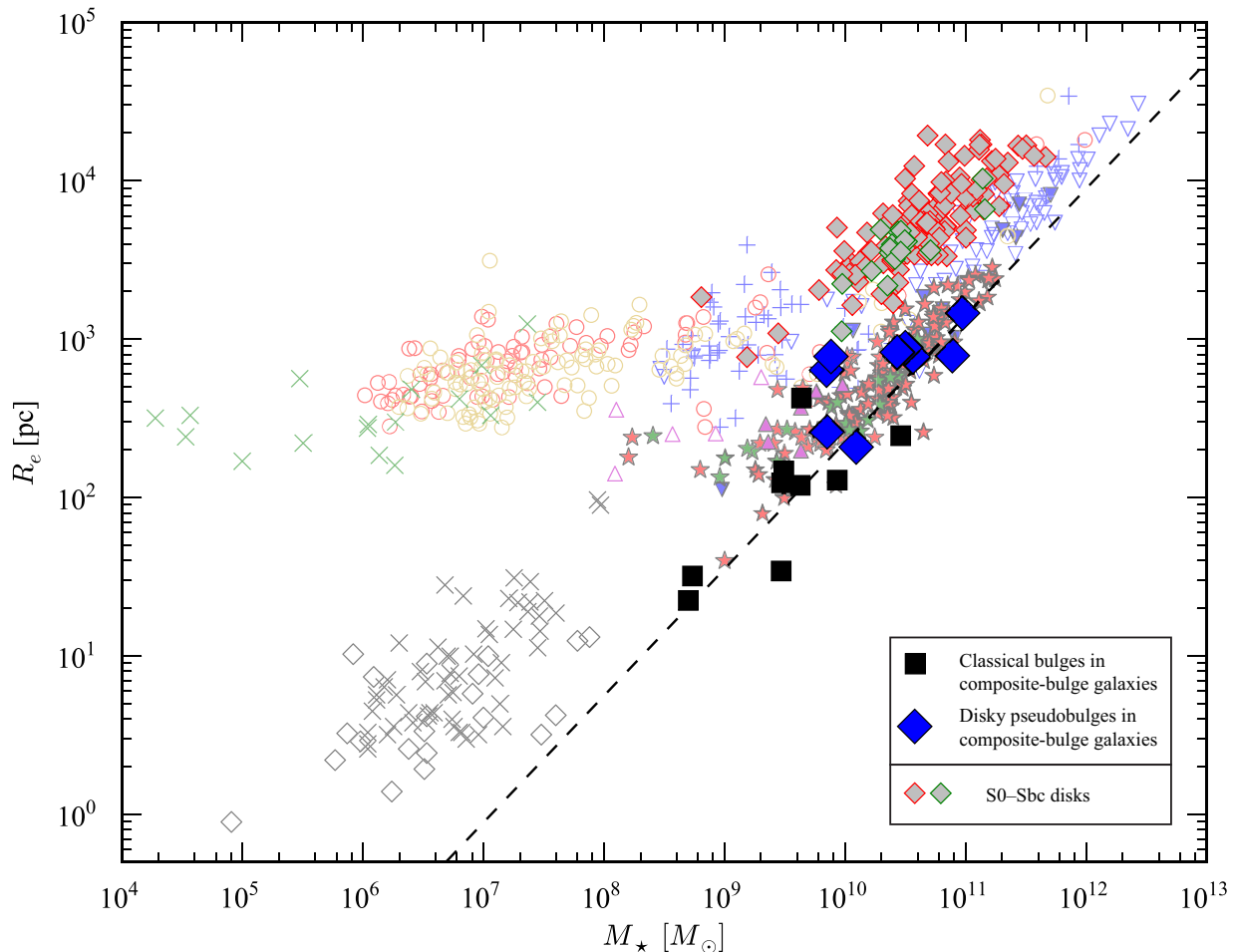


Figure 10. As for Figure 8, but now including the disk pseudobulge components of our composite-bulge galaxies (large blue diamonds), along with the large-scale disks (smaller grey diamonds) from Balcells et al. (2007, green borders) and Laurikainen et al. (2010, red borders). The disk pseudobulges are clearly more compact than large-scale disks of the same mass, and actually fall on the same bulge/elliptical sequence as the classical-bulge components (filled black squares).

large disk pseudobulge (44 per cent of the NGC 1068’s stellar mass) would be formed by such a weak bar. NGC 1553 is classified as unbarred, though it might be possible that its “lens” is either the remnant of a once-strong bar (as argued by, e.g., Kormendy & Kennicutt 2004), or is the projection of the B/P structure of a still-existing, albeit rather weak, bar (see Section A1). The most difficult case is NGC 4699, where the disk pseudobulge is *larger* than the sole bar in the system. This implies that not *all* disk pseudobulges can be formed by bar-driven gas inflow. The alternative would be to postulate a previous, large bar in NGC 4699 which has since vanished. Unfortunately, theories of bar destruction either require unnaturally high central mass concentrations (which should prevent the existence of the *current* small bar in this galaxy), or don’t yield testable predictions that would allow us to unambiguously identify whether a galaxy once had a bar, as opposed to never having had one.

A different formation scenario, which could potentially account for cases like NGC 4699, might be that some disk pseudobulges form *early*, possibly before any large-scale bar, as part of a general inside-out process. For example, Guedes et al. (2013) have presented a cosmologically motivated disk-galaxy simulation which formed with a “pseudobulge” inside

a larger disk; their analysis showed that most of the stars in the pseudobulge formed *in situ* and *prior* to most of the outer disk.

One way of distinguishing between these scenarios would be to look for evidence of significant differences in ages between the stars making up the disk pseudobulge and those making up the bar (if present) or disk outside. Younger ages in the disk pseudobulge would argue for the bar-driven formation mechanism, while a predominantly *older* population in the disk pseudobulge would suggest something more like the inside-out scenario of Guedes et al. (2013).

8.5.2 Possible Clues from Stellar Populations

Unfortunately, we are rather lacking in detailed stellar population analyses for most of our composite-bulge galaxies. Published analyses tend to be patchy and limited, either spatially or in terms of models with multiple populations.

De Lorenzo-Cáceres et al. (2012, 2013) presented an analysis of stellar populations near the centres of five double-barred galaxies, one of which is the composite-bulge system NGC 2859. They found minimal age differences between the stars of the inner and outer bars, with the former being

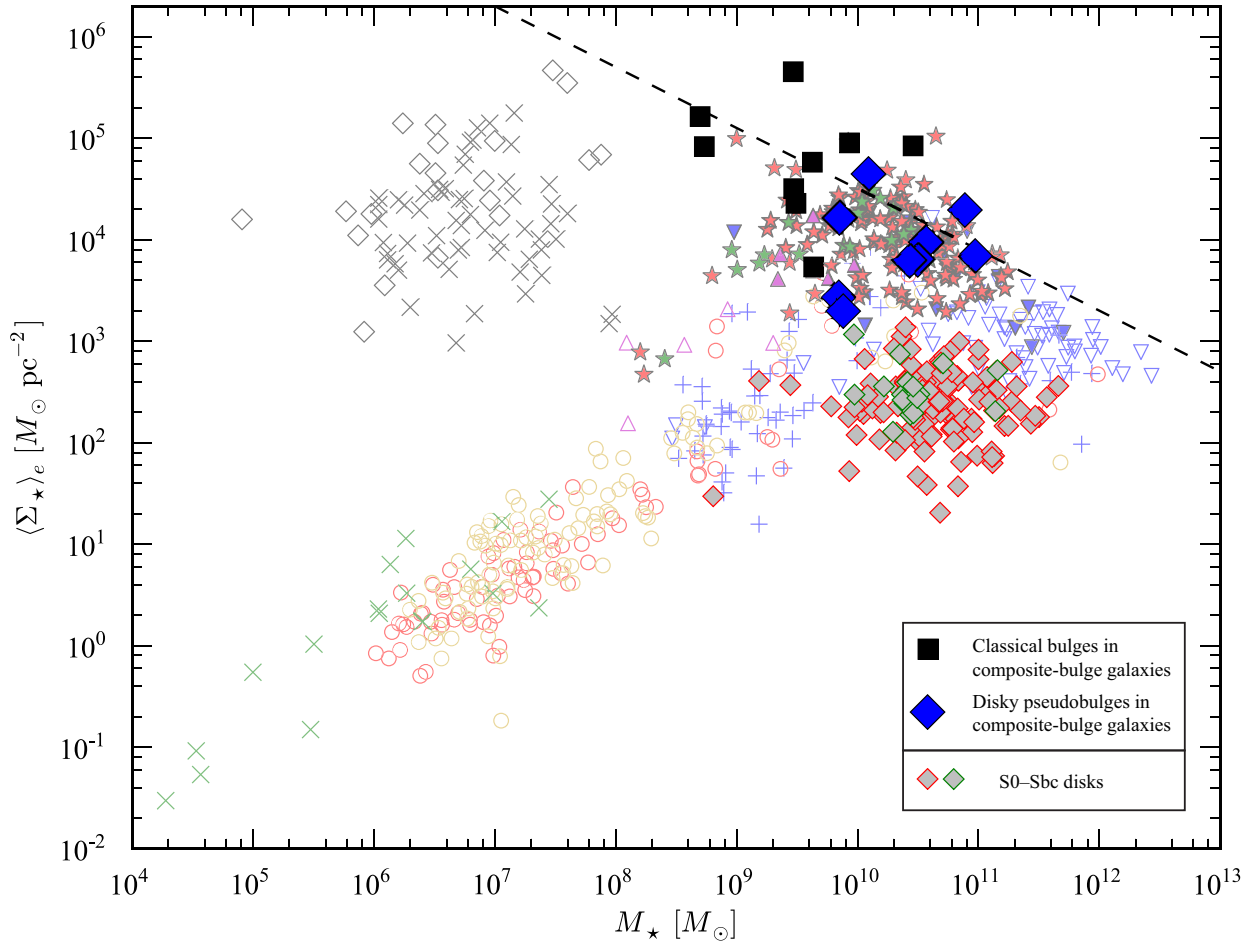


Figure 11. As for Figure 10, but now showing mean stellar mass density within the half-light radius versus total stellar mass for the same systems.

either coeval with or slightly younger than the latter. This seems to suggest that the inner bars – and by implication the rest of the disk pseudobulges – in these galaxies could indeed be (somewhat) younger than the outer bars, and thus formed after the outer bar formed, in agreement with the bar-driven formation model.

For the classical bulges, the existing data are (perhaps) contradictory. In the case of NGC 2859, de Lorenzo-Cáceres et al. (2013) found that they youngest part of the central region of NGC 2859 was what we identify as the classical bulge. While this could be interpreted as evidence that classical bulges form *after* the disk pseudobulges, one should note that de Lorenzo-Caceres et al. measured luminosity-weighted ages from comparisons with single stellar population (SSP) models, so there is the possibility that the measured ages are contaminated by more recent stellar populations.

The relevance of this concern was shown by Sarzi et al. (2005), who used *HST* STIS spectroscopy to estimate the stellar populations in the central 0.2×0.25 arcsec of a number of galaxies, including the composite-bulge system NGC 3368. Their best-fitting SSP models indicated a mean age of ~ 1 Gyr for the nuclear region (dominated by the classical bulge) of NGC 3368, but their best-fitting *multiple*-population models included both younger and older compo-

nents, with a 10 Gyr population contributing 27 per cent of the nuclear light (and the $\lesssim 1$ Gyr components accounting for only 1.4 per cent of the nuclear stellar mass).

Storchi-Bergmann et al. (2012) modeled the near-IR spectra of the central 4.5×5.0 arcsec of NGC 1068 with multiple-age populations and found that the *oldest* component (5–13 Gyr in age) was concentrated in the inner $r < 1$ arcsec, corresponding to what we identify as the classical bulge (Section A6).

So the limited stellar-population evidence is, overall, broadly consistent with the disk pseudobulges being younger than both the bars outside and the classical bulges inside, but there is clearly room for further work.

8.5.3 Classical Bulge Formation?

In the standard picture of galaxy formation, classical bulges are formed at high redshift from the violent merger of smaller galaxies or proto-galactic sub-clumps, resulting in a compact, centrally concentrated object, with stellar kinematics dominated by dispersion and an old, metal-rich stellar population. Although we know of no reason why this couldn't be the case for our classical bulges, the latter *do* tend to be smaller and lower in mass (and certainly in B/T) than what is usually assumed for classical bulges. It is un-

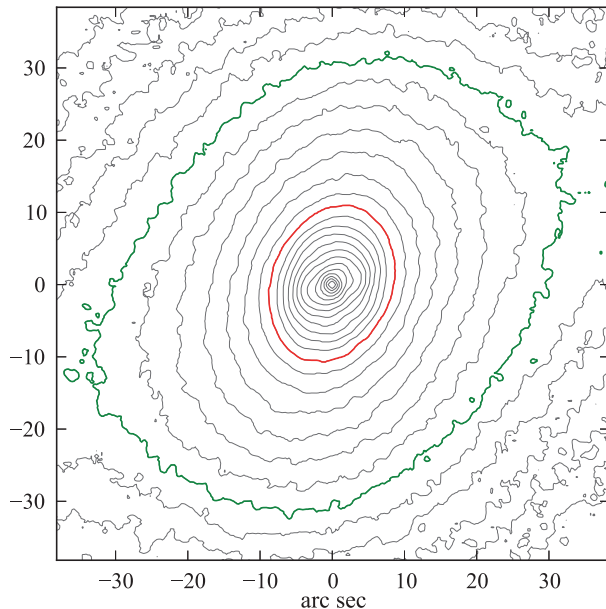


Figure 12. Disky pseudobulge inside a boxy/peanut-shaped bulge. Median-smoothed K -band isophotes for the interior of the outer bar of NGC 3368 (see Figure A5 for larger-scale context). The thicker green contour indicate the region of boxy isophotes, which are probably the projection of the inner, vertically thickened part of the bar – a boxy/peanut-shaped bulge. The region inside which is dominated by the diskly pseudobulge is indicated by the thicker red contour. See also Fig. A1 of Erwin & Debattista (2013).

clear whether this process would produce such *small* structures, or ones with Sérsic indices of ~ 1 –2.5.

Another possibility is the more recent scenario of clump-cluster mergers at high redshift (e.g., Noguchi 2000; Immeli et al. 2004; Elmegreen et al. 2008). In this model, massive star clusters form in turbulent, gas-rich disks and then, due to dynamical friction, spiral in towards the center, where they merge in a fashion not entirely unlike the standard classical-bulge merger-formation. Although some simulations have suggested that the resulting bulge would be relatively massive, with high Sérsic indices (e.g., Elmegreen et al. 2008), it seems possible that smaller, shorter-lived versions of this scenario might form lower-mass, lower-Sérsic-index classical bulges like those we find in the composite-galaxies.

There is also the possibility that the structures we identify as classical bulges in these galaxies are actually byproducts of secular evolution – i.e., that they are produced in some fashion *after* the main disk forms, or even after the diskly pseudobulge forms. We know that nuclear star clusters can host multiple episodes of star formation (e.g., Walcher et al. 2006), and the center of the galaxy is where gas that loses angular momentum will tend to accumulate, which might suggest that compact classical bulges form through a similar process. However, the classical bulges in our galaxies tend to be significantly larger than – and even coexist with – nuclear star clusters (Section 8.2), which argues against that idea.

Our classical bulges might conceivably form directly out of diskly pseudobulges via some kind of instability, though realistic models for such a process are lacking. We *can* rule

out standard bar instabilities, since these produce elongated, boxy/peanut-shaped structures elongated along the parent bar (e.g., Erwin & Debattista 2013, and references therein), in contrast to the round, approximately axisymmetric structures we see, and also because some of the strongest cases, such as NGC 4371, do not have nuclear bars. (The B/P structures of the *large-scale* bars would be far larger than the classical bulges we find, as is clearly the case for at least NGC 3368; see Section 8.4). Similarly, the presence of nuclear bars in many of these galaxies (e.g., NGC 1068, NGC 1543, NGC 1553, NGC 2859, NGC 3945, and possibly NGC 4699) rules out scenarios in which a nuclear bar is “destroyed” in order to form a classical bulge. We also note that the apparent high frequency of pseudobulges in late-type spirals (e.g., Fisher & Drory 2011) suggests that pseudobulges by themselves probably do not *always* give rise to classical bulges.

9 SUMMARY

We have presented a morphological and kinematic analysis of nine disk galaxies (S0 or spiral) in which the photometric bulge region – that is, the excess stellar light above an inward extrapolation of the outer disk profile – is composed of at least two distinct components:

(i) A *diskly pseudobulge*: a structure with flattening similar to that of the outer disk, one or more morphological features characteristics of disks (nuclear rings, bars and/or spirals) and a stellar kinematics which is dominated by rotation.

(ii) A *classical bulge*: a component which is rounder (more spheroidal) than the diskly pseudobulge and which has kinematics dominated by velocity dispersion. These components do, however, tend to have profiles best fitted with Sérsic indices of $n = 1$ –2.2, so they are not classical in the sense of having $R^{1/4}$ profiles.

In at least one galaxy there is also evidence for a boxy/peanut-shaped bulge (the vertically thick inner part of a bar), demonstrating that all three types of “bulge” can coexist, as suggested by, e.g., Athanassoula (2005).

Using Schwarzschild orbit-superposition modeling for three of these galaxies (NGC 3368, NGC 4371 and NGC 4699), taken from Erwin et al. (2014), we investigated the 3D stellar orbital structure of the best-fitting models for each galaxy. We found that the stellar velocity dispersion is approximately isotropic within the classical-bulge regions but is equatorially biased in the diskly pseudobulges (as expected for a highly flattened system), and also that the ratio of azimuthal velocity to total velocity dispersion ($V_\phi/\langle\sigma\rangle$) is typically $\lesssim 0.5$ in the classical bulge and increases towards values $\gtrsim 1$ in the diskly pseudobulge.

Although we are currently unable to put strong limits on the frequency of composite-bulge galaxies, they are probably present in *at least* ~ 10 per cent of barred S0 and early-type spiral galaxies.

Plotting the classical-bulge components of the composite-bulge galaxies in the R_e – M_\star and $\langle\Sigma_\star\rangle_e$ – M_\star planes shows that they fall into the same general sequence as elliptical galaxies and the (larger) bulges of disk galaxies. Even though some of the classical-bulge components are

quite small, with half-light radii ~ 30 pc, they remain distinct from nuclear star clusters (and some in fact harbor nuclear star clusters in their centres). Curiously, the disky pseudobulge components *also* lie along the elliptical/classical-bulge sequences in these planes. While some disky pseudobulges are as massive as the main (outer) disks of S0 and spiral galaxies, they are considerably more compact.

Since almost all of our composite-bulge galaxies are barred, the disky pseudobulge components could plausibly be the result of bar-driven gas inflow and star formation. We note that the “nuclear disks” formed in this fashion in the simulations of Wozniak & Michel-Dansac (2009) and Cole et al. (2014) are similar in size and relative stellar mass to the disky pseudobulges in our galaxies. Cases where disky pseudobulges are found in *unbarred* galaxies (or galaxies where the only bar is *smaller* than the disky pseudobulge) are more difficult to explain, unless disky pseudobulges can form early in a galaxy’s history as part of a general inside-out process (e.g., Guedes et al. 2013).

ACKNOWLEDGEMENTS

We enjoyed helpful and interesting conversations with a number of people, including Niv Drory, Witold Maciejewski and Victor Debattista. We are particularly grateful to Rick Davies, Joris Gerssen, Karl Gebhardt, Erin Hicks and Richard McDermid for supplying us with kinematic data, both long-slit and IFU, and to Jakob Walcher for help with nuclear star cluster data. We would also like to thank Begoña García-Lorenzo for faithfully executing our WHT-ISIS service observations of NGC 4371, and the anonymous referee for comments which helped improve the manuscript.

P.E. was supported in part by DFG Priority Programme 1177 (“Witnesses of Cosmic History: Formation and evolution of black holes, galaxies and their environment”).

This research is (partially) based on data obtained with the William Herschel Telescope; the WHT and its service programme are operated on the island of La Palma by the Isaac Newton Group in the Spanish Observatorio del Roque de los Muchachos of the Instituto de Astrofísica de Canarias.

Based on observations made with ESO Telescopes at the La Silla Paranal Observatory under programme IDs 080.B-0336 and 082.B-0037.

Funding for the creation and distribution of the SDSS Archive has been provided by the Alfred P. Sloan Foundation, the Participating Institutions, the National Aeronautics and Space Administration, the National Science Foundation, the U.S. Department of Energy, the Japanese Monbukagakusho and the Max Planck Society. The SDSS Web site is <http://www.sdss.org/>.

The SDSS is managed by the Astrophysical Research Consortium (ARC) for the Participating Institutions. The Participating Institutions are The University of Chicago, Fermilab, the Institute for Advanced Study, the Japan Participation Group, The Johns Hopkins University, the Korean Scientist Group, Los Alamos National Laboratory, the Max-Planck-Institute for Astronomy (MPIA), the Max-Planck-Institute for Astrophysics (MPA), New Mexico State University, University of Pittsburgh, University of Portsmouth,

Princeton University, the United States Naval Observatory and the University of Washington.

This research made use of the NASA/IPAC Extragalactic Database (NED) which is operated by the Jet Propulsion Laboratory, California Institute of Technology, under contract with the National Aeronautics and Space Administration. It also made use of the Lyon-Meudon Extragalactic Database (LEDA; part of HyperLeda at <http://leda.univ-lyon1.fr/>).

REFERENCES

- Abazajian K. N. et al., 2009, *ApJS*, 182, 543
 Athanassoula E., 2005, *MNRAS*, 358, 1477
 Balcells M., Graham A. W., Peletier R. F., 2007, *ApJ*, 665, 1084
 Barth A. J., Strigari L. E., Bentz M. C., Greene J. E., Ho L. C., 2009, *ApJ*, 690, 1031
 Bell E. F., McIntosh D. H., Katz N., Weinberg M. D., 2003, *ApJS*, 149, 289
 Bender R., 1990, *A&A*, 229, 441
 Bender R., Burstein D., Faber S. M., 1993, *ApJ*, 411, 153
 Bender R., Saglia R. P., Gerhard O. E., 1994, *MNRAS*, 269, 785
 Binney J., 1978, *MNRAS*, 183, 501
 Binney J., 2005, *MNRAS*, 363, 937
 Blakeslee J. P. et al., 2009, *ApJ*, 694, 556
 Böker T., 2008, *Journal of Physics Conference Series*, 131, 012043
 Böker T., Sarzi M., McLaughlin D. E., van der Marel R. P., Rix H.-W., Ho L. C., Shields J. C., 2004, *AJ*, 127, 105
 Bond N. A. et al., 2010, *ApJ*, 716, 1
 Bower G. A., Richstone D. O., Bothun G. D., Heckman T. M., 1993, *ApJ*, 402, 76
 Bureau M., Aronica G., Athanassoula E., Dettmar R.-J., Bosma A., Freeman K. C., 2006, *MNRAS*, 370, 753
 Cappellari M. et al., 2007, *MNRAS*, 379, 418
 Carollo D. et al., 2010, *ApJ*, 712, 692
 Cole D. R., Debattista V. P., Erwin P., Earp S. W. F., Roškar R., 2014, *MNRAS*
 Comerón S., Knapen J. H., Beckman J. E., Laurikainen E., Salo H., Martínez-Valpuesta I., Buta R. J., 2010, *MNRAS*, 402, 2462
 Crenshaw D. M., Kraemer S. B., 2000, *ApJ*, 532, 247
 Davies R. I., Müller Sánchez F., Genzel R., Tacconi L. J., Hicks E. K. S., Friedrich S., Sternberg A., 2007, *ApJ*, 671, 1388
 de Lorenzo-Cáceres A., Falcón-Barroso J., Vazdekis A., 2013, *MNRAS*, 431, 2397
 de Lorenzo-Cáceres A., Falcón-Barroso J., Vazdekis A., Martínez-Valpuesta I., 2008, *ApJL*, 684, L83
 de Lorenzo-Cáceres A., Vazdekis A., Aguerri J. A. L., Corsini E. M., Debattista V. P., 2012, *MNRAS*, 420, 1092
 de Vaucouleurs G., de Vaucouleurs A., Corwin H. G., Buta R. J., Paturel G., Fouqué P., 1993, *Third Reference Catalog of Bright Galaxies*. New York: Springer-Verlag
 Elmegreen B. G., Bournaud F., Elmegreen D. M., 2008, *ApJ*, 688, 67
 Elmegreen D. M., Chromey F. R., Johnson C. O., 1995, *AJ*, 110, 2102
 Emsellem E. et al., 2011, *MNRAS*, 414, 888

- Emsellem E. et al., 2004, *MNRAS*, 352, 721
- Emsellem E., Fathi K., Wozniak H., Ferruit P., Mundell C. G., Schinnerer E., 2006, *MNRAS*, 365, 367
- Erwin P., 2004, *A&A*, 415, 941
- Erwin P., 2011, *Mem. S. A. It. Suppl.*, 18, 145
- Erwin P., 2014a, *MNRAS*, in prep
- Erwin P., 2014b, *MNRAS*, in prep
- Erwin P., Beckman J. E., Pohlen M., 2005, *ApJL*, 626, L81
- Erwin P., Debattista V. P., 2013, *MNRAS*, 431, 3060
- Erwin P., Gadotti D. A., 2012, *Advances in Astronomy*, 2012
- Erwin P., Pohlen M., Beckman J. E., 2008, *AJ*, 135, 20
- Erwin P., Sparke L. S., 1999, *ApJL*, 521, L37
- Erwin P., Sparke L. S., 2003, *ApJS*, 146, 299
- Erwin P. et al., 2014, *MNRAS*, in prep
- Erwin P., Vega Beltrán J. C., Beckman J. E., 2001, in *The Central Kiloparsec of Starbursts and AGN: The La Palma Connection*, J. H. Knapen, J. E. Beckman, I. Shlosman, & T. J. Mahoney, ed., p. 171
- Erwin P., Vega Beltrán J. C., Graham A. W., Beckman J. E., 2003, *ApJ*, 597, 929
- Eskridge P. B. et al., 2002, *ApJS*, 143, 73
- Fabricius M. H., Saglia R. P., Fisher D. B., Drory N., Bender R., Hopp U., 2012, *ApJ*, 754, 67
- Ferrarese L. et al., 2006, *ApJS*, 164, 334
- Fisher D. B., Drory N., 2008, *AJ*, 136, 773
- Fisher D. B., Drory N., 2010, *ApJ*, 716, 942
- Fisher D. B., Drory N., 2011, *ApJL*, 733, L47
- Fisher D. B., Drory N., Fabricius M. H., 2009, *ApJ*, 697, 630
- Freedman W. L. et al., 2001, *ApJ*, 553, 47
- Freeman K. C., 1975, in *IAU Symposium, Vol. 69, Dynamics of the Solar Systems*, Hayli A., ed., p. 367
- Gadotti D. A., 2009, *MNRAS*, 393, 1531
- Gebhardt K. et al., 2003, *ApJ*, 583, 92
- Gerssen J., Allington-Smith J., Miller B. W., Turner J. E. H., Walker A., 2006, *MNRAS*, 365, 29
- Graham A. W., Spitler L. R., 2009, *MNRAS*, 397, 2148
- Greene J. E. et al., 2010, *ApJ*, 721, 26
- Guedes J., Mayer L., Carollo M., Madau P., 2013, *ApJ*, 772, 36
- Gültekin K. et al., 2009, *ApJ*, 695, 1577
- Gutiérrez L., Erwin P., Aladro R., Beckman J. E., 2011, *AJ*, 142, 145
- Hicks E. K. S., Davies R. I., Maciejewski W., Emsellem E., Malkan M. A., Dumas G., Müller-Sánchez F., Rivers A., 2013, *ApJ*, 768, 107
- Ho L. C., Filippenko A. V., 1996, *ApJ*, 472, 600
- Ho L. C., Greene J. E., Filippenko A. V., Sargent W. L. W., 2009, *ApJS*, 183, 1
- Hopkins P. F., Kereš D., Murray N., Quataert E., Hernquist L., 2012, *MNRAS*, 427, 968
- Hu J., 2008, *MNRAS*, 386, 2242
- Illingworth G., 1977, *ApJL*, 218, L43
- Immeli A., Samland M., Gerhard O., Westera P., 2004, *A&A*, 413, 547
- Inoue S., Saitoh T. R., 2012, *MNRAS*, 2819
- Jarvis B. J., Dubath P., Martinet L., Bacon R., 1988, *A&AS*, 74, 513
- Knapen J. H., de Jong R. S., Stedman S., Bramich D. M., 2003, *MNRAS*, 344, 527
- Kormendy J., 1979, *ApJ*, 227, 714
- Kormendy J., 1982, *ApJ*, 257, 75
- Kormendy J., 1984, *ApJ*, 286, 116
- Kormendy J., 1993, in *IAU Symp. 153: Galactic Bulges*, Dejonghe H., Habing H. J., eds., Kluwer, Dordrecht, p. 209
- Kormendy J., Bender R., 2012, *ApJS*, 198, 2
- Kormendy J., Bender R., Cornell M. E., 2011, *Nature*, 469, 374
- Kormendy J., Drory N., Bender R., Cornell M. E., 2010, *ApJ*, 723, 54
- Kormendy J., Kennicutt, Jr. R. C., 2004, *ARA&A*, 42, 603
- Kormendy J., Norman C. A., 1979, *ApJ*, 233, 539
- Kuijken K., Fisher D., Merrifield M. R., 1996, *MNRAS*, 283, 543
- Laurikainen E., Salo H., Buta R., Knapen J., Speltinckx T., Block D., 2006, *AJ*, 132, 2634
- Laurikainen E., Salo H., Buta R., Knapen J. H., 2009, *ApJL*, 692, L34
- Laurikainen E., Salo H., Buta R., Knapen J. H., Comerón S., 2010, *MNRAS*, 405, 1089
- Laurikainen E., Salo H., Buta R., Vasylyev S., 2004, *MNRAS*, 355, 1251
- Longhetti M., Saracco P., 2009, *MNRAS*, 394, 774
- Longo G., Zaggia S. R., Busarello G., Richter G., 1994, *A&AS*, 105, 433
- Lütticke R., Dettmar R.-J., Pohlen M., 2000, *A&AS*, 145, 405
- McDermid R. M. et al., 2006, *MNRAS*, 373, 906
- Mei S. et al., 2005, *ApJ*, 625, 121
- Misgeld I., Hilker M., 2011, *MNRAS*, 414, 3699
- Misgeld I., Hilker M., Mieske S., 2009, *A&A*, 496, 683
- Misgeld I., Mieske S., Hilker M., 2008, *A&A*, 486, 697
- Noguchi M., 2000, *MNRAS*, 312, 194
- Nowak N., Saglia R. P., Thomas J., Bender R., Davies R. I., Gebhardt K., 2008, *MNRAS*, 391, 1629
- Nowak N., Saglia R. P., Thomas J., Bender R., Pannella M., Gebhardt K., Davies R. I., 2007, *MNRAS*, 379, 909
- Nowak N., Thomas J., Erwin P., Saglia R. P., Bender R., Davies R. I., 2010, *MNRAS*, 403, 646
- Ohta K., Hamabe M., Wakamatsu K.-I., 1990, *ApJ*, 357, 71
- Pinkney J. et al., 2003, *ApJ*, 596, 903
- Pohlen M., Trujillo I., 2006, *A&A*, 454, 759
- Price J. et al., 2009, *MNRAS*, 971
- Prieto M., Gottesman S. T., Aguerri J.-A. L., Varela A.-M., 1997, *AJ*, 114, 1413
- Renzini A., 1999, in *The Formation of Galactic Bulges*, Carollo C. M., Ferguson H. C., Wyse R. F. G., eds., p. 9
- Rusli S. P., Thomas J., Erwin P., Saglia R. P., Nowak N., Bender R., 2011, *MNRAS*, 410, 1223
- Rusli S. P. et al., 2013, *AJ*, 146, 45
- Sandage A., Bedke J., 1994, *The Carnegie atlas of galaxies*. Washington, DC: Carnegie Institution of Washington with The Flintridge Foundation
- Sarzi M., Rix H.-W., Shields J. C., Ho L. C., Barth A. J., Rudnick G., Filippenko A. V., Sargent W. L. W., 2005, *ApJ*, 628, 169
- Schinnerer E., Eckart A., Tacconi L. J., Genzel R., Downes D., 2000, *ApJ*, 533, 850
- Scoville N. Z., Matthews K., Carico D. P., Sanders D. B., 1988, *ApJL*, 327, L61
- Seth A. C. et al., 2010, *ApJ*, 714, 713

- Shapiro K. L., Gerssen J., van der Marel R. P., 2003, *AJ*, 126, 2707
- Shaw M., Axon D., Probst R., Gatley I., 1995, *MNRAS*, 274, 369
- Simien F., Prugniel P., 1997, *A&AS*, 126, 519
- Spolaor M., Hau G. K. T., Forbes D. A., Couch W. J., 2010, *MNRAS*, 408, 254
- Storchi-Bergmann T., Riffel R. A., Riffel R., Diniz M. R., Borges Vale T., McGregor P. J., 2012, *ApJ*, 755, 87
- Thomas J., Saglia R. P., Bender R., Erwin P., Fabricius M., 2014, *ApJ*, 782, 39
- Thomas J., Saglia R. P., Bender R., Thomas D., Gebhardt K., Magorrian J., Richstone D., 2004, *MNRAS*, 353, 391
- Tonry J. L., Dressler A., Blakeslee J. P., Ajhar E. A., Fletcher A. B., Luppino G. A., Metzger M. R., Moore C. B., 2001, *ApJ*, 546, 681
- Trager S. C., Worthey G., Faber S. M., Burstein D., González J. J., 1998, *ApJS*, 116, 1
- Vega Beltrán J. C., Pizzella A., Corsini E. M., Funes J. G., Zeilinger W. W., Beckman J. E., Bertola F., 2001, *A&A*, 374, 394
- Walcher C. J., Böker T., Charlot S., Ho L. C., Rix H.-W., Rossa J., Shields J. C., van der Marel R. P., 2006, *ApJ*, 649, 692
- Walcher C. J. et al., 2005, *ApJ*, 618, 237
- Wegner G., et al., 2003, *AJ*, 126, 2268
- Weinzirl T., Jogee S., Khochfar S., Burkert A., Kormendy J., 2009, *ApJ*, 696, 411
- Wozniak H., Friedli D., Martinet L., Martin P., Bratschi P., 1995, *A&AS*, 111, 115
- Wozniak H., Michel-Dansac L., 2009, *A&A*, 494, 11
- Wyse R. F. G., Gilmore G., Franx M., 1997, *ARAA*, 35, 637
- York D. G. et al., 2000, *AJ*, 120, 1579

APPENDIX A: OTHER COMPOSITE BULGES

A1 NGC 1553

NGC 1553 is a nominally unbarred S0 galaxy, notable for its prominent lens (e.g., Freeman 1975; Kormendy 1984). Kormendy & Kennicutt (2004) called attention to it as an example of a pseudobulge in an unbarred galaxy, based on its rather high V_{\max}/σ_0 value.

As Kormendy & Kennicutt noted, this galaxy’s surface-brightness profile looks very similar to that of many barred galaxies: an extended, shallow-surface-brightness “shelf” with a much steeper falloff at its outer edge (located in between the central bulge and the outer exponential disk). The lens *is* more elliptical than the outer disk, and the presence of weak boxyness in the isophotes (strongest at $a \sim 25$ arcsec) might suggest we are seeing the projected box/peanut structure of a (weak) bar, rather than a flattened structure. This would imply an unusually large ratio of B/P size to bar size, since we see little or no sign of the “spurs” which are the projection of the vertically thin outer part of the bar (see Erwin & Debattista 2013). Regardless of its true nature, the presence of the lens leads us to model it as a separate, broken-exponential component in our global decomposition; the result is a relatively good fit to the major-axis profile (panel b of Figure A1).

The photometric bulge region ($r < 16$ arcsec) shows clear evidence for a disky pseudobulge, as previously suggested by Kormendy & Kennicutt (2004) and Laurikainen et al. (2006): the ellipticity of the isophotes is similar to or greater than that of the main disk (panels c and e of Figure A1), and the stellar kinematics are dominated by rotation, with V_{dp}/σ reaching a maximum of ~ 1.4 at $r \sim 8$ arcsec (panel f). Analysis of the *HST* images reveals a previously unrecognized nuclear bar, with surrounding stellar spiral arms (panel d), further evidence that the photometric bulge is disklike.

Inside the nuclear bar, the isophotes are clearly rounder than the outer disk. We also find a clear central excess in the surface-brightness profile, and are able to fit the inner $r < 30$ arcsec major-axis profile quite well using the sum of an inner exponential + Sérsic, added to the contribution from the lens component we used in the global decomposition (panel b of Figure A2). As was the case for NGC 3945 and NGC 4371, the inner photometric bulge (where the inner Sérsic component dominates, at $r < 1.5$ arcsec) corresponds to the round central isophotes. Although the ground-based stellar kinematics of Kormendy (1984) and Longo et al. (1994) which we use to determine V_{dp}/σ may not fully resolve our proposed classical-bulge region,¹⁰ the fact that $V_{\text{dp}}/\sigma < 0.5$ for $r \lesssim 3$ arcsec suggests this region is indeed dominated by velocity dispersion, allowing us to classify the inner photometric bulge as a classical bulge.

A2 NGC 2859

NGC 2859 is a strongly double-barred galaxy, as originally noted by Kormendy (1979); Kormendy (1982) observed a relatively high degree of stellar rotation in the photometric bulge region, with $(V_{\max}/\sigma_0)^* = 1.2$. This makes the galaxy potentially rather similar to NGC 3945.

The similarity with NGC 3945 begins, in fact, with a luminous outer ring (panel a of Figure A3) creating a strongly non-exponential outer-disk profile. We choose to fit the region *interior* to the outer ring ($r \lesssim 70$ arcsec, panel b). This produces a reasonable photometric bulge-disk decomposition, with $R_{bd} \approx 12$ arcsec. If we had tried including the outer ring, the photometric bulge region would only have become larger; e.g., the decomposition in Fabricius et al. (2012) gives $R_{bd} = 30$ arcsec.

Interior to this we find a disky pseudobulge, as evidenced morphologically by the strong inner bar (Figure A3, panels c and d) and kinematically by the V_{dp}/σ curve (panel f), which reaches a maximum of ~ 1.3 – 1.5 at $r \sim 7$ arcsec. The kinematic data combines our WHT-ISIS longslit observations (Appendix B) and a pseudo-longslit constructed from the SAURON data of de Lorenzo-Cáceres et al. (2008); the latter profile was previously presented in Fabricius et al. (2012). We note that de Lorenzo-Cáceres et al. (2013) have also argued for the existence of a distinct inner disk in this galaxy from their 2D analysis of the SAURON kinematics.

Unlike the case of NGC 3945, where the inner bar was a small perturbation within the disky pseudobulge and could

¹⁰ Note, however, that Longo et al. reported seeing of < 1 arcsec for their observations of this galaxy

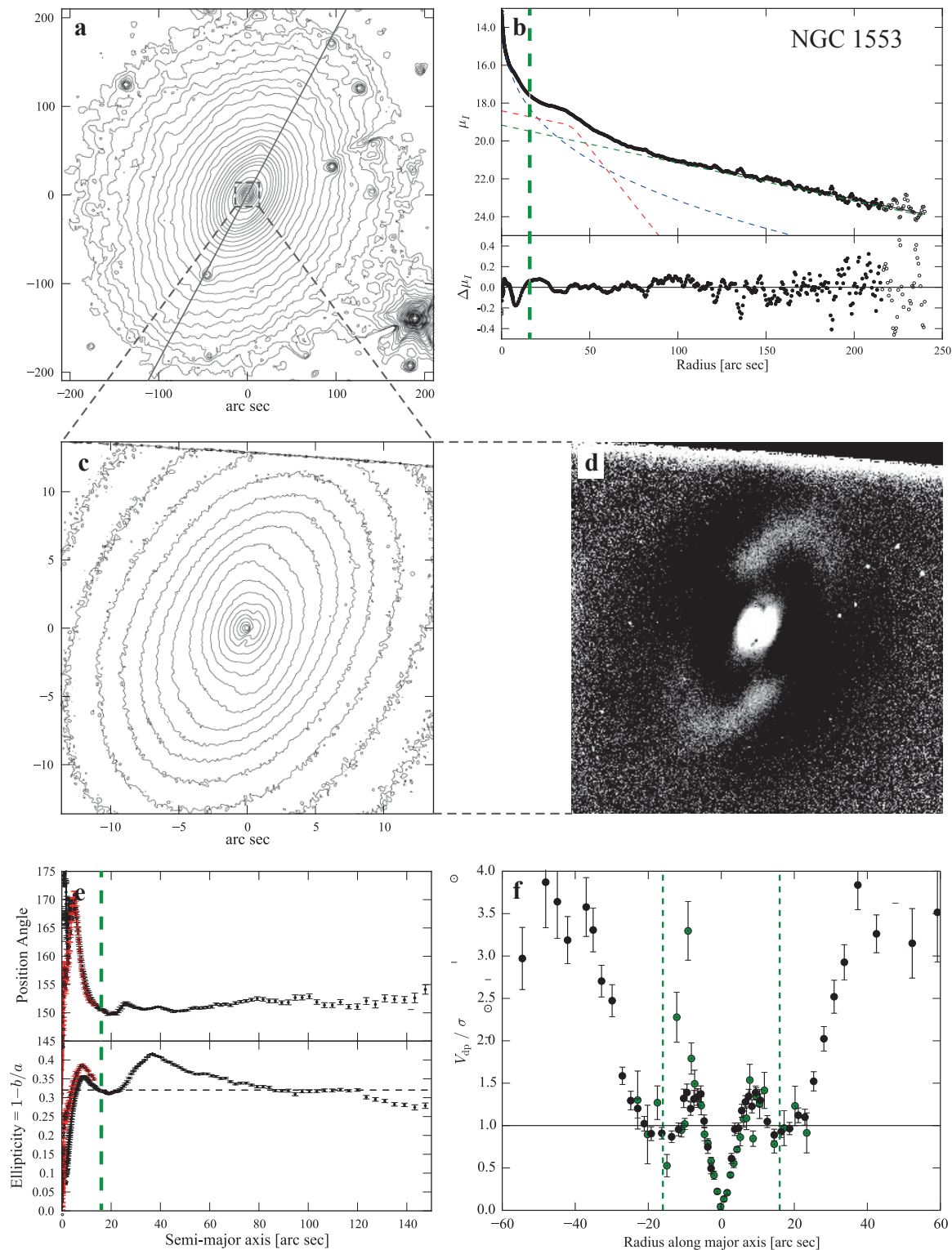


Figure A1. The disk pseudobulge in the S0 galaxy NGC 1553. **a:** log-scaled *Spitzer* IRAC1 isophotes (smoothed with 15-pixel-wide median filter); gray line marks major axis (PA = 152°). **b:** Bulge-disk decomposition of *I*-band major-axis profile (*HST* WFPC2 F814W for $r < 4.1$ arcsec, IRAC1 for larger radii). Dashed lines represent Sérsic + broken-exponential (lens) + exponential fit to the data, with residuals plotted in lower sub-panel. Vertical dashed green line marks “bulge=disk” radius R_{bd} . **c:** Close-up of photometric bulge region (log-scaled contours from WFPC2 F814W PC image). **d:** Unsharp mask of the same image ($\sigma = 30$ pixels), showing the inner bar and partial spiral arms surrounding it. **e:** Ellipse fits to the IRAC1 [black] and WFPC2 F814W [red] images. **f:** Deprojected stellar rotation velocity divided by local velocity dispersion V_{dp}/σ along the major axis, using data from Kormendy (1984) [black] and Longo et al. (1994) [green]. Vertical dashed lines mark the photometric bulge region $|R| < R_{bd}$. Both datasets show that V_{dp}/σ rises to well over 1 within this region, indicating a kinematically cool region more like a disk.

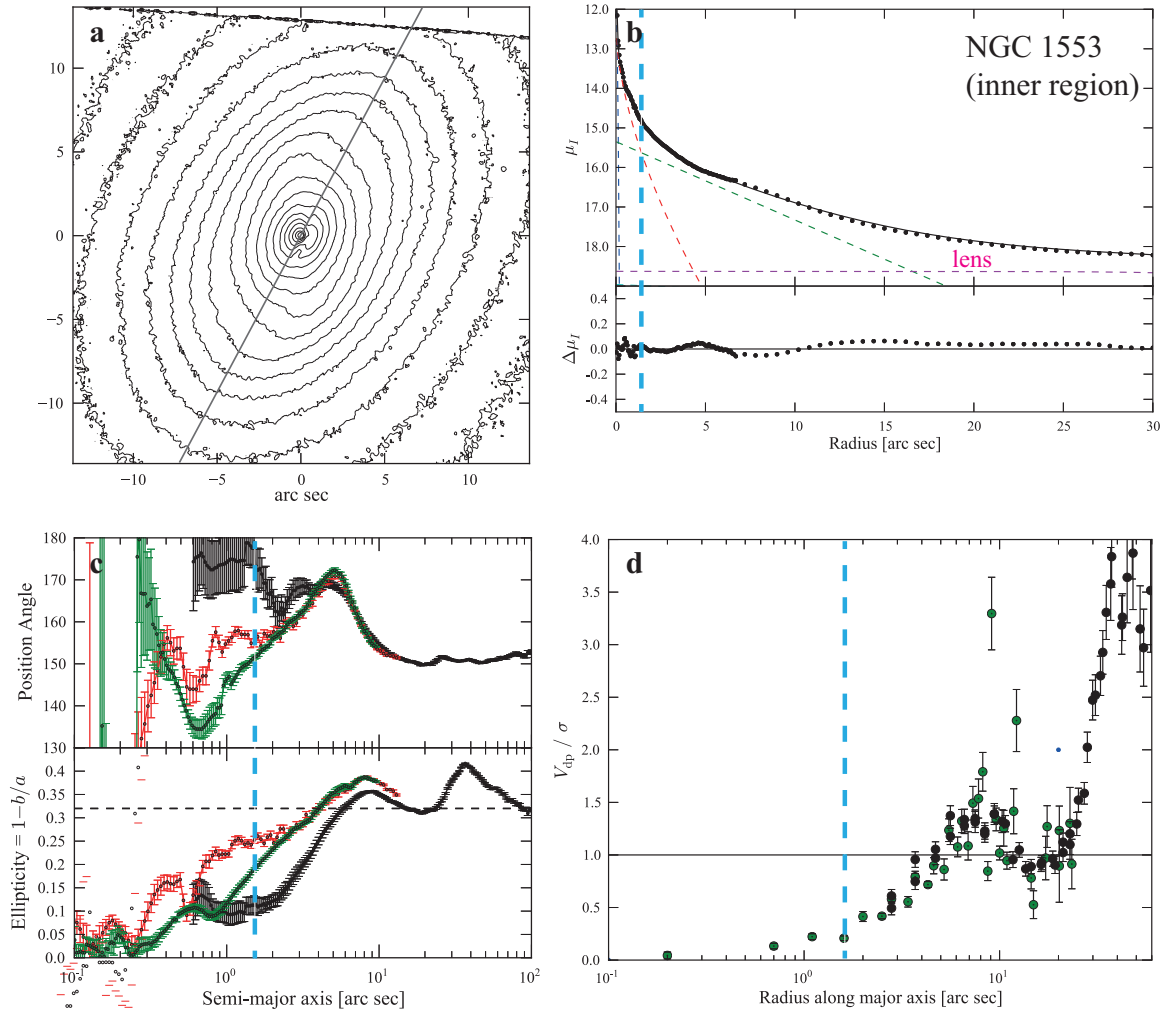


Figure A2. The classical bulge inside the diskly pseudobulge of NGC 1553. **a:** Close-up of main photometric bulge region (see Figure A1); gray line marks the major axis. **b:** major-axis profile, with fit (Sérsic + exponential + broken-exponential; dashed blue, green and red lines, respectively) and residuals from fit in lower sub-panel. Vertical dashed blue line marks inner “bulge=disk” radius $R_{bd,i}$. **c:** Ellipse fits (see Figure A1; additional green fit is from NICMOS2 F160W image); note that the ellipticity in the inner photometric bulge region ($a \lesssim 1.5$ arcsec) is < 0.25 (and ~ 0.05 – 0.15 for $a \lesssim 0.6$ arcsec), clearly less than that of the diskly pseudobulge outside, or the outer disk. **d:** Deprojected, folded stellar rotation velocity divided by local velocity dispersion V_{dp}/σ along galaxy major axis; see Figure A1. Vertical dashed blue and green lines mark the inner and main photometric bulge regions $|R| < R_{bd,i}$, respectively. In the inner region ($r \lesssim 1.4$ arcsec) and immediately outside, V_{dp}/σ remains well below 1, suggesting a kinematically hot region (i.e., a classical bulge).

thus be ignored in the fitting process (particularly as it was oriented almost perpendicular to the major axis), the inner bar in NGC 2859 is much larger and stronger relative to the diskly pseudobulge; indeed, it could perhaps be argued that the diskly pseudobulge is largely just the inner bar plus its surrounding lens. However, we can take advantage of this fact by using the inner bar itself to guide our decomposition. A more detailed discussion of this approach, along with an analysis of the inner bar’s structure, will be presented elsewhere (Erwin 2014a).

As Figure A4 shows, we can use a cut along the inner bar’s major axis and decompose this into an underlying exponential, a broken-exponential profile for the bar itself and a central Sérsic component. The latter defines the inner photometric bulge, with $R_{bd,i} = 0.94$ arcsec. This region is associated with a position angle close to that of the outer disk and an ellipticity of ~ 0.05 (panel c of Figure A4),

so we have morphological evidence for a classical bulge. Finally, the stellar kinematics (panel d of the figure) show that V_{dp}/σ remains < 1 for $r \lesssim 3$ arcsec, in both the SAURON and the (higher-resolution) WHT-ISIS data.

A3 NGC 3368

The case of NGC 3368 was originally considered in Nowak et al. (2010); our analysis here is very similar. The large-scale major-axis decomposition (panel b of Figure A5) shows a fairly plausible Sérsic + exponential fit, with $R_{bd} = 52$ arcsec. We note that this is rather larger than the value of $R_{bd} = 23.3$ arcsec which Fabricius et al. (2012) found from their 1-D decomposition, which may reflect the effects of masking intermediate parts of the profile in the latter study. A similar fit to a partially masked 1D profile of this galaxy by Fisher & Drory (2008) resulted in $R_{bd} \sim 35$ arcsec.

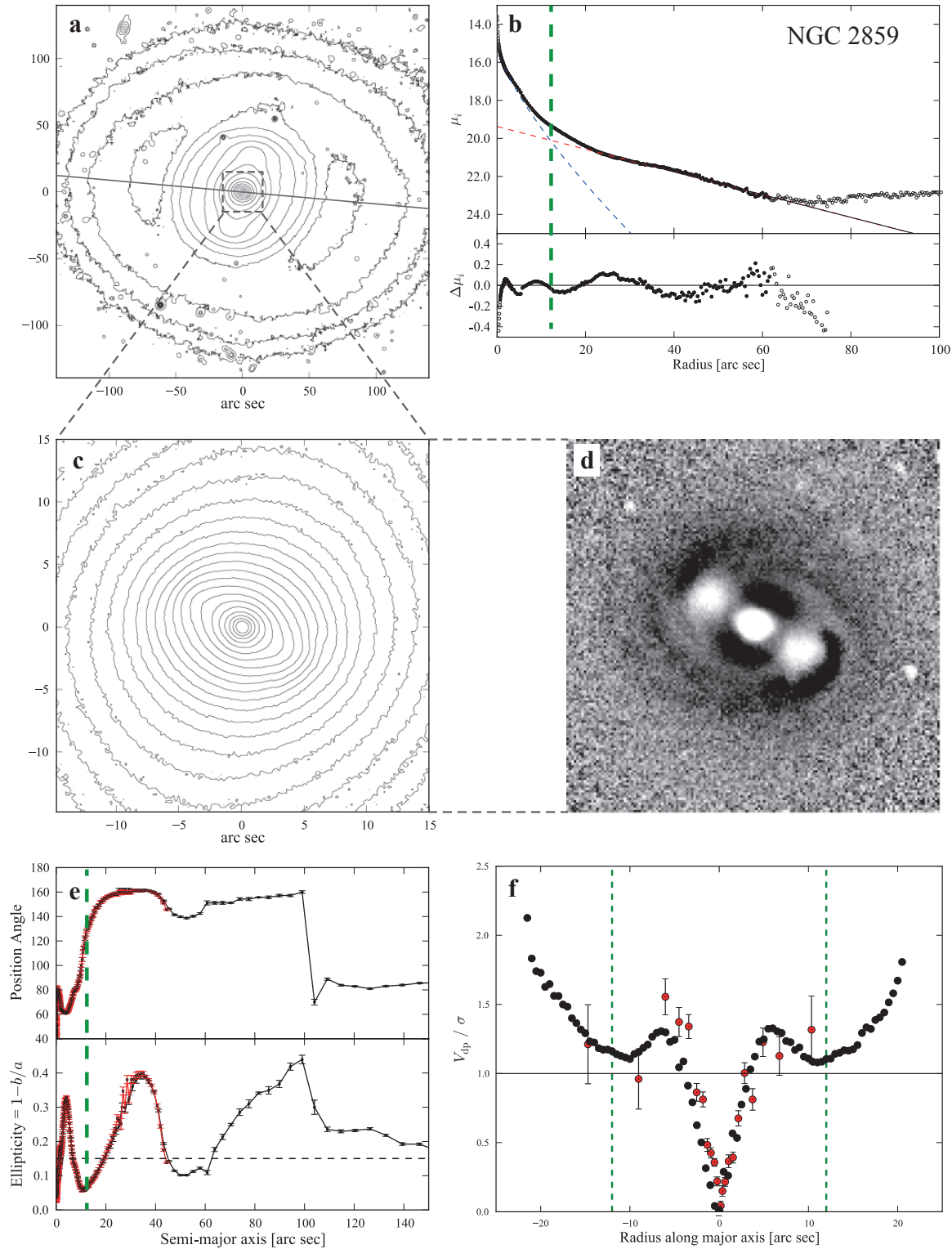


Figure A3. The disk pseudobulge in the S0 galaxy NGC 2859. **a:** log-scaled R -band isophotes (WIYN image, smoothed with 15-pixel-wide median filter); gray line marks major axis (PA = 86°). **b:** Bulge-disk decomposition of i -band major-axis profile (HST ACS-WFC F814W for $r < 3.4$ arcsec, SDSS i -band for larger radii). Dashed lines represent Sérsic + exponential fit to the data, with residuals plotted in lower sub-panel. Vertical dashed green line marks “bulge=disk” radius R_{bd} , where the Sérsic and exponential components are equally bright; this sets the boundary of the “photometric bulge”. **c:** Close-up of photometric bulge region (log-scaled contours from R -band image). **d:** Unsharp mask of the R -band image ($\sigma = 5$ pixels), showing the inner bar and partial spiral arms surrounding it. **e:** Ellipse fits to the SDSS i -band [black] and ACS-WFC F814W [red] images. **f:** Deprojected stellar rotation velocity divided by local velocity dispersion V_{dp}/σ along the major axis, using WHT-ISIS long-slit data [red] and SAURON data [black]. Vertical dashed lines mark the photometric bulge region $|R| < R_{bd}$. Both datasets show that V_{dp}/σ rises to well over 1 within this region, indicating a kinematically cool region more like a disk.

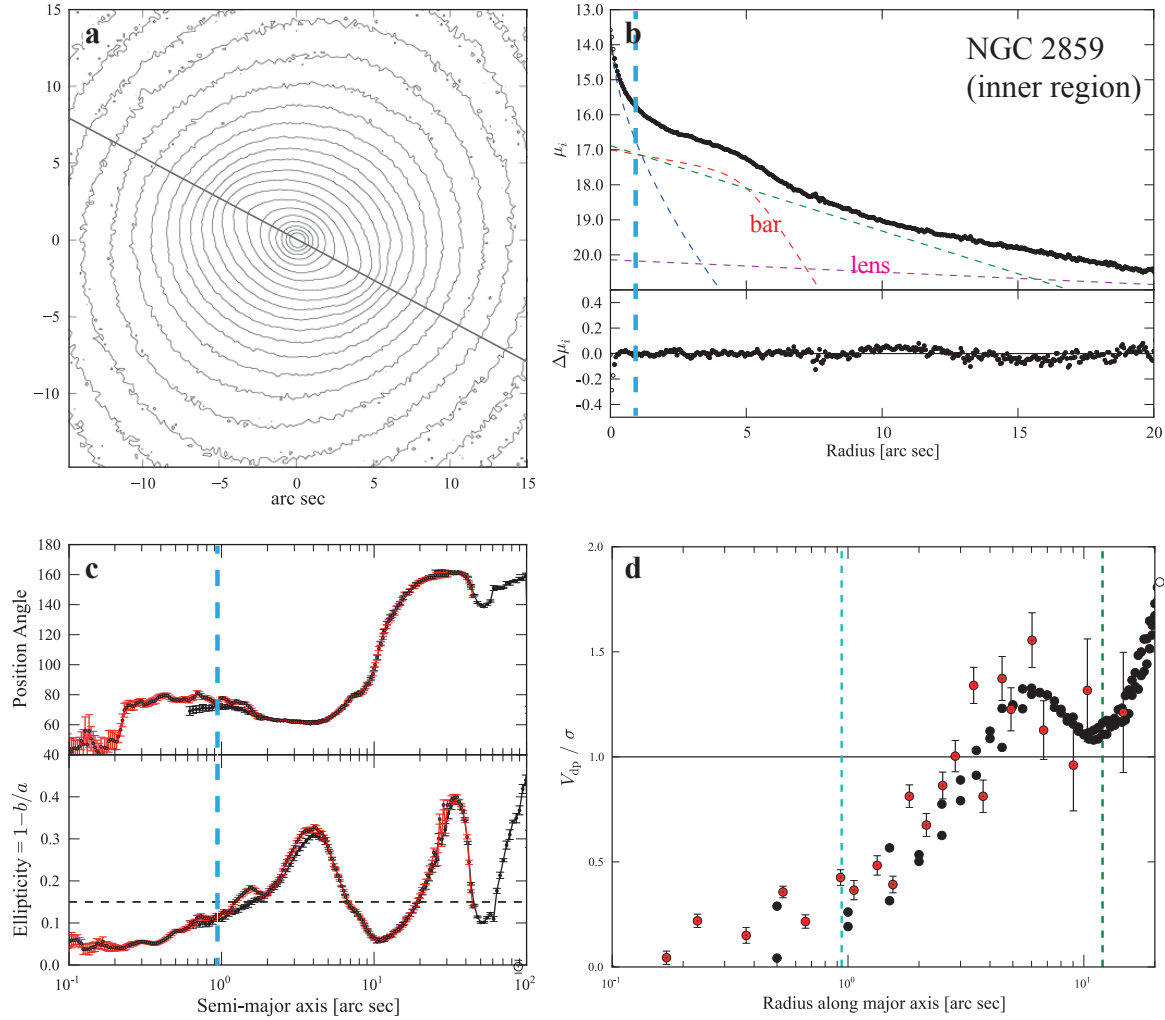


Figure A4. The classical bulge inside the disk pseudobulge of NGC 2859. **a:** Close-up of main photometric bulge region (see Figure A3); gray line marks the major axis of the inner bar. **b:** inner-bar major-axis profile (from ACS F814W image), with fit (Sérsic + broken-exponential + exponential; dashed lines) and residuals from fit in lower sub-panel. Vertical dashed blue line marks inner “bulge=disk” radius $R_{bd,i}$, where Sérsic component is as bright as the sum of the other two components. **c:** Ellipse fits (see Figure A3); note that the ellipticity in the inner photometric bulge region ($a \lesssim 1$ arcsec) is ~ 0.05 – 0.1 , less than that of the disk pseudobulge outside. **d:** Deprojected, folded stellar rotation velocity divided by local velocity dispersion V_{dp}/σ along galaxy major axis; see Figure A3. Vertical dashed blue and green lines mark the inner and main photometric bulge regions $|R| < R_{bd,i}$, respectively. In the inner region ($r \lesssim 1$ arcsec) and immediately outside, V_{dp}/σ remains well below 1, suggesting a kinematically hot region (i.e., a classical bulge).

Adopting either of these smaller radii as the outer boundary of the photometric bulge region has no significant effect on our analysis, however.

The isophotes and ellipse fits (panels c and e) show two regions of high ellipticity, corresponding to the “inner disk” and inner bar of Erwin (2004); unsharp masking (panel d) shows the inner bar more clearly (panel d). The stellar kinematics from Fabricius et al. (2012) clearly shows a peak in the V_{dp}/σ profile (panel f), which reaches a maximum of ~ 1.3 at $r \approx 7$ arcsec; the improved S/N of the HET spectrum shows this more clearly that the older kinematics from Vega Beltrán et al. (2001) used by Nowak et al. (2010).

Thus we appear to have reasonable evidence for a disk pseudobulge, as argued in Nowak et al. (2010). As in the cases of NGC 1553 and NGC 2859, the ellipticity profile (panel e of Figure A5) is more complicated than those of NGC 3945 and NGC 4371, both because of the strong con-

tribution from the inner bar (which is indirect evidence for disk-like structures, but is not a disk itself) and because the intermediate ellipticity peak (at $a \sim 21$ arcsec) is probably associated with the structure of the outer bar – specifically, with the projection of the vertically thick inner part of the bar (see Section 8.4).

Figure A6 shows the evidence for a classical bulge inside the disk pseudobulge of this galaxy. The inner decomposition presented here is somewhat different from that of Nowak et al. (2010), because we are now including an additional (exponential) component to represent the contribution of the (outer) bar and the lens; consequently, the parameters of the best-fitting inner exponential and Sérsic components are somewhat different. None the less, our main conclusions are unchanged: we find evidence that the light at $r \lesssim 1$ arcsec is due to a separate photometric component with much rounder isophotes than either the disk

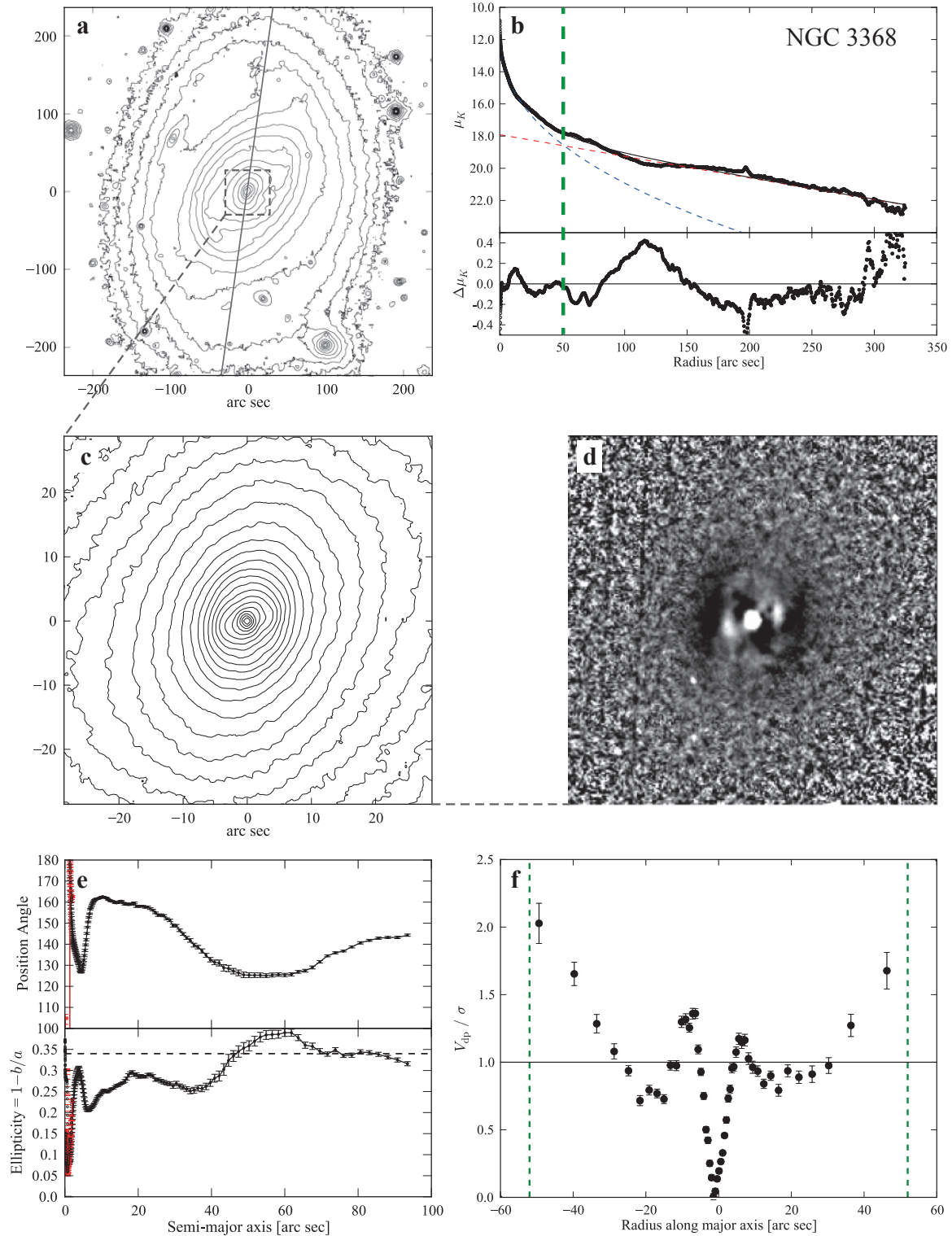


Figure A5. The disk pseudobulge in the Sab galaxy NGC 3368. **a:** log-scaled SDSS r -band isophotes (smoothed with 15-pixel-wide median filter); gray line marks major axis (PA = 172°). **b:** Bulge-disk decomposition of major-axis profile (combines NICMOS2 F160W, Knapen et al. (2003) K -band and SDSS r -band data). Dashed lines represent Sérsic + exponential fit to the data, with residuals plotted in lower sub-panel. Vertical dashed green line marks “bulge=disk” radius R_{bd} , where the Sérsic and exponential components are equally bright; this sets the boundary of the “photometric bulge”. **c:** Close-up of photometric bulge region, using Knapen et al. (2003) K -band image (smoothed with 5-pixel-wide median filter, log-scaled contours). **d:** Unsharp mask of the same image ($\sigma = 5$ pixels), showing the inner bar and dust lanes in the vicinity. **e:** Ellipse fits to the K -band and SINFONI (red) images. **f:** Projected stellar rotation velocity divided by local velocity dispersion V_{dp}/σ along the major axis, using HET long-slit data. Vertical dashed lines mark the photometric bulge region $|R| < R_{bd}$. V_{dp}/σ rises to ~ 1.36 within this region, indicating a kinematically cool region more like a disk.

pseudobulge or the outer disk. The V_{dp}/σ plot incorporates major-axis values from the SINFONI datacubes of Nowak et al. (2010) and Hicks et al. (2013) and the lower-resolution major-axis long-slit spectroscopy of Fabricius et al. (2012). The innermost SINFONI kinematics from Nowak et al. (2010), obtained with an AO-corrected seeing of ~ 0.17 arcsec FWHM, clearly show that this inner component has dispersion-dominated stellar kinematics, with V_{dp}/σ significantly < 1 .

A4 NGC 4262

NGC 4262 is a low-inclination barred S0 galaxy in the Virgo Cluster, classified by Erwin (2004) as possessing an inner disk inside the bar, based in part on observations by Shaw et al. (1995). Although the galaxy is quite close to face-on, we do find evidence for both a (possibly) disk pseudobulge and a very small classical bulge.

The decomposition of the major-axis profile (Figure A7, panel b) is relatively simple and clean, with the resulting photometric bulge region defined by $r < R_{\text{bd}} = 7.2$ arcsec. The main morphological evidence for a disk pseudobulge is a distinct stellar nuclear ring with $a \sim 2.9$ arcsec (panel d), also noted by Comerón et al. (2010); the isophotes in this region have an ellipticity only marginally less than that of the outer disk, and greater than that of the inner $a \lesssim 1$ arcsec (see also panel c of Figure A8). Kinematically, we find that V_{dp}/σ reaches a peak value of almost 1.6 at approximately the same radius as the nuclear ring. The stellar kinematic data are from major-axis cuts through SAURON IFU data from the SAURON public archive,¹¹ originally published in Emsellem et al. (2004), and higher-resolution OASIS IFU data from McDermaid et al. (2006).

Closer inspection of the ACS-WFC isophotes shows that the isophotes become gradually rounder interior to the stellar nuclear ring, reaching values of ~ 0.05 before PSF effects dominate (Figure A8). Decomposition of the inner major-axis profile (panel b of Figure A8) shows a small central excess, reasonably well fit by a Sérsic component with $n \sim 0.9$. Stellar kinematics with the necessary resolution for this inner photometric-bulge region ($r < 0.32$ arcsec) are unavailable; however, the fact that V_{dp}/σ is < 1 for radii $\lesssim 2$ arcsec suggests that the inner stellar kinematics are probably dispersion-dominated, and that the central photometric excess corresponds to a (very compact) classical bulge.

A5 NGC 4699

This is a luminous, intermediate-type (Sb) spiral galaxy with a very extended, Type III outer disk (Erwin et al. 2008). In our analysis, we ignore the very outer part of this disk (visible in the azimuthally averaged profile of Erwin et al. at $r \gtrsim 120$ arcsec), and so our “outer” decomposition (panel b of Figure A9) is restricted to $r < 120$ arcsec. This fit yields a significant photometric bulge which dominates the light at $r \lesssim 45$ arcsec; this clearly corresponds to what Sandage & Bedke (1994) call “the bulge” of this galaxy.

Inspection of the photometric bulge region shows that it is as elliptical as the outer disk, or even more so (panels

c and e of Figure A9), and is dominated by tightly wrapped spiral arms and a relatively strong bar (panels c and d of the same figure). Although the long-slit stellar kinematics of Bower et al. (1993) only extend to $r \sim 20$ arcsec, they clearly show that V_{dp}/σ reaches values > 1 in the photometric-bulge region, so we are confident in identifying a disk pseudobulge in NGC 4699.

Figure A10 shows the previously identified photometric bulge region. In the case of this galaxy, the major axis is close to the bar’s major axis, but this produces only a very weak bump in the major-axis profile, similar to that due to spiral structure further out, so we do not include a separate component for the bar. The resulting fit (including two exponential components for the outer disk) is rather good, with a clear inner excess (modeled as a Sérsic component with $n = 1.4$) creating an inner photometric-bulge zone with $R_{\text{bd},i} = 2.8$ arcsec. The stellar kinematics from the ground-based data of Bower et al. (1993) suggest a relatively low value of V_{dp}/σ within $R_{\text{bd},i}$, and the SINFONI AO data appear to confirm this, since the SINFONI V_{dp}/σ values reach a plateau of only ~ 0.5 . Strictly speaking, we cannot rule out the possibility that V_{dp}/σ might reach values ~ 1 between $r \approx 1.5$ and 3 arcsec, since this is beyond the range of our SINFONI data but within a region where seeing effects might reduce V_{dp}/σ from the ground-based data. None the less, we suggest that the inner photometric bulge region of NGC 4699, associated with very round isophotes (panel c of Figure A10) and V_{dp}/σ values $\lesssim 0.5$, is most likely another example of a compact classical bulge.

Our decomposition and identification of the classical bulge is similar to that of Weinzirl et al. (2009), who performed a 2D bulge/bar/disk decomposition of an H -band image of NGC 4699 from the OSU Bright Spiral Galaxy Survey Eskridge et al. (2002). (Inspection of the OSU-BSGS H -band image shows that the main disk of the galaxy is not visible in that image, so Weinzirl et al. treated the disk pseudobulge as the galaxy’s only disk.) They found a bulge with $n = 2.08$ and $r_e = 2.62$ arcsec – values within ~ 35 per cent of the corresponding values from our fit.

A6 Ambiguous Case: NGC 1068

In most respects, the Sb galaxy NGC 1068 appears to be similar to the previous composite-bulge galaxies: it has a large, disk pseudobulge combined with a much smaller central component. The sole ambiguity concerns the morphology of the central component – is it rounder than the galaxy disk, or is it more of a nuclear disk? – and stems from uncertainty about the galaxy’s inclination.

Both Schinnerer et al. (2000), using H I data, and Davies et al. (2007), using stellar kinometry analysis of their SINFONI data, suggest an inclination of $\approx 40^\circ$, which implies an observed ellipticity of ≈ 0.22 for an early-type disk. On the other hand, Gutiérrez et al. (2011) used SDSS images and found an outer-disk ellipticity of ~ 0.14 , implying an inclination of $\sim 31^\circ$. Since, as we will see below, the inner component has an ellipticity of ~ 0.15 , the question of whether the inner component is disklike or spheroidal depends on the adopted galaxy inclination – thus, we consider this galaxy a somewhat ambiguous case, though we include it with the other composite-bulge galaxies in our analysis.

¹¹ <http://www.strw.leidenuniv.nl/sauron/>

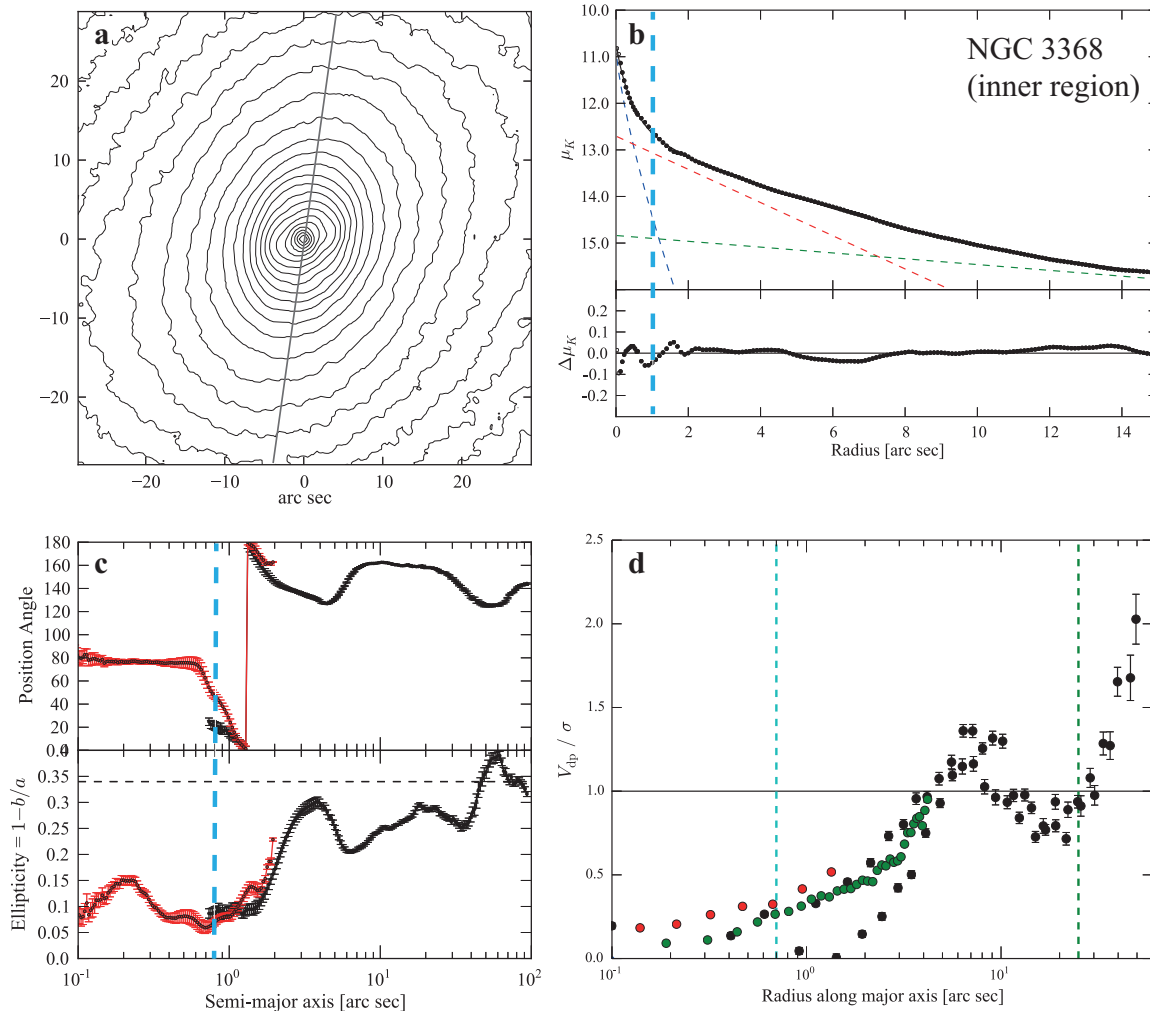


Figure A6. The classical bulge inside the diskly pseudobulge of NGC 3368. **a:** Close-up of main photometric bulge region from the K -band image; gray line marks major-axis PA. **b:** major-axis profile combining SINFONI, NICMOS2 and ground-based K -band data, with fit (Sérsic + exponential + exponential; dashed lines) and residuals from fit in lower sub-panel. Vertical dashed blue line marks inner “bulge=disk” radius $R_{bd,i}$. **c:** Ellipse fits to the K -band and SINFONI (red) images.; note that the ellipticity in the inner photometric bulge region ($a \lesssim 1$ arcsec) is ~ 0.1 , less than that of the diskly pseudobulge outside. **d:** Deprojected, folded stellar rotation velocity divided by local velocity dispersion V_{dp}/σ along the major axis, combining AO SINFONI (red), non-AO SINFONI (green) and HET (black) data. Vertical dashed blue and green lines mark the inner and main photometric bulge regions $|R| < R_{bd,i}$, respectively. In the inner region ($r \lesssim 1$ arcsec), V_{dp}/σ remains well below 1, suggesting a kinematically hot region (i.e., a classical bulge).

A6.1 Disky Pseudobulge

Our global analysis of NGC 1068’s surface-brightness profile uses the light at $r \lesssim 100$ arcsec and is very similar to that carried out by Shapiro et al. (2003) for this galaxy (their Fig. 2). As both Pohlen & Trujillo (2006) and Gutiérrez et al. (2011) showed, there is considerable stellar light further out in a shallower profile, much of which is due to the outer pseudoring. The global fit for this galaxy is thus similar to those for NGC 3945 and NGC 2859, where we deliberately exclude light due to extended outer rings.

The decomposition (Figure A11, panel b) is relatively straightforward, and the resulting photometric bulge has $R_{bd} = 24$ arcsec. The morphology interior to this radius is strikingly disklike: the near-IR stellar light is dominated by the very strong (inner) bar first noted by Scoville et al. (1988), with star-forming spiral arms forming a pseudoring just outside the bar (panels c and d); due to this bar, the

isophotes have an ellipticity much higher than that of the outer disk (panel e).

The long-slit stellar-kinematic data of Shapiro et al. (2003) show $V_{dp}/\sigma > 1$ at all radii $\gtrsim 1$ arcsec, and in fact the ratio reaches a value of almost ~ 3 at $r \sim 15$ arcsec (panel f), so this an even more extreme case of a photometric bulge with disklike kinematics than NGC 3945. We are certainly not the first to suggest that the kinematics in this part of the galaxy are more disklike than bulgelike: in particular, Emsellem et al. (2006) pointed this out using 2D stellar kinematics from the SAURON instrument, in conjunction with N -body/hydrodynamical modeling.

A6.2 Nuclear Disk or Classical Bulge?

Optical and near-IR images of NGC 1068 are strongly contaminated by light from the bright AGN. To get around this

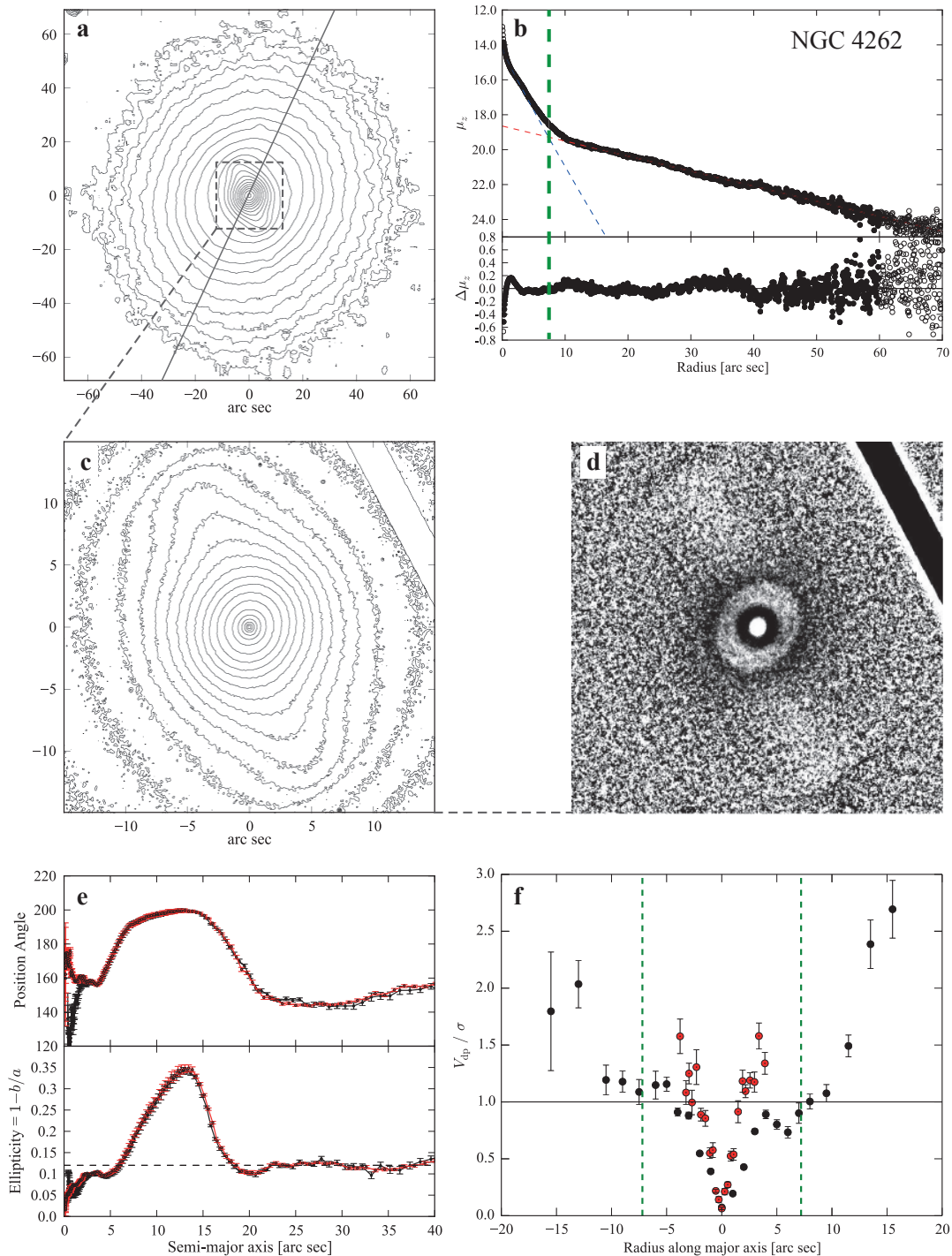


Figure A7. The disk pseudobulge in the S0 galaxy NGC 4262. **a:** log-scaled SDSS *i*-band isophotes (smoothed with 15-pixel-wide median filter); gray line marks major axis ($PA = 155^\circ$). **b:** Bulge-disk decomposition of major-axis profile, from SDSS *i*-band and *HST* ACS-WFC F850LP images. Dashed lines represent Sérsic + exponential fit to the data, with residuals plotted in lower sub-panel. Vertical dashed green line marks “bulge=disk” radius R_{bd} , where the Sérsic and exponential components are equally bright; this sets the boundary of the “photometric bulge”. **c:** Close-up of photometric bulge region (log-scaled contours from ACS-WFC F850LP image, smoothed with 3-pixel-wide median filter). **d:** Unsharp mask of the *HST* image ($\sigma = 15$ pixels), showing the nuclear ring. **e:** Ellipse fits to the SDSS [black] and *HST* [red] images; note that the ellipticity interior to the bar is only slightly below that of the outer disk. **f:** Deprojected stellar rotation velocity divided by local velocity dispersion V_{dp}/σ along the major axis, using OASIS data (red) from McDermid et al. (2006) and SAURON data (black) from Emsellem et al. (2004); the former has much higher spatial resolution (FWHM = 0.6 versus 2.6 arcsec). Vertical dashed lines mark the photometric bulge region $|R| < R_{bd}$. V_{dp}/σ in the high-resolution OASIS data rises to ~ 1.57 within this region, indicating a kinematically cool region more like a disk.

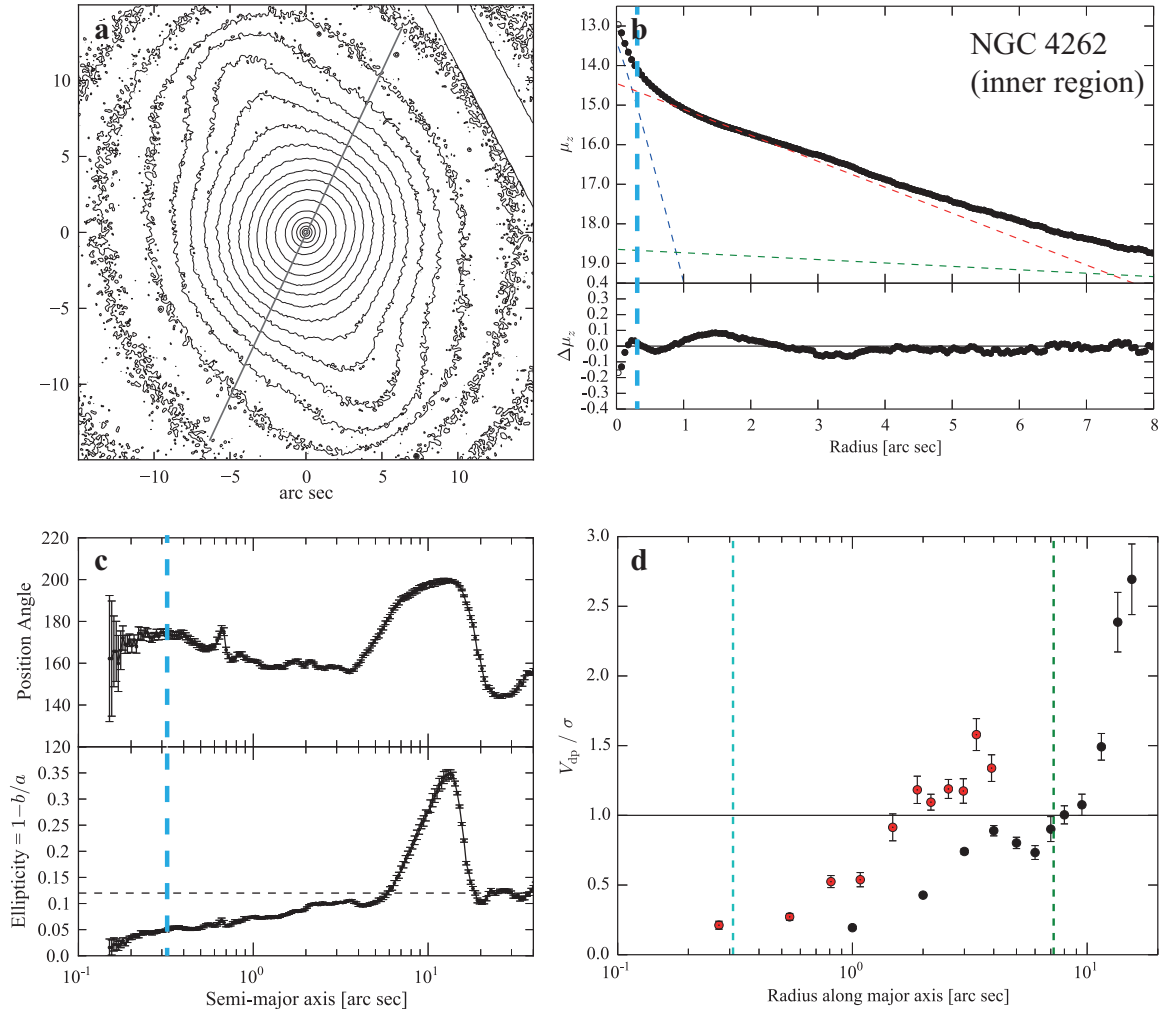


Figure A8. The classical bulge inside the diskypseudobulge of NGC 4262. **a:** Close-up of main photometric bulge region from *HST* ACS-WFC F850LP image; gray line marks major-axis PA. **b:** major-axis profile from the *HST* image, with fit (Sérsic + exponential; dashed lines) and residuals from fit in lower sub-panel. Vertical dashed blue line marks inner “bulge=disk” radius $R_{bd,i}$. **c:** Ellipse fits to the *HST* image; note that the ellipticity in the inner photometric bulge region ($a \lesssim 0.32$ arcsec is ~ 0.05 , less than that of the diskypseudobulge outside. **d:** Deprojected, folded stellar rotation velocity divided by local velocity dispersion V_{dp}/σ along the major axis. Vertical dashed blue and green lines mark the inner and main photometric-bulge regions $|R| < R_{bd,i}$, respectively. Although there is essentially no kinematic data for the inner photometric-bulge region, the fact that V_{dp}/σ is below 1 for $r < 1.8$ arcsec suggests that the latter is almost certainly kinematically hot (i.e., a classical bulge).

problem, we make use of an *H*-band image from the 100mas SINFONI observations (1.5 arcsec field of view) of Davies et al. (2007), where the AGN emission (assumed to come mostly from hot dust in the circumnuclear torus) has been spectroscopically modeled and removed, leaving behind a “pure stellar” continuum which is then collapsed along the wavelength axis to form an image. We matched the surface-brightness profile extracted from this image to a profile from a larger-scale *HST* NICMOS3 F200N image.

For the stellar kinematics, we supplement the large-scale (but low-spatial-resolution) data of Shapiro et al. (2003) with data from the Gemini GMOS IFU observations of Gerssen et al. (2006), which had a seeing of FWHM = 0.5 arcsec, and with the VLT-SINFONI kinematics of Davies et al. (2007), observed in AO mode with a corrected FWHM of 0.10 arcsec.

We perform our inner decomposition by choosing a po-

sition angle which avoids most of the inner bar (PA = 137° , perpendicular to the bar). Since the galaxy is seen at a relatively low inclination, the projection effects are relatively small; however, this does mean that our decomposition does not exactly mirror the major-axis stellar kinematics.

Comparison of the NICMOS3 image with the PA = 137° profile shows that the increase in surface brightness starting at $r \sim 6$ arcsec is actually due to the profile crossing into the bright part of the bar, along its minor axis. Since we consider bars to be disk phenomena, this excess light should be treated as part of the diskypseudobulge. There is a second, much steeper increase in the profile which sets in for $r \lesssim 1$ arcsec, associated with rounder isophotes; this is the best candidate for an embedded bulge.

Our best fit to the surface-brightness profile thus uses *three* components: an exponential for the main part of the pseudobulge outside the bar itself (in analogy with large-

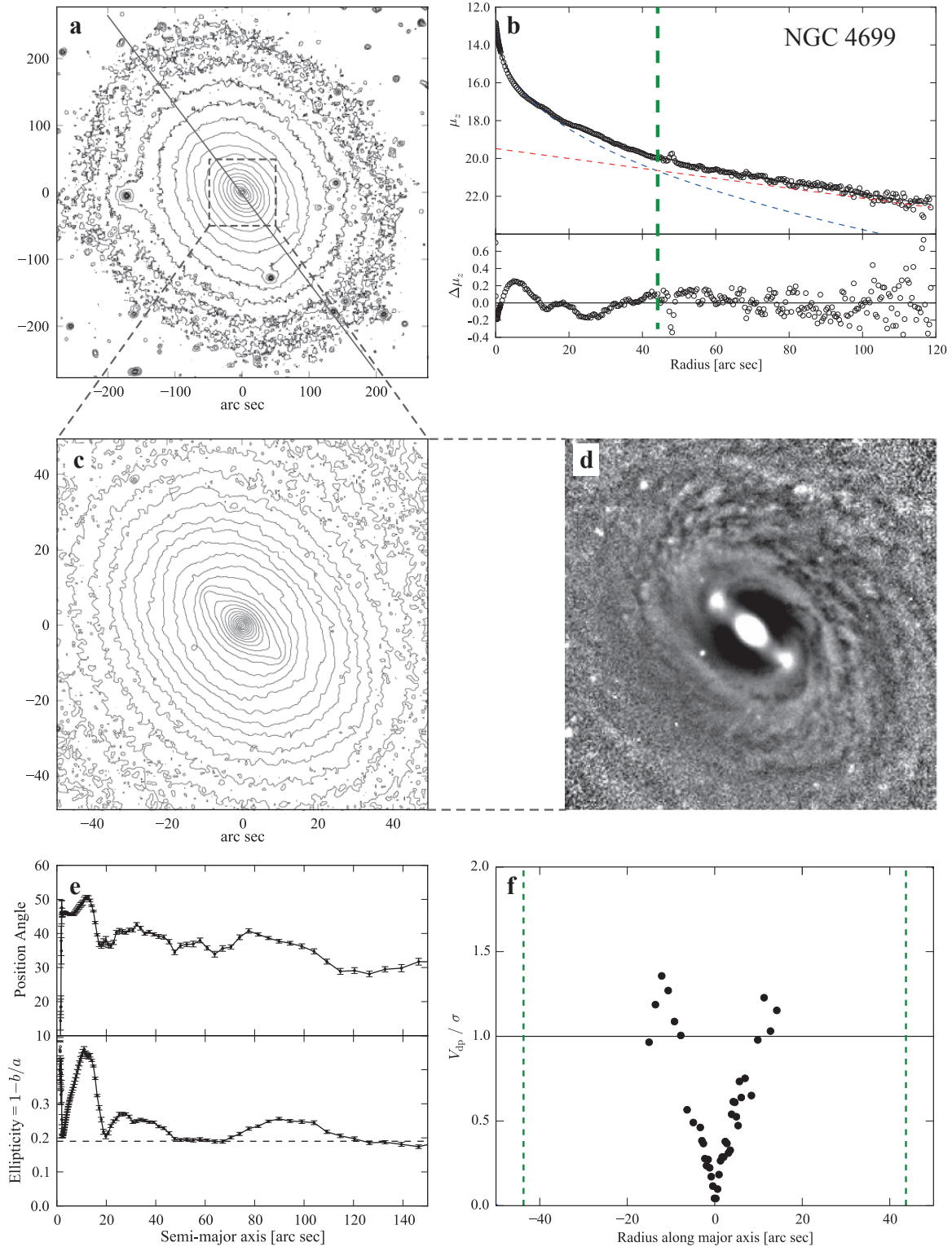


Figure A9. The disk pseudobulge in the Sb galaxy NGC 4699. **a:** log-scaled i -band isophotes (SDSS image, smoothed with 15-pixel-wide median filter); gray line marks major axis (PA = 37°). **b:** Bulge-disk decomposition of SDSS z -band major-axis profile. Dashed lines represent Sérsic + exponential fit to the data, with residuals plotted in lower sub-panel. Vertical dashed green line marks “bulge=disk” radius R_{bd} , where the Sérsic and exponential components are equally bright; this sets the boundary of the “photometric bulge”. **c:** Close-up of photometric bulge region (log-scaled contours from SDSS z -band image, smoothed with 3-pixel-wide median filter). **d:** Unsharp mask of the z -band image ($\sigma = 20$ pixels), showing the bar and spiral immediately structure outside it. **e:** Ellipse fits to the SDSS i -band image; note that the ellipticity in the photometric bulge region remains essentially unchanged from the outer disk value (horizontal dashed line), except for the peak associated with the bar, indicating the photometric bulge has flattening similar to the outer disk. **f:** Deprojected stellar rotation velocity divided by local velocity dispersion V_{dp}/σ along the major axis, using long-slit data from Bower et al. (1993). Vertical dashed lines mark the photometric bulge region $|R| < R_{bd}$. Although the kinematics do not extend very far out from the centre, V_{dp}/σ does rise to ~ 1.35 within this region, indicating a kinematically cool region more like a disk.

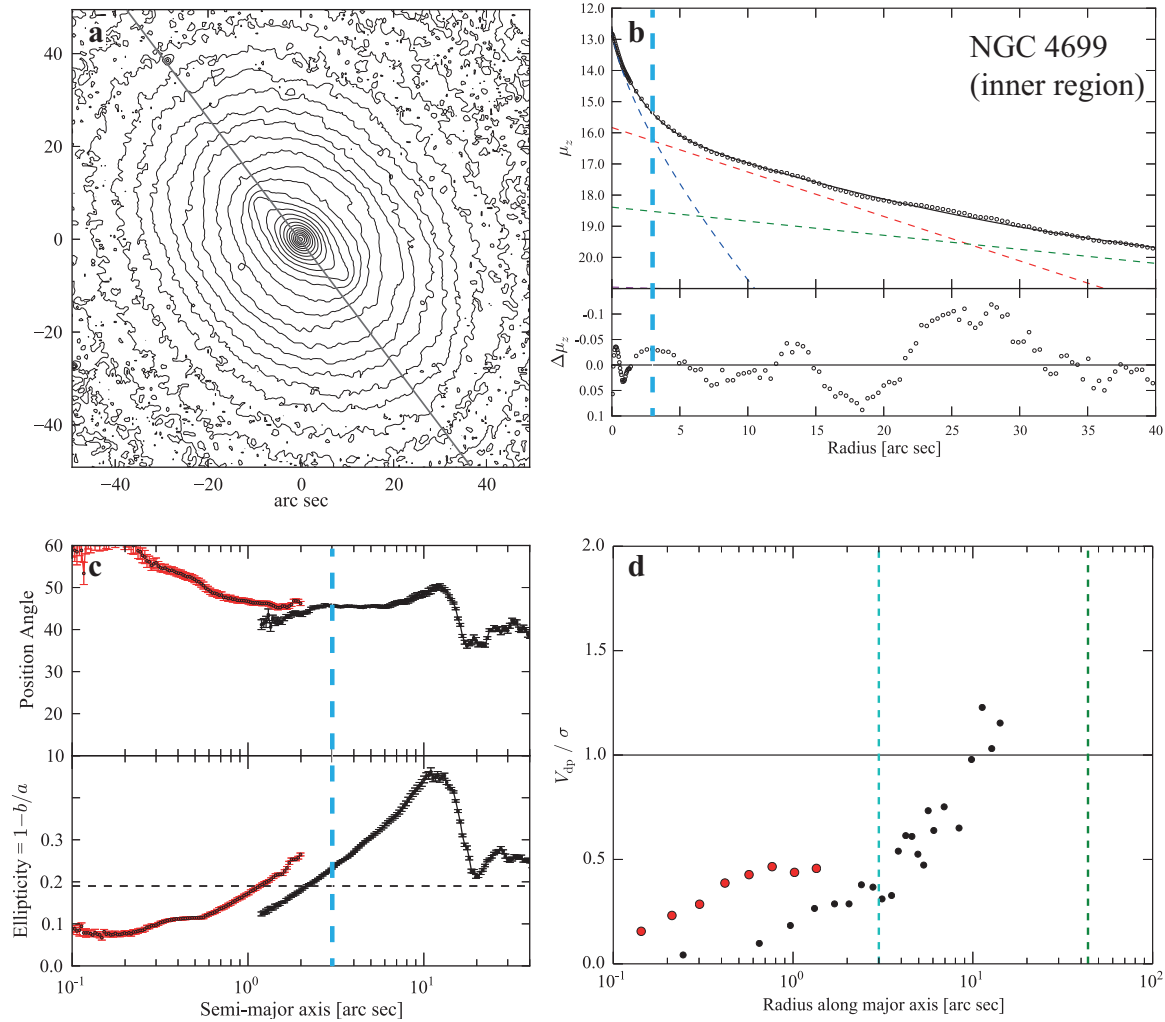


Figure A10. The classical bulge inside the diskly pseudobulge of NGC 4699. **a:** Close-up of main photometric bulge region from SDSS z -band image; gray line marks major-axis PA. **b:** major-axis profile combining data from SINFONI K -band image ($r < 1.3$ arcsec) and SDSS z -band and i -band images, with fit (Sérsic + multiple exponentials; dashed lines) and residuals from fit in lower sub-panel. Vertical dashed blue line marks inner “bulge=disk” radius $R_{bd,i}$. **c:** Ellipse fits to the SINFONI K -band [red] and SDSS z -band images; note that the ellipticity in the inner photometric bulge region ($a \lesssim 3$ arcsec) is $\lesssim 0.15$, less than that of the diskly pseudobulge outside. **d:** Deprojected, folded stellar rotation velocity divided by local velocity dispersion V_{dp}/σ along the major axis, using long-slit data from Bower et al. (1993) [black] and SINFONI AO data [red]. Vertical dashed blue and green lines mark the inner and main photometric bulge regions $|R| < R_{bd,i}$, respectively. In the inner region ($r \lesssim 3$ arcsec), V_{dp}/σ remains well below 1, suggesting a kinematically hot region (i.e., a classical bulge).

scale bars, one could perhaps call this a “lens”); a Gaussian for the minor axis profile of the bar;¹² and a Sérsic for the innermost component. The innermost (Sérsic) component corresponds to the “extra emission” at $r < 1$ arcsec noted by Davies et al. (2007), although we identify their 1–5 arcsec “ $R^{1/4}$ bulge” profile as being due to the inner bar, not to a larger-scale bulge. The final R_e value recorded in Table 4 for this Sérsic component has been corrected to its major-axis value assuming an ellipticity of 0.15, based on the ellipse fits (Figure A12).

As in the other galaxies, the V_{dp}/σ profile shows

dispersion-dominated stellar kinematics in the inner $r < R_{bd,i}$ region: V_{dp}/σ reaches a maximum of only ~ 0.7 .

Is the innermost component a compact classical bulge, or is it something more disklike? Davies et al. (2007) argued for a disk, and suggested (based on indirect arguments about the estimated M/L ratio of the inner component) that its stellar population was relatively young: ~ 300 Myr. If we adopt an inclination of 31° for the galaxy, then the inner ellipticity of ~ 0.15 is consistent with that of a disk having a flattening similar to the outer disk’s.

However, Crenshaw & Kraemer (2000) and Storchi-Bergmann et al. (2012) have both presented high-resolution spectroscopic evidence – including fits to the near-nuclear spectra – indicating that the $r < 1$ arcsec region is actually dominated by *old* stars, with an age of at least 2 Gyr according to Crenshaw & Kraemer’s optical STIS spec-

¹² Evidence that the minor-axis profiles of at least some bars are Gaussian can be found in Ohta et al. (1990) and Prieto et al. (1997).

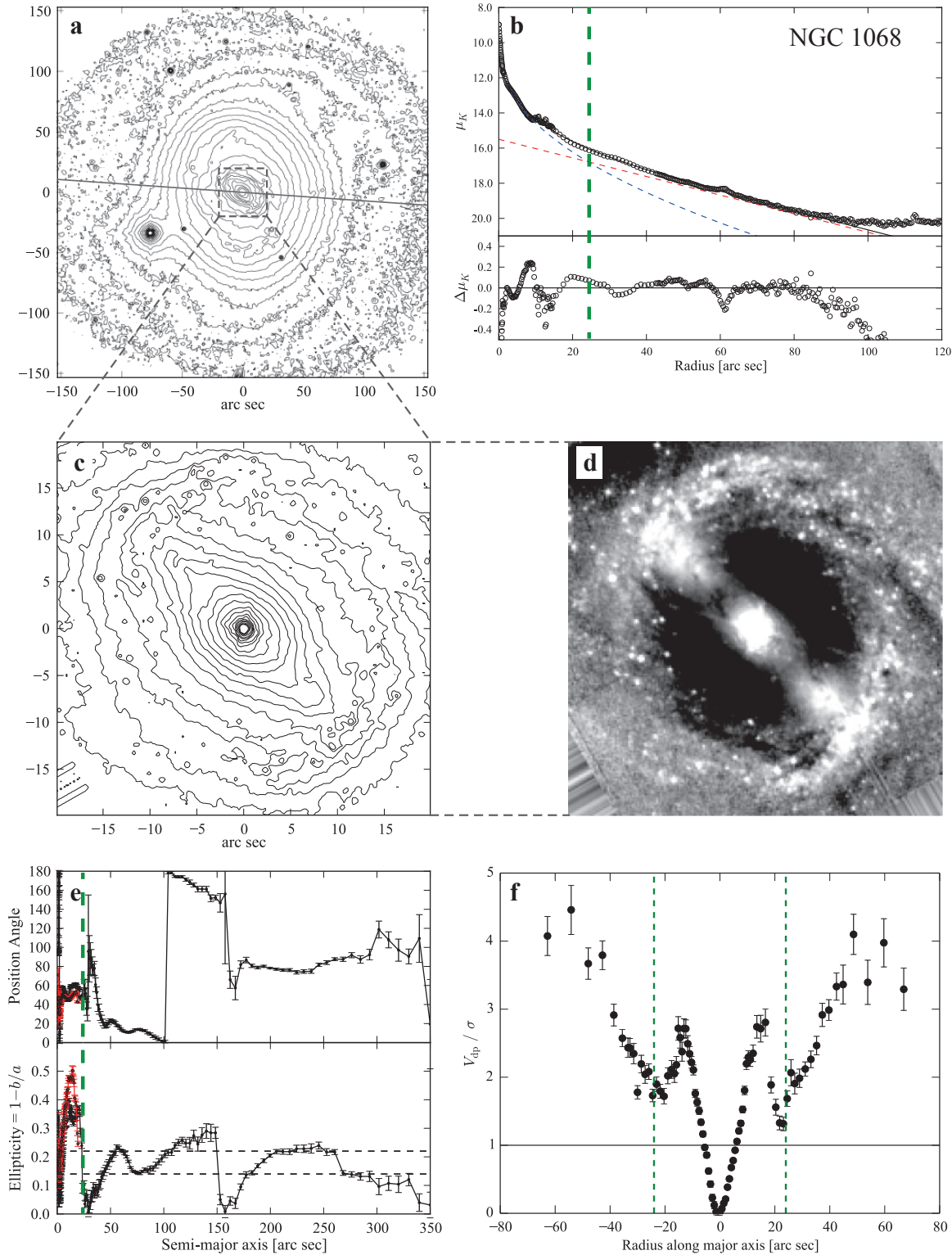


Figure A11. The disk pseudobulge in the Sb galaxy NGC 1068. **a:** log-scaled i -band isophotes (SDSS image, smoothed with 7-pixel-wide median filter); gray line marks major axis (PA = 86°). **b:** Bulge-disk decomposition of major-axis profile (profile combines AGN-subtracted SINFONI data from Davies et al. (2007) for $r < 1.3$ arcsec, *HST* NICMOS3 F200N for $r = 1.3$ –15 arcsec, 2MASS K -band for $r = 15$ –42 arcsec, SDSS i -band for $r > 42$ arcsec). Dashed lines represent Sérsic + exponential fit to the data, with residuals plotted in lower sub-panel. Vertical dashed green line marks “bulge=disk” radius R_{bd} , where the Sérsic and exponential components are equally bright; this sets the boundary of the “photometric bulge”. **c:** Close-up of photometric bulge region (log-scaled contours from NICMOS3 image). **d:** Unsharp mask ($\sigma = 20$ pixels) of same region, showing bar and spiral arms. **e:** Ellipse fits to SDSS i (black) and NICMOS (red) images. **f:** Deprojected stellar rotation velocity divided by local velocity dispersion V_{dp}/σ along major axis, using long-slit data from Shapiro et al. (2003). Vertical dashed lines mark the photometric bulge region $|R| < R_{bd}$; V_{dp}/σ rises to almost 3 in this region.

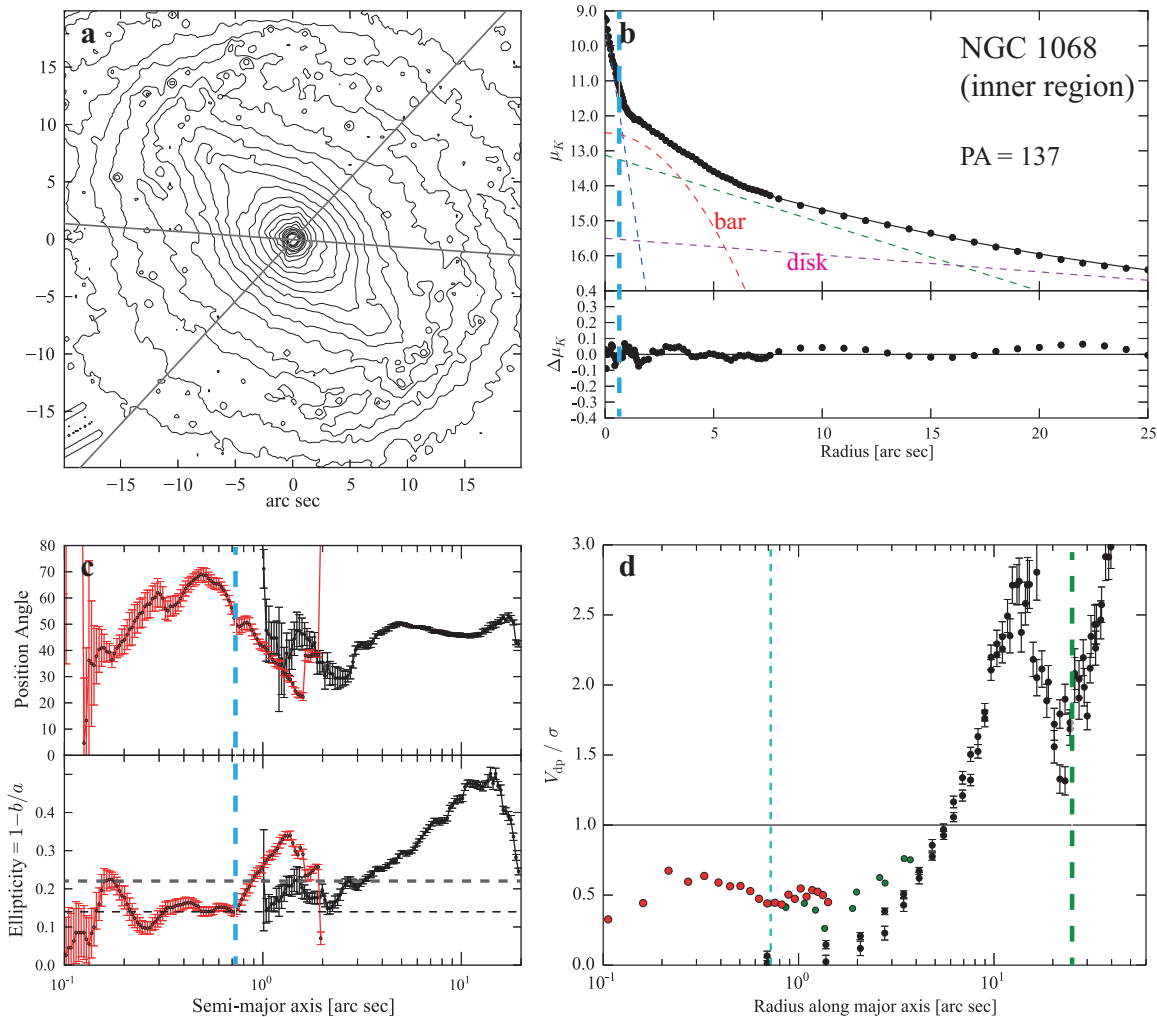


Figure A12. Evidence for a possible classical bulge inside the disk pseudobulge of NGC 1068. **a:** Close-up of main photometric bulge region from *HST* NICMOS3 F200N image; gray lines marks major-axis PA (86°) and PA perpendicular to inner bar (137°). **b:** Profile at 137° from AGN-subtracted SINFONI *H*-band image of Davies et al. (2007) ($r < 1.7$ arcsec) and NICMOS3 F200N image, with fit (Sérsic + Gaussian + exponential + exponential; dashed lines) and residuals from fit in lower sub-panel. Vertical dashed blue line marks inner “bulge=disk” radius $R_{bd,i}$. **c:** Ellipse fits to the SINFONI [red] and NICMOS3 [black] images; the two estimates for the outer-disk ellipticity (0.13 and 0.22) are marked by the horizontal black and gray lines. **d:** Deprojected, folded stellar rotation curve divided by local velocity dispersion V_{dp}/σ along the galaxy major axis. Data from Shapiro et al. (2003, black), GMOS IFU kinematics of Gerssen et al. (2006, green) and SINFONI IFU kinematics of Davies et al. (2007, red).

troscopy, and an age of 5–15 Gyr according to the near-IR spectroscopy of Storchi-Bergmann et al. If we combine this with the dispersion-dominated kinematics *and* assume an inclination of 40° for the galaxy, then the central stellar component is rounder than a disk, kinematically hot, *and* made up of old stars – a good case for a classical bulge, albeit one with a nearly-exponential profile.

A7 Possible Case: NGC 1543

NGC 1543 is something of a borderline case, primarily because we do not have a good handle on the stellar kinematics. The galaxy is so close to face-on that it is difficult to determine the major axis with any accuracy, and thus long-slit data cannot really be used. (We need to know the major axis accurately in order to properly deproject the observed velocities to their major-axis, edge-on values.) The

only available stellar kinematics are two long-slit observations by Jarvis et al. (1988). Since both their “major-axis” and “minor-axis” profiles (at position angles of 90° and 0° , respectively) show stellar rotation, all we really can say is that the major axis is not close to 0° or 90° . Thus we are unable to perform a proper kinematic analysis for NGC 1543.

None the less, the *morphology* of the galaxy is very suggestive of a composite-bulge system (Figure A13). Full details of the disk pseudobulge decomposition, including analysis of the structure of the inner bar, will be presented elsewhere (Erwin 2014a); see Erwin (2011) for a preliminary discussion. Because the the major axis of the inner bar is relatively close to the minor axis of the outer bar, we use a profile along the position angle of the inner bar for our decomposition (as in the case of NGC 2859; see Section A2).

Figure A13 summarizes both the global, “naive” bulge/disk decomposition (panel b) and the inner,

composite-bulge decomposition (panel d). We construct our surface-brightness profile using an *HST* WFPC2 F814W image at small radii and a Spitzer IRAC2 image at large radii (we use the IRAC2 image instead of the IRAC1 image because the galaxy position on the former is slightly better for purposes of measuring the sky background). Excluding the broad outer ring (similar to those of NGC 2859 and NGC 3945), a decomposition of the inner ~ 100 arcsec (panel a) yields a photometric bulge with $n = 1.6$, $r_e = 9.4$ arcsec and $R_{bd} \approx 26$ arcsec; this is similar to, but slightly larger than, the “pseudobulge” reported by Fisher & Drory (2010) from their 1-D IRAC1 decomposition ($n = 1.51$, $r_e = 6.5$ arcsec). The photometric bulge region thus defined ($r \lesssim 26$ arcsec) is dominated by a very strong inner bar, with a very weak stellar nuclear ring surrounding it (Erwin 2014a). We take this as strongly suggestive evidence for a disk pseudobulge, though as noted above we lack the necessary kinematic data for full confirmation.

In the central regions, the isophotes become very round (panels c and f of Figure A13), and there is a central excess of light above the inner bar. Simultaneous decompositions along the major and minor axes of the inner bar support the presence of an inner Sérsic component with $n = 1.5$, $r_e = 2.7$ arcsec and ellipticity $\lesssim 0.05$ (panel d of the figure shows the decomposition along the inner-bar major axis). So there is morphological and photometric evidence for a distinct, classical-bulge-like component in the centre of this galaxy as well. There is in addition evidence for a very compact, distinct feature inside the classical bulge, which is probably a nuclear star cluster (see Erwin 2011 and Erwin 2014a).

A8 The Uncertain Case of NGC 3489

Nowak et al. (2010) considered two cases of composite-bulge galaxies: the double-barred spiral NGC 3368 and the barred S0 galaxy NGC 3489. Although we confirm the previous classification of NGC 3368 (see Section A3, above), NGC 3489 has proved to be more ambiguous (Figure A14).

Careful analysis of the isophotes of NGC 3489 suggests that the broad, slightly boxy region inside the bar may well be an example of a projected box/peanut (B/P) structure (outlined isophote in panel a of Figure A14), even though Erwin & Debattista (2013) did not classify this galaxy as such. The presence of a B/P structure certainly does not prevent the simultaneous existence of a composite bulge in this galaxy – indeed, Section 8.4 argues that NGC 3368 has a clear B/P structure in addition to its composite bulge – but it does mean that the major-axis decomposition in Nowak et al. (2010) needs to be revised, since what they considered to be the inner-disk component, dominating the major-axis light from ≈ 4 –12 arcsec, is more likely to be a combination of the B/P structure and the lens region immediately outside the bar.

For our revised inner decomposition (panel d of Figure A14), we include the contribution from the outer disk component (panel b) and treat the B/P structure as a separate component with a Sérsic profile; we also include an additional Sérsic component for the nuclear luminosity excess which Nowak et al. (2010) modeled with a Gaussian. The resulting fit has an inner exponential with scale length ~ 55 pc, corresponding to the original “classical bulge” component in Nowak et al. (2010), as well as an extremely com-

pact Sérsic component with $n = 0.7$ and $R_e = 0.19$ arcsec. The R_{bd} radii for these two components are 2.7 and 0.2 arcsec, respectively.

As shown by the ellipticity plot (panel e), the inner exponential component, which dominates the light at $r \lesssim 2.7$ arcsec, is in fact highly elliptical – almost as elliptical as the outer disk. This is very similar to the disk pseudobulges identified in our other galaxies. On the other hand, the stellar kinematics in this region (panel f) are rather dispersion-dominated, with $V_{dp}/\sigma \sim 0.7$; even at the outer edge of this region, V_{dp}/σ is never larger than ~ 0.9 . So this structure is both flattened like a disk and at the same time kinematically *hot*, making it unlike any of the disk pseudobulges in the other galaxies of our sample.

The innermost (Sérsic) component is associated with rounder isophotes and a lower V_{dp}/σ value, but it is so small¹³ that it could more plausibly be classified as a nuclear star cluster than as a genuine classical bulge.

We are thus left with a curiosity: our revised analysis identifies a structure in NGC 3489 which morphologically resembles a disk pseudobulge, but is kinematically hot, along with a distinct nuclear component that might best be classified as a nuclear star cluster. NGC 3489 may thus be a kind of transition object, and an indication that the central regions of early-type disk galaxies can be even more diverse and complicated than our main “composite-bulge” argument suggests.

¹³ The Sérsic R_e is ≈ 9 pc, but this does not account for PSF convolution.

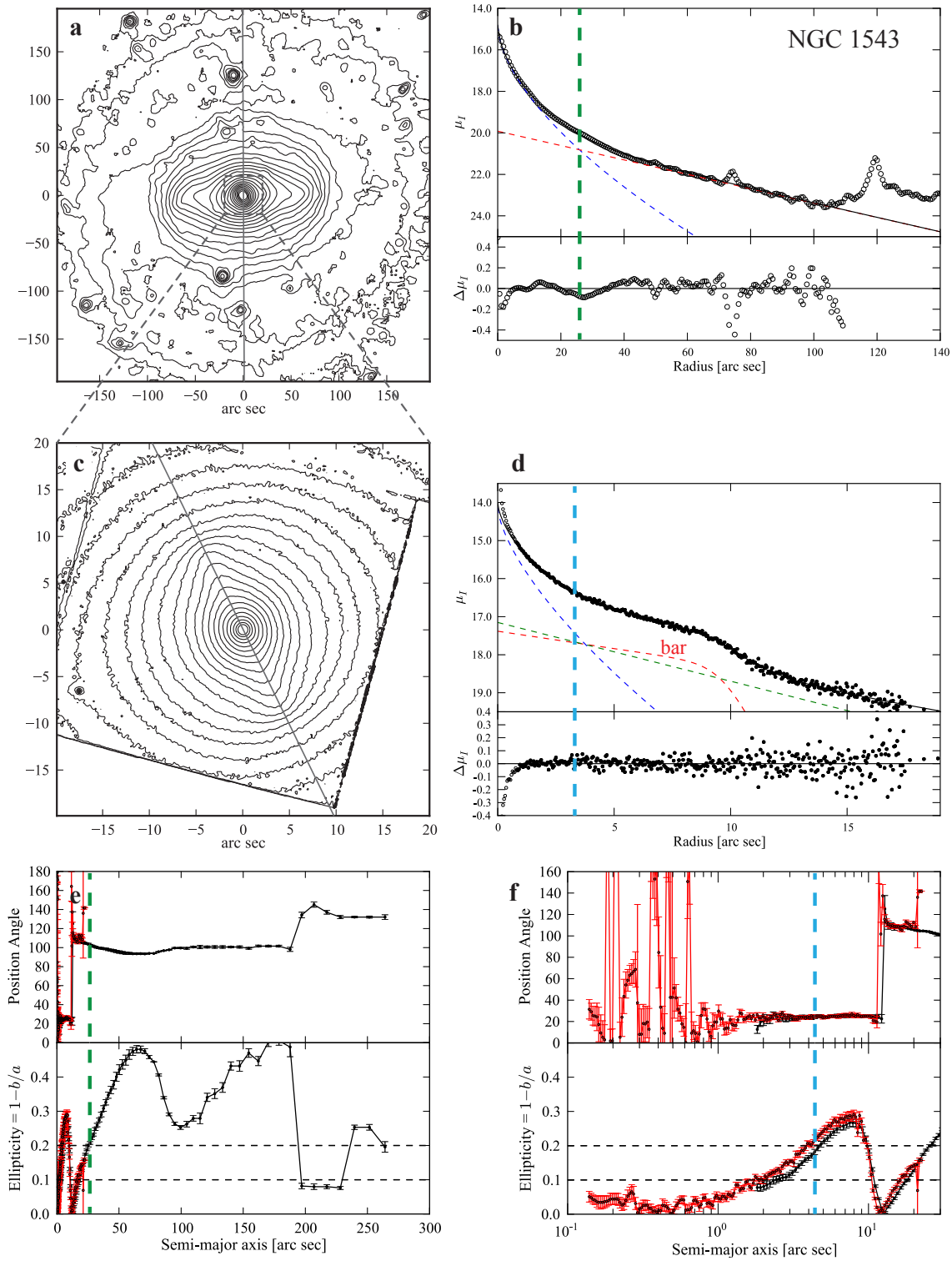


Figure A13. Photometric and morphological evidence for a possible composite bulge in the SB0 galaxy NGC 1543. **a:** Logarithmically scaled isophotes from Spitzer IRAC2 image. **b:** Bulge-disk decomposition of major-axis IRAC2 profile. Dashed lines represent Sérsic + exponential fit to the data, with residuals plotted in lower sub-panel. Vertical dashed green line marks “bulge=disk” radius R_{bd} . **c:** Close-up of photometric bulge region (WFPC2 F814W image). **d:** Profile from WFPC2 image ($r < 18$ arcsec) and IRAC2 image ($r > 18$ arcsec) along the inner bar’s major axis (PA = 26°), fit using Sérsic + broken-exponential (red, inner bar) + exponential fit (fit also includes outer-disk exponential component, not visible here); vertical dashed blue line marks inner “bulge=disk” radius $R_{bd,i}$. **e:** Ellipse fits to Spitzer IRAC2 data [black] and HST-WFPC2 F814W data [red]. **f:** Same as panel e, but on a logarithmic semi-major-axis scale.

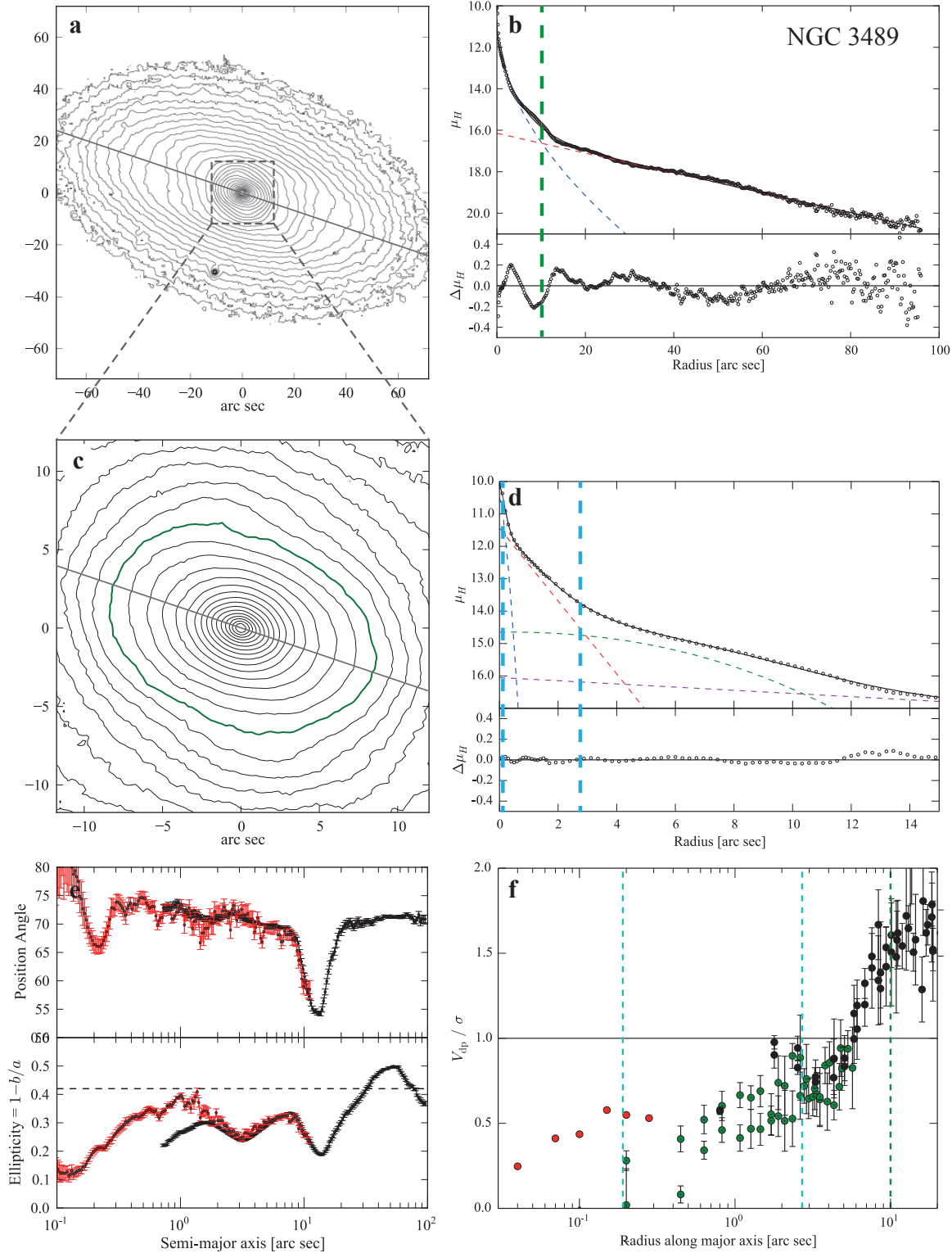


Figure A14. Possible kinematically hot, diskly pseudobulge in the S0 galaxy NGC 3489. **a:** log-scaled INGRID H -band isophotes (smoothed with 9-pixel-wide median filter); gray line marks major axis (PA = 71°). **b:** Bulge-disk decomposition of major-axis profile, from H -band and WFPC2 F814W images. Dashed lines show Sérsic + exponential fit, with residuals in lower sub-panel. Vertical dashed green line marks R_{bd} . **c:** Close-up of photometric bulge region; thick green contour shows approximate location of bar's projected box/peanut structure. **d:** Decomposition of inner major-axis profile, using outer exponential + Sérsic (for B/P structure) + inner exponential + inner Sérsic; residuals from fit are in lower sub-panel. Vertical dashed blue lines indicate R_{bd} for the inner exponential and the inner Sérsic components. **e:** Ellipse fits to H -band image (black) and WFPC2 F814W image (red); horizontal dashed line indicates outer-disk ellipticity. **f:** Deprojected stellar rotation velocity divided by local velocity dispersion V_{dp}/σ along the major axis, using SAURON data (black) from Emsellem et al. (2004), OASIS data (green) from McDermid et al. (2006) and SINFONI AO data from Nowak et al. (2010). Vertical dashed lines mark the previously identified photometric bulge regions $|R| < R_{bd}$.

Table B1. WHT-ISIS Instrumental Setup

Parameter	NGC 2859	NGC 4371
Date	2000 Dec 13	2001 Jun 4
Grating (lines mm ⁻¹)	R600B	R600B
Central wavelength (Å)	5498	5498
Detector	EEV12	EEV12
Pixel binning	1 × 1	1 × 1
Scale (arcsec pix ⁻¹)	0.36	0.36
Reciprocal dispersion (Å pix ⁻¹)	0.45	0.45
Slit width (arcsec)	0.93	1.2
Slit length (′)	4.0	4.0
Slit position angle (°)	85	92
Instrumental σ (km s ⁻¹)	60	60
Seeing FWHM (arcsec)	1.0	1.0
Galaxy exposure	3 × 1200s	3000s + 2 × 2400s
Sky exposure	900s	1200s

Instrumental setup for the blue arm of the WHT-ISIS spectrograph, as used for observations of NGC 2859 and NGC 4371.

APPENDIX B: WHT-ISIS SPECTROSCOPY

We obtained long-slit spectroscopy of NGC 2959 with the ISIS spectrograph of the William Herschel Telescope on 2000 December 13, using the blue arm with the R600B grating; further details of the observing setup are listed in Table B1. Because the galaxy was large enough to fill most of the slit, we obtained a separate 900s exposure of the nearby blank sky, offset 6′ to the east of the galaxy centre. We also observed two kinematic standard stars (HR941 and HR2660) with the same setup.

NGC 4371 was observed with an almost identical instrumental setup as part of ING service-time observations on 2001 June 4 (see Table B1). A separate 1200s sky exposure was taken with a 3′ offset to the north of the galaxy centre, and observations of four kinematic standard stars (HR5200, HR5966, HD5340, HR5340) were also obtained.

Following standard MIDAS¹⁴ reduction of the ISIS observations, including bias-subtraction, flat-fielding and wavelength calibration using CuAr and CuNe+CuAr lamp exposures, the extracted galaxy spectra were analysed using the Fourier Correlation Quotient method (Bender 1990; Bender et al. 1994) in order to determine the stellar kinematics. The resulting kinematic values – radial velocity, velocity dispersion and the Gauss-Hermite coefficients h_3 and h_4 – are presented in Table B2.

¹⁴ MIDAS is developed and maintained by the European Southern Observatory.

Table B2. WHT-ISIS Major-Axis Stellar Kinematics for NGC 2859 and NGC 4371

Galaxy	PA °	R arcsec	V km s ⁻¹	σ km s ⁻¹	h_3	h_4
NGC 2859	85	-14.70	1554.6 ± 39.5	203.1 ± 35.2	-0.124 ± 0.081	-0.072 ± 0.149
NGC 2859	85	-9.03	1586.1 ± 32.6	194.3 ± 28.1	-0.125 ± 0.067	-0.026 ± 0.120
NGC 2859	85	-6.03	1552.8 ± 13.4	160.4 ± 10.3	-0.083 ± 0.050	-0.019 ± 0.065
NGC 2859	85	-4.50	1575.0 ± 11.2	151.2 ± 8.2	-0.076 ± 0.044	0.085 ± 0.057

Stellar kinematics along the major axes of NGC 2859 and NGC 4371, as determined from spectra obtained with WHT-ISIS; see Table B1 for the instrumental setup. This table is published in its entirety in the online edition of this paper; a sample is provided here for guidance in terms of form and content.